
Molecular simulations of Hofmeister ion pairing and solvation of protein building blocks in aqueous interfacial environments

Vom Fachbereich Chemie
der Technischen Universität Darmstadt

zur Erlangung des akademischen Grades eines
Doktor rerum naturalium (Dr. rer. nat.)

genehmigte

Dissertation

vorgelegt von

Timir Hajari,

Master of Science (M. Sc.)

aus Rasulpur, Hooghly, Indien

Referent: Prof. Dr. Nico F. A. van der Vegt

Korreferent: apl. Prof. Michael C. Böhm

Tag der Einreichung: 1. Juni 2015

Tag der mündlichen Prüfung: 13. Juli 2015

Darmstadt, 2015

D17

to

my parents

Contents

Summary	ii
Zusammenfassung	v
Acknowledgments	viii
Publications	x
1 Introduction	1
2 Free Energy Calculations Using Molecular Simulations	9
3 Peptide Backbone Effect on Hydration Free energies of Amino Acid Side Chains	27
4 Solvation Thermodynamics of Amino Acid Side Chains on a Short Peptide Backbone	43
5 The Influence of Graphite Surface on Ion-Pairing of Hofmeister Ions and Hydrophobic Association	54
6 Enthalpy-Entropy of Cation Association with the Acetate Anion in Water	66
7 Conclusions and Outlook	74

Summary

In current days, computer simulation is a scientific tool to study material properties. Using computer simulation, equilibrium and nonequilibrium properties of materials can be estimated with a detailed atomistic picture which is not easily accessible with experimental techniques. It is widely used to get the atomistic resolution of various chemical and biophysical processes for better understanding of these processes. Molecular level understanding of stability, conformational changes and solvation properties of proteins or peptides in water or in ionic solution or in water-cosolvent (osmolytes) mixtures are research areas where lots of simulations and experimental works are ongoing. To understand these problems, we mainly focus in this thesis on two types of thermodynamic processes, solvation of different amino acid side-chains and ion pairing/ion-ion interaction in bulk water and near hydrophobic surfaces using molecular dynamics simulations.

A detailed understanding of aqueous solvation of protein building blocks, namely amino acids, is very useful to understand the structural stability of proteins or peptides. The free energy estimation using molecular simulations is a useful tool to rationalize protein thermodynamics. In chapter 2, a short description of different methods to estimate free energies is presented. Most of the studies to understand thermodynamics of protein have used solvation data of small molecules or analogs as a representative of amino acid side-chains in protein or peptide. In reality, these side-chains are not free but rather attached to a peptide backbone. In chapter 3, we estimate the solvation free energy of different polar and nonpolar amino acid side-chains when they are attached to a peptide backbone to assess the reliability of such small molecules solvation data in explaining phenomena like protein folding and protein-protein association. We find all the nonpolar side-chains become remarkable less hydrophobic than what is expected from the solvation free energy data of the side-chain analogs. This finding challenges many hydrophobicity scales based on the solvation free energy data of small molecules. To analyze the origin of such reductions in hydrophobicity, solvation entropies and enthalpies of nonpolar and polar side chains in peptide backbone are also estimated in chapter 4. Solvation entropies of nonpolar side-chains in peptide backbone are found to be less unfavorable than solvation entropies of free side-chains which causes an overall hydrophobicity reduction. Cavity and dispersion contributions in the solvation free

energies of nonpolar side-chains are also estimated. We find that a nonpolar side-chain sized cavity formation next to a tripeptide backbone is entropically favored over formation of similar sized cavities in bulk water, which effectively makes nonpolar side-chains less hydrophobic. The solvation enthalpies and entropies of the polar side chains are negative, but in absolute magnitude smaller compared with the corresponding analogue data. These effects almost perfectly cancel out in the solvation free energies and because of that the solvation free energies of polar side chains remain largely unaffected by the peptide backbone.

Aqueous ionic solutions have vast applications from protein folding to colloidal stability, water surface tension, osmotic property. Ion specificity in protein precipitation and ion specific propensity toward air-water and hydrophobic interfaces are well known. Most of the studies focus on the single ion behavior. The nature of ion-ion interaction near those mentioned water interfaces has not been well investigated. In chapter 5, ion pairing of halide anions with K^+ , Na^+ and Cs^+ is studied in bulk water and near to a model hydrophobic surface (graphite) to shed some more knowledge on ion specific phenomena. Small sized cations tend to pair strongly with small sized anions near hydrophobic interfaces compared with that in bulk water, whereas ion-pairing for salts with small(cation)-large(anion) combinations and large-large ion combinations is affected in a lesser extend. The solvent shared ion pair state is the ion-pairing mode that becomes more favorable owing to the higher ion-ion association near hydrophobic interfaces. Ion-ion association free energy profile is further decomposed into entropic and enthalpic components for better molecular level understanding. A positive entropic component in the free energy of the solvent shared and contact ion pair states near graphite surface is found alike in bulk solution. Hydrophobic association near graphite interface is also analyzed. The contact pair state becomes more favorable because of that the overall association is more feasible near hydrophobic interfaces.

The electrostatic interaction between the surface charge from protein and the ion from ionic solution is another important aspect that also contributes significantly in peptide or protein stability. Negatively charged acetate group from glutamate and aspartate side-chains can bind specifically with different cations that contributes to ion specific protein-cation interaction. In chapter 6, the structural details and the free-energy, entropy and enthalpy of ion-pairing between acetate ion, a model charge group present in protein or peptide and cations, K^+ , Na^+ , Li^+ are discussed. The different affinities of Na^+ and K^+ toward acetate anion is explained using an enthalpy-entropy reinforcement mechanism at solvent shared ion-pair (SIP) state which involves a water-mediated hydrogen bonding

interaction between the oppositely charged ions. Finally in chapter 7, we conclude the thesis and provide some future outlook.

Zusammenfassung

In der heutigen Zeit sind computergestützte Simulationen ein wichtiges Hilfsmittel um Materialeigenschaften zu untersuchen. Sie ermöglichen es die Gleichgewichts- und Nicht-Gleichgewichtseigenschaften von Stoffen auf Basis einer atomistischen Auflösung zu berechnen, welche mit herkömmlichen experimentellen Techniken nicht ohne weiteres realisierbar wäre. Daher werden Computersimulationen weitestgehend verwendet um ein besseres Verständnis von chemischen und biochemischen Prozessen auf atomarer Ebene zu erlangen. Viele experimentelle und computergestützte Methoden dienen dazu Erkenntnisse über die Stabilität, die Konformationsänderungen und die Löslichkeitseigenschaften von Proteinen oder Peptiden in wässrigen, ionischen oder osmolythaltigen Lösungen auf molekularer Ebene zu erlangen. Ziel dieser Arbeit ist es diese Phänomene mit Hilfe molekuldynamischer Simulationen anhand zweier thermodynamischer Prozesse zu erklären: Dem Solvatieren verschiedener Seitenketten von Aminosäuren und der Ionenpaarung/Ion-Ion Wechselwirkung in Wasser und in der Nähe hydrophober Oberflächen.

Ein detailliertes Verständnis über die Solvation der Proteinbausteine, den Aminosäuren, in Wasser ist zur Erklärung des thermodynamischen Verhaltens von Proteinen und Peptiden sehr nützlich. Die Berechnung der freien Energie durch molekulare Simulationen ist hierfür ein geeignetes Hilfsmittel. Verschiedene Methoden, die der Berechnung der freien Energie dienen sind in Kapitel 2 zusammengefasst. Die meisten Studien über das Verständnis der Solvationsthermodynamik der Proteine basieren auf der Solvation kleiner Moleküle oder Seitenkettenanaloge, welche das Verhalten von Aminosäureseitenketten in Proteinen oder Peptiden darstellen sollen. In Wirklichkeit sind diese Seitenketten aber nicht frei in Lösung, sondern vielmehr an das Rückgrat des Peptids gebunden. Kapitel 3 beinhaltet daher die Berechnung der freien Energie für verschiedene polare und unpolare Aminosäureseitenketten, die an ein Rückgrat gebunden sind. Dies dient dazu die Verlässlichkeit der Daten, die auf Basis der Solvation kleiner Molekül erhalten wurden, zur Erklärung von Prozessen wie Proteinfaltung oder Protein-Protein Assoziierung zu überprüfen. Aus diesen Berechnungen kann geschlossen werden, dass alle unpolaren Seitenketten signifikant weniger hydrophob sind als es aufgrund dieser Daten zu erwarten wäre. Skalen, die die Hydrophobizität der Seitenketten ordnen und auf

diesen Daten basieren, werden also durch die erhaltenen Ergebnisse hinterfragt. Um den Ursprung des Rückgangs der Hydrophobizität zu untersuchen werden in Kapitel 4 die Solvatationsentropien und Solvatationsenthalpien polarer und unpolarer Seitenketten in Kontakt mit dem Peptidrückgrat berechnet. Daraus geht hervor, dass die Solvatationsentropien unpolarer Seitenketten in Anwesenheit des Rückgrates weniger negativ sind als die der freien unpolaren Seitenketten. Darüber hinaus wird ebenfalls der Anteil der Kavitätsbildung und der Anteil der Dispersion an der freien Solvatationsenergie unpolarer Seitenketten berechnet. Anhand dieser Berechnungen kann herausgefunden werden, dass die Bildung eines Hohlraums in der Größe einer Seitenkette in der Nähe der Rückgrates eines Tripeptids im Vergleich zur Bildung eines ähnlich großen Hohlraumes in purem Wasser entropisch favorisiert wird. Dieser Unterschied in der Entropie bewirkt eine geringere effektive Hydrophobizität der unpolaren Seitenketten in Anwesenheit des Rückgrates. Für die polaren Seitenketten ist sowohl die Solvatationsenthalpie als auch die Solvatationsentropie negativ. Jedoch ist auch hier der Gesamtbeitrag kleiner verglichen mit den Daten, die auf Basis der entsprechenden Seitenkettenanaloge erhalten wurden. Die beiden Effekte, Entropie und Enthalpie, gleichen sich fast vollständig aus in ihrem Betrag zur freien Löslichkeitsenergie. Aus diesem Grund wird die freie Energie im Falle der polaren Seitenketten kaum von der Anwesenheit des Rückgrates beeinflusst.

Wässrige Ionenlösungen spielen in verschiedenen Anwendungsgebieten eine entscheidende Rolle. Angefangen bei der Faltung von Proteinen, über kolloidale Stabilität, bis zum Einfluss auf die Oberflächenspannung von Wasser und dem osmotischen Verhalten. Ionen spezifisches Ausfällen von Proteinen und die Ionen spezifische Affinität sowohl an die Luft-Wasser-Grenzfläche zu wandern als auch zu hydrophoben Grenzflächen sind wohl bekannt. Die meisten Studien über dieses Verhalten basieren auf einzelnen Ionen. Die Charakteristika der Wechselwirkung zwischen zwei Ionen in der Nähe der beschriebenen Wassergrenzfläche sind dagegen bis dato nicht besonders detailliert untersucht worden. Um mehr Wissen über die spezifischen Wechselwirkungen zwischen Ionen zu erlangen, wird in Kapitel 5 die Ionenpaarung von Halogenidionen mit K^+ , Na^+ und Cs^+ in reinem Wasser und nahe einer hydrophoben Modelloberfläche, Graphit, untersucht. Aus diesen Berechnungen ist erkennbar, dass kleine Kationen bevorzugt Paare mit kleinen Anionen in der Nähe hydrophober Oberflächen bilden im Vergleich zu reinem Wasser. Dieser Effekt wird nicht in diesem Maße zwischen großen Anionen und Kationen und zwischen kleinen und großen Ionen beobachtet. Aufgrund des höheren Ionen-Ionen Assoziierungsgrad in der Nähe der hydrophoben Grenzfläche, ist die Art der Paarung zwischen den Ionen eine durch das Lösungsmittel vermittelte Paarung. Für ein besseres

Verständnis auf molekularer Ebene wird das Profil der freien Energie der Ionenassoziiierung in einen entropischen und enthalpischen Teil zerlegt. Daraus geht hervor, dass der entropische Beitrag zur freien Energie für die Zustände des durch das Lösungsmittel verbundene Ionenpaar und für das im direkten Kontakt stehende Ionenpaar sowohl in reinem Wasser als auch in der Nähe einer hydrophoben Oberfläche positiv ist. Ebenfalls wird die hydrophobe Assoziierung in der Nähe einer Graphitoberfläche untersucht. Hierbei wird der direkte Kontakt zwischen Ionen ohne verbindendes Lösungsmittel verstärkt beobachtet. Dies ermöglicht eine leichtere Ionen-Assoziierung in der Nähe hydrophober Oberflächen.

Die elektrostatische Wechselwirkung zwischen der Oberflächenladung des Proteins und der Ionen in Lösung ist ein weiterer wichtiger Aspekt, der zur Stabilität des Proteins oder Peptids beiträgt. Die negativ geladene Acetatgruppe der Glutamat- und Aspartatseitenkette kann spezifisch Kationen binden, welche zur Ionen spezifischen Protein-Kation-Wechselwirkung beitragen. In Kapitel 6 werden sowohl die strukturellen Details als auch die freie Energie, Entropie und Enthalpie der Ionenpaarung zwischen dem Acetation, einer Modellverbindung eines geladenen Teilchens, und den Kationen K^+ , Na^+ und Li^+ unter Anwesenheit eines Proteins oder Peptids diskutiert. Die verschiedenen Affinitäten von K^+ und Na^+ zum Acetatanion sind anhand eines Entropie-Enthalpie-Verstärkungsmechanismus zu erklären. Dieser tritt bei bei der Bildung eines Ionenpaares, welches durch das Lösungsmittel verbunden wird, auf. Diese Verbindung wird über die Bildung von Wasserstoffbrückenbindungen zwischen den Wasserstoffatomen des Wassers und den gegensätzlich geladenen Ionen gebildet. Abschließend ist in Kapitel 7 eine Schlussfolgerung und ein Ausblick auf zukünftige Forschungsschwerpunkte basierend auf den Ergebnissen dieser Arbeit gegeben.

Sincere Thanks to...

First of all, I am indebted to Prof. Dr. Nico van der Vegt for giving me the opportunity to work as a PhD student in his group. His scientific knowledge, positive attitude, enthusiasm and friendly gestures always worked as a motivation to me. His willingness to explain any scientific doubt or query during my past few years journey will be memorable for me. I thank him sincerely for sharing his enormous knowledge on solvation thermodynamics with me.

I am very grateful to Prof. Michael C. Böhm, Prof. Dr. Markus Biesalski, Prof. Dr. Herbert Plenio for agreeing to be my co-examiners and for reading my thesis critically. I also thank Prof. Dr. Christian Hess for agreeing to be the Chairman. I would like to thank Prof. Dr. Florian Müller-Plathe and his group for sharing their ongoing research works in the weekly theory-seminar. I am really thankful to Prof. Dr. B. L. Tembe for introducing me to the field of molecular dynamics simulations and for his caring attitude. I sincerely thank all my school, college and university teachers/professors who shared their knowledges. I would not have reached this point without them. Many many thanks to Bapi Da, Gourango babu, Subrata babu for your enormous contributions to enrich my basic knowledge in physics, mathematics and chemistry. I am grateful to Naba Da whose teaching enhanced my interest in Physical Chemistry During my college days. I would like to thank Goutam Da for many useful discussions.

Thanks go to all present and former members of the CPC group: Pritam Da, Fereshte, Francisco, David, Valentina, Gregor, Kaustubh, Philipp, Mari Angeles, Imke, Marianne, Emiliano, Pim, Chunli, Pranay, Claudia, Samira, Bin, Ran, Tingting and other colleagues. My Ph.D.-life would not have been the same without your constant involvement and support. I would like to express my gratitude to Prof. Nico van der Vegt and all of the members for keeping a social climate within the group.

Thanks go to my friends in Darmstadt during my PhD days – Amit, Ravi, Tamal, Nishad, Sandeep, Andre, Vignesh, sharath, Ehsanul, Upendra, Mani, Titu, Prashant, Rajesh, Abhinav, Mekap, Aniruddh, Supratik, Evangelos, Debayan Da, Ali, Ani, Salman and all others. Thanks go to all my friends outside Darmstadt for their constant supports during my PhD days — Popy, Bachcha, Bhakta, Arka, Sanyal, Jambu, Tuhin, Mayank, Manna, Anup, Biswajit, Shyamal, Mrityunjoy, Ekadashi Da, Gouranga, Bapi, Debashish Da — I wish I

could go on with the names! I would like to thank all my school and college friends: Tanmay(Sau), Sucheta, Kankan, Maidul, Zaved, Yadav, Suman, Milan, Hemanta, Raghu, Swarup, Amitava, Manika, Tanmay(Samanta), Sarbartha, Maitri, Gourhari, Modak, Mavo, Bijit, Sujoy, Aniket, Bisak Da, Atanu, Soumya, Abhijnan, Soumendra, Nitai and others. All my friends from IIT Bombay deserve a special thanks: Alokesh, Prasenjit, Mallick, Anamitra, Krish, Raja, Tuseeta, Ushak, Pritam, Pratyay, Abhirup, Pal, Arpan, Sushanta, Buddha, Supriya, Madan, Tamal, Kalyan and others — the enjoyment I got for you guys, is and will be memorable for me.

I would like to thank all my relatives for their constant support. Thanks go to my cousins, Pinki, Munu Da, Payel, Rana, Chhattu, Lattu, Silpi, Pikai, Dolon, Tusi Di, Raju Da, Bakul Da, Puti Di, and to my childhood friends for offering me such wonderful childhood days. Last but not least, I would like to say "maa, baba, dada thanks for everything".

Timir

Publications

This thesis is based on the following publications:

T. Hajari, P. Ganguly, and N. F. A. van der Vegt, *Enthalpy-Entropy of Cation Association with the Acetate Anion in Water*, *J. Chem. Theory Comput.*, 8:3804 (2012).

Reprinted (adapted) with permission from *J. Chem. Theory Comput.*, 8:3804 (2012).
Copyright (2012) American Chemical Society.

T. Hajari, and N. F. A. van der Vegt, *Peptide Backbone Effect on Hydration Free Energies of Amino Acid Side Chains*, *J. Phys. Chem. B*, 118:13162 (2014).

Reprinted (adapted) with permission from *J. Phys. Chem. B*, 118:13162 (2014).
Copyright (2014) American Chemical Society.

T. Hajari, and N. F. A. van der Vegt, *Solvation thermodynamics of amino acid side chains on a short peptide backbone*, *J. Chem. Phys.*, 142:144502 (2015).

Reprinted with permission from *J. Chem. Phys.*, 142:144502 (2015). Copyright [2015],
AIP Publishing LLC.

T. Hajari, F. Teherian, and N. F. A. van der Vegt, *The Influence of Graphite Surface on Ion-Pairing of Hofmeister ions and Hydrophobic Association*, (in preparation).

Related publications (not included in the thesis):

P. Ganguly, T. Hajari, and N. F. A. van der Vegt, *Molecular Simulation Study on Hofmeister Cations and the Aqueous Solubility of Benzene*, *J. Phys. Chem. B*, 118:5331 (2014).

P. Ganguly, T. Hajari, J. E. Shea, and N. F. A. van der Vegt, *Mutual Exclusion of Urea and Trimethylamine N-Oxide from Amino Acids in Mixed Solvent Environment*, *J. Phys. Chem. Lett.*, 6:581 (2015).

1 Introduction

Molecular level understanding of stability, conformational changes and solvation properties of protein or peptide in water or in water-cosolvent (osmolytes, ions etc) mixture is one of interesting and challenging research area till now. Several experimental and simulation works have been done on this regard and these studies provide various contradictory opinions as an outcome. The complete understanding regarding the thermodynamic driving force behind protein's conformation change due to the changes in thermodynamic conditions (pressure, temperature) and chemical environment is still limited. Heat induced (thermal) protein unfolding is often explained using hydrophobic solvation free energy of nonpolar groups in water.^[1] The effect of hydrophilic interaction arising from hydrophilic groups (peptide backbone or polar side-chains) is not quite clear and several contradictory views are reported in literature. Similarly the mechanism behind protein or peptide folding/unfolding in ionic solutions or in presence of osmolytes is still under debate. Whether the direct interaction between protein and ion or osmolyte leads to a conformation change or an indirect effect from ion or osmolyte plays more important role is not yet completely resolved.^[2-4] However it is well accepted that the interaction between the protein building blocks, amino acid side-chains and the solvent molecules and the intramolecular interactions inside protein have important roles to bias the protein structure toward folded or unfolded form. The balance of these two types of interactions is influenced by the pressure or temperature change or by addition of osmolytes and ions that all leads protein's conformational changes. So, a detailed understanding of aqueous solvation of different polar and nonpolar amino acid side-chains is very useful to understand the thermodynamics of protein or peptide. Many hydrophobicity scales are established using the transfer free energies of amino acids to understand protein folding and protein-protein association. However, the solvation free energy of each amino acid is not enough as solvation of amino acid in protein is quite different than solvation of free amino acid. The reason is all amino acid side-chains are attached to peptide backbone. A proper understanding of solvation of side-chains with more realistic aqueous environment is not well quantified and is important to study. On the other hand, for better understanding of the ion-protein interactions, the electrostatic interactions between ions and charge groups from protein and ion-ion interactions near

aqueous interfacial environment are important to quantify. Instead of using real protein, small molecules to represent model charge groups from protein can potentially provide useful information on ion-protein electrostatic interaction. Similarly a model hydrophobic surface could be useful to mimic aqueous interface to study ion-ion interaction at interface. Molecular simulation is one of the scientific tool to access the detail atomistic picture of various biomolecular systems. In this thesis, computer simulations of three biochemically relevant aqueous systems will be discussed. Firstly, the solvation thermodynamics (solvation free energies, solvation entropies, enthalpies) of different polar and nonpolar amino acid side-chains in tripeptides are discussed in details. A systematic study of ion-ion interaction or ion-pairing of different sets of cations and anions near model hydrophobic interface is also addressed. This thesis then discusses the thermodynamics of ion pairing of acetate ion, a model charge group present in protein, with Na^+ , K^+ and Li^+ ions.

Solvation thermodynamics of amino acid side-chains

It is commonly believed that the hydrophobicity of nonpolar amino acid side-chains plays dominating role in processes like protein folding or protein-protein association.^[5-7] The alternative views about protein folding has put more emphasis on the role of peptide backbone hydrogen bonding.^[8,9] Whether the dominating role behind this folding phenomena is from the nonpolar amino side-chains or from the backbone hydrogen bonding, is an ongoing debate.^[8,10] Once protein folds, the nonpolar side-chains are buried inside protein interior from its water exposed state. Kauzmann^[5] made an analogy between protein folding and the transferring of hydrophobic molecules from water to an organic solvent, a representative of protein interior. He proposed that the transfer free energies of small molecules or amino acid side-chain analogs from water to a reference organic solvent are a good estimate of the role of hydrophobicity in protein stability. Several attempts were made to make a hydrophobicity scale using Kauzmann model or water-organic solvent partitioning approach. Most of the studies using Kauzmann model, either amino acids or side-chain analog molecules have been used.^[11,12] The associated entropy, enthalpy, heat capacity change upon unfolding of a protein is often explained based on the information about the solvation entropy, enthalpy, heat capacity data of small molecules.^[1,13-17] Similarly the information on the transfer free energies of amino acid side-chain analogs from water to water+osmolyte mixture are key ingredients to explain thermodynamics of protein stability in water-osmolyte medium.^[8,18] On the Contrary, the side-chains in peptide or protein are attached to peptide backbone.

Backbone partially excludes solvent molecules around the side-chains and also the nature of charge distribution present in the backbone can potentially influence the solvent orientation around the side-chains.^[19] The contribution from a side-chain in solvation of protein is often estimated by scaling the side-chain analog's solvation free energy with the solvent accessible area of that particular side-chains. Many implicit solvent models and solvation study of protein follow this approach. The reliability of such small molecule's solvation data or the mentioned scaling approach in understanding solvation or stability of protein is not well addressed so far. In this thesis, we estimated the solvation free energy contributions of nonpolar and polar side-chains, given each of the side-chain is attached to a tripeptide backbone. The nonpolar side-chains in presence of backbone become remarkably less hydrophobic compared to the same side-chains without backbone and even the above mentioned scaling approach can not predict that. The impact of backbone on polar side-chains is found to be less pronounced. Our work evidences that the hydrophobicity of nonpolar side-chains provides a driving force in protein folding that is smaller than what is assumed based on analog molecules (small molecules) solvation data combined with solvent accessible area information. In chapter 3, a detailed discussion is available in this regard. The effect of peptide backbone on the solvation process of nonpolar side-chains is further analysed in terms of solvation entropy, enthalpy and cavity/dispersion contributions. The backbone reduces significantly the unfavorable solvation entropic contribution in the solvation free energy of nonpolar side-chains that leads such hydrophobicity reductions. This result is in contrast with hydration entropy of small nonpolar molecules which is highly unfavorable. Hence this work demonstrates that the use of small molecules solvation data in protein stability studies, hydrophobicity scale and implicit solvent model is not adequate. It also hints the urgency to include the role of nonadditivity in the solvation process of amino acid side-chains in peptide. Chapter 4 contains a detailed discussion on solvation thermodynamics of amino acid side-chains in tripeptide backbone.

Ion pairing in bulk and near interface

The ionic solution of water has vast applications from protein folding to colloidal stability, water surface tension, osmotic property and viscosity B coefficient.^[2,20,21] Hofmeister noticed that the precipitation of protein occurs in ionic solutions and different ions have distinctly different abilities to precipitate the protein. Such ion specific behavior is known as *Hofmeister effect*. Generally ions with higher charge density are prone to induce protein precipitation. Based on precipitation ability, Hofmeister ranked series of

ions (cation/anion) which is known as Hofmeister ion series. The propensity of ions to reach near air-water interface^[22] or solid(hydrophobic)-water interface follows similar kind of Hofmeister ordering. The tendency of an ion to reach near such interfaces (protein interface, air interface or solid-interface) is determined by the ion-water, ion-ion, water-water interactions in bulk water and near the interface. The ion specificity in protein precipitation and the ion specific propensity toward air-water interface and hydrophobic interface are mainly analyzed based on single ion behavior. The nature of ion-ion interaction at aqueous interface is not yet well understood.^[23] Few works correlated thermodynamic properties like water activity coefficient, air-water surface tension, solubility of model protein with ion cooperativity or ion pairing in bulk solution.^[24,25] However the water in bulk solution behaves differently than at interface. The ion-ion interaction strength can be influenced at interfacial region. The extend of influence on ion-pairing of Hofmeister ions at such interfaces is not well quantified. In this thesis (chapter 5), ion-pairing of Hofmeister anions with K^+ , Na^+ and Cs^+ are studied in bulk water and near to a model hydrophobic surface (graphite) to shed some more knowledge on ion-ion interaction near aqueous interface. Pairing between large cations and large anions near the surface becomes highly favorable compared with that in bulk. However ion pairing for small-large, large-large ion combinations is weakly affected at interface. The water density near hydrophobic interface plays crucial role to govern such specific enhancement in ion-pairing. A general explanation is established on how hydrophobic surfaces influence ion pairing propensity of salt solutions using Collins's law of matching water affinities. The solvent shared ionpair state is the pairing mode that becomes systematically more stable near graphite interface. Ion-ion association free energy profile is further decomposed into entropic and enthalpic components for a deeper understanding.

Electrostatic interactions between surface charges from protein and ions from ionic solution is another important aspect that also contributes significantly in Hofmeister phenomena. Negatively charged acetate group from glutamate and aspartate side-chains can bind specifically with different cations.^[26,27] These specific interactions between different alkali cations and the acetate group from the side-chain of amino acids like glutamate and aspartate plays important role in peptide or protein stability. Even inside the cell, the K^+ and Na^+ ions are in different proportions which is often explained using the binding affinities of Na^+ and K^+ toward acetate group. A simulation study about ion-pairing propensities of bulk ionic solution of alkali acetate salts is useful to understand the detailed picture behind such ion specific binding toward acetate group. The impact of ion pairing is not restricted there, it also governs many thermodynamic properties of ionic

solutions. Interestingly, salt activity coefficient of the aqueous alkali acetate solutions increases with increasing size of cation which is in contrast with normal ionic solution i.e. alkali chloride. To address all these questions, the affinities of K^+ , Na^+ and Li^+ ions to acetate ion, a model charge group present in protein or peptide, are estimated by computing the potential of mean force between cation and anion at different temperatures. Work from Hess and van der Vegt^[28] showed the excess population at solvent shared ion-pair (SIP) states governs the activity coefficient of different alkali acetate solutions. Contrarily, the excess population at contact ion pair (CIP) states determines the trends for the activity coefficients of alkali chloride solutions. Here the thermodynamic properties, entropy and enthalpy changes, in the CIP state and SIP state for K^+ , Na^+ and Li^+ acetates are estimated using MD simulations and also compared with primitive model. The different affinities of K^+ and Na^+ are discussed in terms of the water mediated hydrogen bonding between two oppositely charged ions at SIP state and an entropy-enthalpy reinforcement mechanism is established.

Outline

This thesis is organised as follows:

In chapter 2, we discuss the theories behind different methods for free energy estimations.

In chapter 3, we compute the solvation free energies of amino acid side-chain analogs and compared with the respective conditional solvation free energies that accounts the effect of peptide backbone. The conditional solvation free energies are further compared with hydrophobicity scale based on surface accessibility of amino acid side-chain obtained from known protein structures.

In chapter 4, the solvation entropies and enthalpies of the various amino acid side chains in tripeptides are estimated and compared with existing side chain analogue data. The nonpolar solvation free energies are further decomposed into repulsive van der Waals cavity and attractive dispersion interaction contributions and these two contributions are compared with the solvent accessible surface area (SASA).

In chapter 5, ion pairing of different Hofmeister ions and hydrophobic association at bulk aqueous solution and near a model hydrophobic (graphite) surface are discussed.

In chapter 6, the thermodynamics of ion-pairing of alkali acetate solutions are focused in detail. The thermodynamic properties of contact and solvent shared ion-pair states are characterized in terms of their enthalpic and entropic contributions.

Finally in chapter 7, we conclude the thesis and provide some future outlooks.

Bibliography

- [1] Baldwin, R. L. Temperature Dependence of the Hydrophobic Interaction in Protein Folding. *Proc. Natl. Acad. Sci. USA* **1986**, *83*, 8069-8072.
- [2] Zhang, Y.; Cremer, P. S. Chemistry of Hofmeister Anions and Osmolytes. *Annu. Rev. Phys. Chem.* **2010**, *61*, 63-83.
- [3] Canchi, D. R.; García, A. E. Cosolvent Effects on Protein Stability. *Annu. Rev. Phys. Chem.* **2013**, *64*, 273-293.
- [4] Ganguly, P.; Hajari, T.; Shea, J. E.; van der Vegt, N. F. Mutual Exclusion of Urea and Trimethylamine N-oxide from Amino Acids in Mixed Solvent Environment. *J. Phys. Chem. Lett.* **2015**, *6*, 581-585.
- [5] Kauzmann, W. Some Factors in the Interpretation of Protein Denaturation. *Adv. Protein Chem.* **1959**, *14*, 1-63.
- [6] Tanford, C. The Hydrophobic Effect and the Organization of Living Matter. *Science* **1978**, *200*, 1012-1018.
- [7] Dill, K. A. Dominant Forces in Protein Folding. *Biochemistry* **1990**, *29*, 7133-7155.
- [8] Auton, M.; Bolen, D. W. Predicting the Energetics of Osmolyte-Induced Protein Folding/Unfolding. *Proc. Natl. Acad. Sci. USA* **2005**, *102*, 15065-15068.
- [9] Bolen, D. W.; Rose, G. D. Structure and Energetics of the Hydrogen-Bonded Backbone in Protein Folding. *Annu. Rev. Biochem.* **2008**, *77*, 339-362.
- [10] Moeser, B.; Horinek, D. Unified Description of Urea Denaturation : Backbone and Side Chains Contribute Equally in the Transfer Model. *J. Phys. Chem. B* **2014**, *118*, 107-114.
- [11] Nozaki, Y.; Tanford, C. The Solubility of Amino Acids and Two Glycine Peptides in Aqueous Ethanol and Dioxane Solutions. *J. Biol. Chem.* **1971**, *246*, 2211-2217.
- [12] Radzicka, A.; Wolfenden, R. Comparing the Polarities of the Amino Acids: Side-Chain Distribution Coefficients between the Vapor Phase, Cyclohexane, 1-Octanol, and Neutral Aqueous Solution. *Biochemistry* **1988**, *27*, 1664-1670.
- [13] Baldwin, R. L. Properties of Hydrophobic Free Energy Found by Gas-Liquid Transfer. *Proc. Natl. Acad. Sci. USA* **2013**, *110*, 1670-1673.

-
- [14] Murphy, K. P.; Privalov, P. L.; Gill, S. J. Common Features of Protein Unfolding and Dissolution of Hydrophobic compounds. *Science* **1990**, *247*, 559-561.
- [15] Spolar, R. S.; Livingstone, J. R.; Record Jr, M. T. Use of Liquid Hydrocarbon and Amide Transfer Data to Estimate Contributions to Thermodynamic Functions of Protein Folding from the Removal of Nonpolar and Polar Surface from Water. *Biochemistry* **1992**, *31*, 3947-3955.
- [16] Sturtevant, J. M. Heat Capacity and Entropy Changes in Processes Involving Proteins. *Proc. Natl. Acad. Sci. USA* **1977**, *74*, 2236-2240.
- [17] Huang, D. M.; Chandler, D. Temperature and Length Scale Dependence of Hydrophobic Effects and Their Possible Implications for Protein Folding. *Proc. Natl. Acad. Sci. USA* **2000**, *97*, 8324-8327.
- [18] Tanford, C. Isothermal Unfolding of Globular Proteins in Aqueous Urea Solutions. *J. Am. Chem. Soc.* **1964**, *86*, 2050-2059.
- [19] Ben-Naim, A. *Molecular Theory of Water and Aqueous Solutions, Part II: The Role of Water in Protein Folding Self Assembly and Molecular Recognition*; World Scientific: Singapore, 2010.
- [20] Jungwirth, P.; Cremer, P. S. Beyond Hofmeister. *Nature Chemistry* **2014**, *6*, 261-263.
- [21] Lo Nostro, P.; Ninham, B. W. Hofmeister Phenomena: An Update on Ion Specificity in Biology. *Chem. Rev.* **2012**, *112*, 2286-2322.
- [22] Jungwirth, P.; Tobias, D. J. Specific Ion Effects at the Air/Water Interface. *Chem. Rev.* **2006**, *106*, 1259-1281.
- [23] Venkateshwaran, V.; Vembanur, S.; Garde, S. Water-Mediated Ion-Ion Interactions are Enhanced at the Water Vapor-Liquid Interface. *Proc. Natl. Acad. Sci. USA* **2014**, *111*, 8729-8734.
- [24] Xie, W. J.; Gao, Y. Q. A Simple Theory for the Hofmeister Series. *J. Phys. Chem. Lett.* **2013**, *4*, 4247-4252.
- [25] Collins, K. D. Ions from the Hofmeister Series and Osmolytes: Effects on Proteins in Solution and in the Crystallization Process. *Methods* **2004**, *34*, 300-311.
- [26] Vrbka, L.; Vondrasek, J.; Jagoda-Cwiklik, B.; Vácha, R.; Jungwirth, P. Quantification and Rationalization of the Higher Affinity of Sodium over Potassium to Protein Surfaces. *Proc. Natl. Acad. Sci. USA* **2006**, *103*, 15440-15444.

-
- [27] Kahlen, J.; Salimi, L.; Sulpizi, M.; Peter, C.; Donadio, D. Interaction of Charged Amino-Acid Side Chains with Ions: An Optimization Strategy for Classical Force Fields. *J. Phys. Chem. B* **2014**, *118*, 3960-3972.
- [28] Hess, B.; van der Vegt, N. F. A. Cation Specific Binding with Protein Surface Charges. *Proc. Natl. Acad. Sci. USA* **2009**, *106*, 13296-13300.

2 Free Energy Calculations Using Molecular Simulations

Free energy calculation is extremely important and useful in understanding various chemical and biological processes like protein-protein association, protein-ligand binding and in the research areas such as drug designing and solvation free energy, solubility, partition coefficient estimations.^[1-5] The most common theories to compute free energy were developed long ago, nevertheless the free energy calculation in practice was started after the advancement in computer simulations. Computer simulation generates a detail information on ensemble of atomic configurations of a molecular system that helps to estimate the free energy difference. The absolute free energy estimation is restricted only for the system with a simple Hamiltonian, whereas the free energy difference is generally estimated for larger and complicated system because of the lacking of an analytical formulation of the partition function.^[2] Our discussion will focus on the estimation of the free energy differences. We will briefly discuss the basic theories of free energy calculations which are used in the next four chapters. There are several methods to estimate the free energy differences, a detail review on this topic is out of scope and we would recommend interested readers to go through the book^[3] written by C. Chipot and A. Pohorille.

Theory

In the canonical (NVT) ensemble, the probability of a configuration specified by the positions (r^N) and the associated momenta (p^N) of N-particles, can be expressed from statistical thermodynamics in the following way

$$P(r^N, p^N) = P(\Gamma) = \frac{1}{Q} e^{-\beta H(r^N, p^N)} = \frac{1}{Q} e^{-\beta H(\Gamma)} \quad (2.1)$$

Where any phase space point in this N-particle system is expressed by $\Gamma \equiv (r^N, p^N) \equiv (r_1, p_1, r_2, p_2, \dots, r_N, p_N)$ and Q is the canonical partition function and $\beta = (k_B T)^{-1}$ with k_B the Boltzmann constant and T the temperature. The total energy of the system at a given

configuration is represented by the Hamiltonian $H(\Gamma)$. At thermodynamic equilibrium, the canonical partition function can be described in terms of positions and momenta,

$$Q = \frac{1}{h^{3N}N!} \int e^{-\beta H(\Gamma)} d\Gamma \quad (2.2)$$

The relation between the free energy (F) of a system and the partition function (Q) in the canonical ensemble or (N,V,T) ensemble is

$$F = -\frac{1}{\beta} \ln Q \quad (2.3)$$

Now the free energy difference between two states 0 and 1, can be expressed in terms of their partition functions Q_0, Q_1 .

$$\Delta F = F_1 - F_0 = -\frac{1}{\beta} \ln \frac{Q_1}{Q_0} \quad (2.4)$$

This is the difference that our discussion will focus on. As pV work is negligible in the condensed phase at atmospheric ambient pressure, our discussion will not distinguish Gibbs free energy and Helmholtz free energy.

Molecular dynamics simulations

Before explaining the details of free energy estimations, a short introduction of molecular dynamic (MD) simulations is needed. We utilize the MD simulations to generate the ensemble of configurations defined by (r^N, p^N) for a N -particle system. The Hamiltonian of the N -particle system can be expressed as

$$H(r^N, p^N) = \sum_{i=1}^N \frac{1}{2} m_i v_i^2 + V(r^N) \quad (2.5)$$

Here, the mass, position and velocity of particle i , are defined by m_i, r_i and v_i respectively. The potential energy of the system is $V(r^N)$. $V(r^N)$ contains all the nonbonded and bonded interactions present in the system. The functional forms of the nonbonded and bonded interactions and the associated parameters to represent these interactions

are collectively referred to as force field. Using all the necessary force field parameters, the force (f_i) on particle i can be obtained by differentiating the $V(r^N)$ with respect to r_i .

$$f_i = -\frac{\partial V(r^N)}{\partial r_i} \quad (2.6)$$

Using Newton's equation of motion, the force acting on particle i can be correlated with r_i and time (t) in the following way

$$\frac{d^2 r_i}{dt^2} = \frac{dv_i}{dt} = \frac{f_i}{m_i} \quad (2.7)$$

One can integrate the Eq. 2.7 and get the time evolution of the particle. Alternatively, one can break down the integration into several small steps and get the time dependent position information of any particle i , using the leap-frog algorithm. If we know the position at time t and the velocity at $(t - \frac{1}{2}\Delta t)$, the leap-frog algorithm gives us the position at $(t + \Delta t)$ and the velocity at $(t + \frac{1}{2}\Delta t)$ using the force at time t obtained from Eq. 2.6.

$$v_i(t + \frac{1}{2}\Delta t) = v_i(t - \frac{1}{2}\Delta t) + \frac{\Delta t}{m_i} f_i(t) \quad (2.8)$$

$$r_i(t + \Delta t) = r_i(t) + \Delta t v_i(t + \frac{1}{2}\Delta t) \quad (2.9)$$

Here the time interval Δt should be sufficiently small and is typically around 10^{-14} sec - 10^{-15} sec. Using Eq. 2.8 and 2.9, the positions and velocities of all N -particles can be updated with time (t) proceeds. Finally, the time average of an observable, $X(r^N, p^N)$ can be estimated as

$$\langle X \rangle_t = 1/M \sum_{i=1}^M X(r^N, p^N) \quad (2.10)$$

Where M is the total number of times the positions and velocities are updated. Assuming ergodicity, the time average, $\langle X \rangle_t$ is equal to the ensemble average, $\langle X \rangle_{en}$.

$$\langle X \rangle_{en} = 1/\Omega \int dr^N dp^N X(r^N, p^N) \delta(E(r^N, p^N) - E) \quad (2.11)$$

Here $\Omega = \int dr^N dp^N \delta(E(r^N, p^N) - E)$ and the Delta function (δ) makes sure the conservation of the total energy (E).

Methods to estimation free energy differences

Depending on the nature of the thermodynamic transfer from one state to another state, there are two types of free energy differences, alchemical and conformational; which are commonly seen in literature. In **alchemical** free energy changes, two states are different by the energy expression or Hamiltonian. Solvation free energy and protein-ligand binding free energy estimations belong to this category. In **conformational** free energy changes, two states of interest are just separated by geometry criteria and a pathway called as reaction coordinate connects these two states. The conformational free energy difference is measured along this reaction coordinate and the corresponding free energy profile along this pathway or reaction coordinate is known as the potential of mean force (PMF).

The commonly used methods to estimate free energy differences follow three main approaches. First type of approach calculates directly the ΔF and the free energy perturbation method^[6] follows this route. In second type of approach, instead of direct ΔF computation, the derivative of ΔF with respect to a general coupling parameter, λ , is estimated to get the ΔF . The thermodynamic integration method^[7] follows this route. In third approach, the information on the probability density of different microstates is used to get ΔF . We will mainly discuss about the free energy perturbation method and the thermodynamic integration method here.

Free energy Perturbation

One of the common method of computing ΔF in computer simulations is free energy perturbation (FEP) method. Robert Zwanzig introduced about this FEP theory in 1954.^[6] The term perturbation is because of the theoretical formalism. As the free energy difference is computed between a reference system and a target system which differs from it by a perturbation, it is called FEP method.

Suppose a N-particle system with the Hamiltonian $H_0(\Gamma)$ is the reference system and the Hamiltonian of the target system is $H_1(\Gamma)$. So, $\Delta H(\Gamma) = H_1(\Gamma) - H_0(\Gamma)$ is the perturbation here. Let us consider the solvation of a solute is the process we are interested, then $\Delta H(\Gamma)$ represents the solute-solvent interactions.

By substituting the values of Q_0 and Q_1 in the Eq. 2.4, we obtain the ΔF as

$$\Delta F = -\frac{1}{\beta} \ln \frac{\int e^{-\beta H_1(\Gamma)} d\Gamma}{\int e^{-\beta H_0(\Gamma)} d\Gamma}$$

$$\Delta F = -\frac{1}{\beta} \ln \frac{\int e^{-\beta \Delta H(\Gamma)} e^{-\beta H_0(\Gamma)} d\Gamma}{\int e^{-\beta H_0(\Gamma)} d\Gamma}$$

Then we derive the final formula for FEP method (Eq. 2.12). The ΔF can be estimated based on the configurational phase space sampled from the reference system.

$$\Delta F = -\frac{1}{\beta} \ln \langle e^{-\beta \Delta H(\Gamma)} \rangle_0 \quad (2.12)$$

In this regard, it is worth to point out that the Widom test particle insertion method^[8] can be seen as an example of simple one step free energy perturbation calculation. Free energy difference estimation using Eq. 2.12 brings poor convergence in case of complex systems with lots of degrees of freedom. The main reason behind such poor convergence is because of the poor phase space overlap between the important phase space points from the target system and the accessible phase space points from the reference system (see Fig 2.1).^[9,10] A detail explanation is also available in the second chapter from the book by C. Chipot and A. Pohorille.^[3]

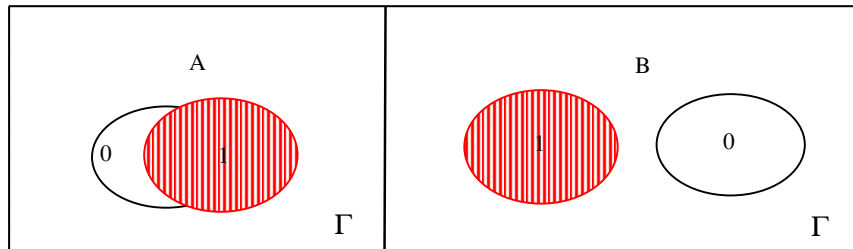


Figure 2.1: Schematic representations of poor overlaps between the important phase spaces from the target system(1) and the reference system(0): (A) partial overlap, (B) no overlap.^[3] The total phase space is represented by Γ . Here the important phase spaces from the target system and the reference system are red shaded oval and open oval respectively.^[3]

The phase space overlap problem in one step perturbation calculation can be overcome by considering multistage calculations using several intermediate states in between reference and target state. If there is 'n' numbers of intermediate states between two end states, then the free energy change between two successive states can be obtained using Eq. 2.12 and the total free energy change will be following:

$$\Delta F = \sum_{i=0}^n \Delta F_{i,i+1} = -\frac{1}{\beta} \sum_{i=0}^n \ln \langle e^{-\beta \Delta H_{i,i+1}(\Gamma)} \rangle_i \quad (2.13)$$

Eq. 2.14 provides the Hamiltonian for any state λ_i , using coupling parameter approach, where λ_i , a coupling parameter, which varies between 0 and 1. The Hamiltonian, $H_{\lambda_i}(\Gamma)$ in Eq. 2.14 is also called as the combined Hamiltonian.

$$H_{\lambda_i}(\Gamma) = \lambda_i H_1(\Gamma) + (1 - \lambda_i) H_0(\Gamma) \quad (2.14)$$

Further improvement in the accuracy of free energy estimation at state i can be done by combining forward and backward free energy perturbation averages appropriately.^[11]

Thermodynamic Integration

The thermodynamic integration (TI) is a common and well used method to estimate free energy difference. The idea behind this approach is given by Kirkwood.^[7] Suppose a system with Hamiltonian $H_\lambda(\Gamma)$ which depends on a general coupling parameter λ . The relation between absolute free energy (F) and canonical partition function is as $F(\lambda) = -\beta^{-1} \ln \int \exp[-\beta H_\lambda(\Gamma)] d\Gamma$. Here the $H_\lambda(\Gamma)$ is the Hamiltonian at a state defined by its respective λ . In TI method, the derivative of free energy with respect coupling parameter (λ) is the key quantity to estimate the correspond free energy change.

$$\frac{\partial F(\lambda)}{\partial \lambda} = \frac{\int \frac{\partial H_\lambda}{\partial \lambda} e^{-\beta H_\lambda(\Gamma)} d\Gamma}{\int e^{-\beta H_\lambda(\Gamma)} d\Gamma} = \left\langle \frac{\partial H_\lambda}{\partial \lambda} \right\rangle_\lambda$$

The total free energy change in going from state $\lambda = \lambda_0$ to state $\lambda = \lambda_1$ can be written as

$$\Delta F = \int_{\lambda_0}^{\lambda_1} \frac{\partial F(\lambda)}{\partial \lambda} d\lambda = \int_{\lambda_0}^{\lambda_1} \left\langle \frac{\partial H_\lambda}{\partial \lambda} \right\rangle_\lambda d\lambda \quad (2.15)$$

Here $\lambda=\lambda_0$ and $\lambda=\lambda_1$ corresponds to the reference state and the target state like we discussed in the FEP section. If the difference between the reference state and the target state is the energy expression (alchemical free energy change), for example: solvation free energy calculation, then the λ varies between 0 and 1 and the corresponding Hamiltonian can be written as Eq. 2.14. In that case, the estimation of $\frac{\partial H_\lambda}{\partial \lambda}$'s ensemble average is trivial.^[12] As we perform molecular simulation, so the integration in the Eq. 2.15 is performed numerically. The number of λ points is generally chosen in such a way so that the numerical integration can be done. The nature of the variation of $\left\langle \frac{\partial H_\lambda}{\partial \lambda} \right\rangle$ with λ is also very important to chose the number of λ points. Advantage of TI method is that any additional λ point can be added easily to make the variation of $\left\langle \frac{\partial H_\lambda}{\partial \lambda} \right\rangle$ smoother. In chapter 3 and 4, we will use the TI method to compute solvation free energy of different amino acid side-chains. In solvation free energy calculation, the atomic site becomes noninteracting site (dummy) at one of end point depending upon our choice of reference state. In that case, the representation of the Hamiltonian at any λ using Eq. 2.14 encounters some numerically instability. A detail discussion will be given in later stage.

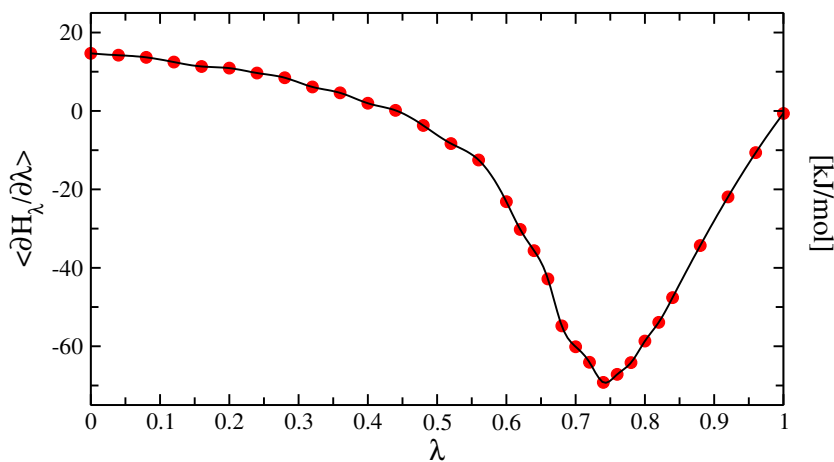


Figure 2.2: The values of $\left\langle \frac{\partial H_\lambda}{\partial \lambda} \right\rangle$ at different λ points in the solvation free energy calculation of Isoleucine side-chain analog in water. At $\lambda=0$ the analog molecule fully interacts with water and the analog molecule has no interaction with water at $\lambda=1$. The soft core scaling is used to represent the H_λ .

When $\lambda=\lambda(r)$, which means the interested free energy change is due to conformational or geometric changes, the estimation of $\left\langle \frac{\partial H_\lambda}{\partial \lambda} \right\rangle_\lambda$ is not straight forward. Here the reference and the target state both has same energy expression and a pathway or a reaction

coordinate (ζ) is required to connect them. The free energy profile along ζ is known as the potential of mean force (PMF). The relation between free energy and ζ is following

$$F(\zeta) = -\beta^{-1} \ln \frac{\int \exp[-\beta H(x, p)] \delta(\zeta - \zeta(x)) dx dp}{\int \exp[-\beta H(x, p)] dx dp} \quad (2.16)$$

Where x and p are used to express positions and momenta of all particles. Here the Dirac delta function makes sure that the integration is performed over Cartesian coordinate space defined by x and momentum space (p) keeping the value of reaction coordinate $\zeta(x) = \zeta$. In free energy calculations with reaction coordinates like torsion angle, radius of gyration; instead of using (x, p) coordinate system, an internal coordinate system is used.^[3] On the other hand, the delta function which is used in Eq. 2.16, is not so easy to deal with. It would be more convincing to use a general coordinate system for avoiding the delta function. The free energy with ζ for N -particles system is defined in a general coordinate system $(\zeta, q_1, q_2, \dots, q_{N-1})$ and associated momenta $(p_\zeta, p_1^q, p_2^q, \dots, p_{N-1}^q)$.^[3]

$$F(\zeta) = -\beta^{-1} \ln \frac{\int \exp[-\beta H] dq_1 dq_2 \dots dq_{N-1} dp_\zeta dp_1^q \dots dp_{N-1}^q}{\int \exp[-\beta H] d\zeta dq_1 dq_2 \dots dq_{N-1} dp_\zeta dp_1^q \dots dp_{N-1}^q} \quad (2.17)$$

Now Eq. 2.17 is differentiated with respect to ζ

$$\frac{\partial F(\zeta)}{\partial \zeta} = \left\langle \frac{\partial H}{\partial \zeta} \right\rangle_\zeta \quad (2.18)$$

If $U(x)$ is the potential energy function of this N -particle system in normal Cartesian coordinate system, the relation between $U(x)$ and $\left\langle \frac{\partial H}{\partial \zeta} \right\rangle_\zeta$ from general coordinate system can be shown as

$$\left\langle \frac{\partial H}{\partial \zeta} \right\rangle_\zeta = \left\langle \frac{\partial U}{\partial \zeta} - k_B T \frac{\partial \ln |J|}{\partial \zeta} \right\rangle_\zeta \quad (2.19)$$

Here the second term containing the determinant of the Jacobian matrix (J) which arises due to this coordinate transformation. In chapter 5, we compute the PMF or the free energy along the distance (r) between two particles as a reaction coordinate. These two particles are moving in a 2D plane and in that case, the value of $|J|$ is r itself.^[3] Hence a correction term $k_B T \ln(r)$ is included in final free energy estimation.

Due to the presence of several energy barriers (see Fig. 2.3), a proper sampling along ζ is not achievable in normal molecular dynamic simulations. The method of constraints or blue moon ensemble method^[13,14] is an useful method in this regard. At each ζ value, a constraint force is applied to keep ζ constant. From the constraint force at each ζ , the $[\frac{\partial F(\zeta)}{\partial \zeta}]_{\zeta}$ can be obtained.

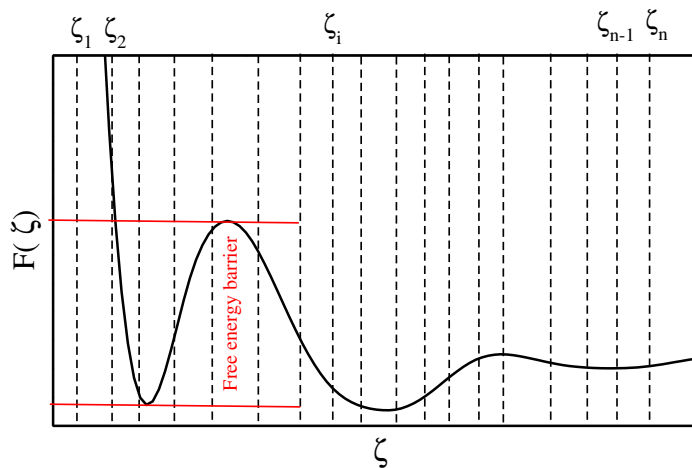


Figure 2.3: A free energy profile along a reaction coordinate ζ with having free energy barriers. Each vertical dotted line represents a specific ζ value and in the blue moon ensemble method, at each of these different specific ζ , a constraint force is applied to keep the ζ into it's respective ζ value.

Alternative approach called Adaptive bias force (ABF) method^[15,16] where $\lambda(r)$ can freely change. In ABF method, the mean force on $\lambda(r)$ is computed and subsequently removed in order to get better sampling along $\lambda(r)$. Once a complete removal of mean force is done, a random work along $\lambda(r)$ will be achieved.

Soft core potential

The coupling parameter approach is commonly used in estimating ΔF in TI method. So the Hamiltonian of the system, $H(\lambda)$ is a function of the coupling parameter, λ like in Eq. 2.14. By putting $\lambda=0$ and $\lambda=1$ in Eq. 2.14, the Hamiltonians from the reference state and the target state can be recovered. It is also common to represent the $H(\lambda)$ in term of nonlinear function of λ

$$H(\Gamma, \lambda) = \lambda^n H_1(\Gamma) + (1 - \lambda)^n H_0(\Gamma) \quad (2.20)$$

$$\frac{\partial H(\Gamma, \lambda)}{\partial \lambda} = n[\lambda^{n-1}H_1(\Gamma) + (1 - \lambda)^{n-1}H_0(\Gamma)] \quad (2.21)$$

In TI method, the ensemble average of the observable, $\frac{\partial H(\Gamma, \lambda)}{\partial \lambda}$ is estimated using combined Hamiltonian as Eq. 2.20. In alchemical free energy change with particle appearing or disappearing at end states, the ensemble average of $\frac{\partial H(\Gamma, \lambda)}{\partial \lambda}$ diverges when n from Eq. 2.20 is less than 4.^[17] The solvation free energy calculation of a solute is an example as the appearing or disappearing of solute particle happens at end states. If we consider at $\lambda=1$ the solute particle does not interact and at $\lambda=0$ the particle fully interact. So at $\lambda \rightarrow 1$, the solute particle almost does not interact with the rest of particles in the system, then other particles can overlap with the solute and eventually the observable, $\frac{\partial H(\Gamma, \lambda)}{\partial \lambda}$ diverges. The work of Beutler et al.^[17] proposed a Lennard Jones potential interaction function at different λ state to express the solute and the rest of the particles interaction and this function efficiently removes the singularity issue.

$$U^{LJ}(r, \lambda) = (1 - \lambda)^n 4\epsilon \left(\frac{1}{[\alpha_{LJ}\lambda^2 + (r/\sigma)^6]^2} - \frac{1}{[\alpha_{LJ}\lambda^2 + (r/\sigma)^6]} \right) \quad (2.22)$$

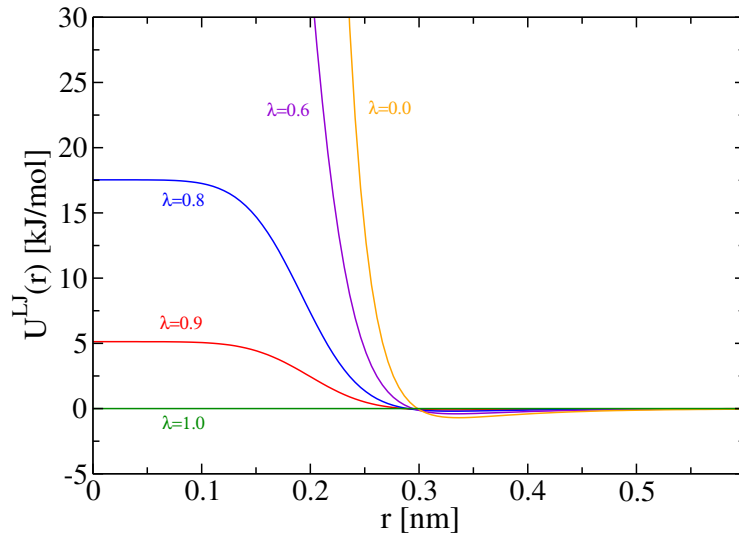


Figure 2.4: Soft core potential function for Lennard-Jones potential as Eq. 2.22 at $\lambda=0.0, 0.6, 0.8, 0.9, 1.0$. Here, $n=1$, $\epsilon=1$ kJ/mol, $\sigma=0.3$ nm, $\alpha_{LJ}=0.3$ nm are considered.

Here this $\alpha_{LJ}\lambda^n$ term makes the potential to a soft core interaction potential and helps to sample the shorter solute-water distances without any divergence issue (Fig 2.4). In this way, the soft core potential, expressed by Eq. 2.22 removes the divergence issue. For

creating or annihilating a partial charged containing particle, if we use Eq. 2.20 for the combined Hamiltonian $H(\lambda)$, the coulomb interaction may grow faster than the repulsive part from the Lennard-Jones interaction.^[17] Due to the stronger electrostatic force and less Lennard-Jones repulsive force, other particles will sit on top of the solute particle. Similarly a soft core form of coulomb interaction potential (Eq. 2.23) can be used to avoid this singularity.

$$U^C(r, \lambda) = \frac{q_1 q_2}{4\pi\epsilon_0\epsilon_r[\alpha_C\lambda^2 + (r)^m]^{1/m}} \quad (2.23)$$

In chapter 3 and 4, we have used similar types of soft core potentials^[18] for treating the Lennard-Jones and the Coulomb interaction in amino acid side-chains' solvation free energy estimations.

Bennett Acceptance Ratio Method

The Bennett Acceptance Ratio Method (BAR)^[19] is another promising method to compute free energy difference. Suppose the potential energy functions for reference state and target state are U_0 and U_1 respectively, in a canonical ensemble with N number of particles. The ratio of their partition functions

$$\frac{Q_0}{Q_1} = \frac{Q_0 \int W \exp[\beta(-U_0 - U_1)] dq_1 \dots dq_N}{Q_1 \int W \exp[\beta(-U_1 - U_0)] dq_1 \dots dq_N} = \frac{\langle W \exp[-\beta U_0] \rangle_1}{\langle W \exp[-\beta U_1] \rangle_0} \quad (2.24)$$

Here $W(q_1, q_2, \dots, q_N)$ is an arbitrary weighting function and is always a finite function with respect to any value of (q_1, q_2, \dots, q_N) . The work from Bennett^[19] had shown that for getting optimised free energy difference ($\Delta F = -\beta^{-1} \ln \frac{Q_1}{Q_0}$) or achieving minimum error in ΔF estimation, the optimum W function is as

$$W(q_1, \dots, q_N) = \text{const} \times \left(\frac{Q_0}{n_0} \exp(-\beta U_1) + \frac{Q_1}{n_1} \exp(-\beta U_0) \right)^{-1} \quad (2.25)$$

n_0 and n_1 are the numbers of statistically independent configurations from the reference state and target state respectively. Substituting the optimum W into Eq. 2.24 gives

$$\frac{Q_0}{Q_1} = \frac{\langle f(U_0 - U_1 + C) \rangle_1}{\langle f(U_1 - U_0 + C) \rangle_0} \exp(+C) \quad (2.26)$$

$$C = \ln \frac{Q_0 n_1}{Q_1 n_0} \quad (2.27)$$

Here f represents the Fermi function, $f(x) = \frac{1}{1 + \exp(+x)}$. As $\frac{Q_0}{Q_1}$ is unknown, the optimal value of C is unknown and is obtained in a self consistent manner. The value of C is adjusted until Eq. 2.26 and 2.27 become self consistent for a given n_0 and n_1 . So the optimum estimation of ΔF is achieved in BAR method in this self consistent manner.

Other Methods

There are many other methods to compute free energy differences. In this regard, the λ **dynamics** is a useful method to compute free energy differences like protein-ligand binding free energies, solvation free energies, conformational changes. Unlike TI method, λ can vary during simulation and λ is treated as a degree of freedom in extended ensemble. The detail of this method can be found in the paper of Kong et al. [25]

In conformational changes related free energy difference estimations or PMF calculations, **umbrella sampling** (US) [20] is an very commonly used method. To compute free energy along the reaction coordinate, the reaction coordinate (ζ) is splitted into a series of windows. Each window has a specific value of ζ_i and a bias potential, often a harmonic potential, is added to keep ζ around ζ_i . Finally the weighted histogram analysis (WHAM) [21] method or umbrella integration [22] is generally used to obtain the free energy profile along ζ . More information about US technique and other methods to estimate PMFs are available in the recent review papers. [23,24] Methods like **local elevation** [26] and **Metadynamics** [27] use the information about the number of times a certain ζ_i is visited by the system and based on that a repulsive Gaussian function is added on that ζ_i to explore other ζ values. Finally the free energy profile is recovered from the information on the added Gaussian functions along ζ .

The solvation free energy calculations are extremely useful in modern days in developing and validating force field, in understanding solvation process, in estimating the partitioning of a certain type of compound into different phases.^[4] Ben-Naim's definition of solvation free energy is utilized here.^[28] The normal solvation process is defined as the associated free energy change in bringing a molecule from a fixed position in an ideal gas phase to a fixed position in the liquid phase like in the Figure 2.5A.^[28] Thus the solvation free energy can be defined as Eq. 2.28, where B_S is the binding energy between the molecule S and solvent molecules (see Eq. 2.29). The solute-solvent distance is represented by r_{v_i} .

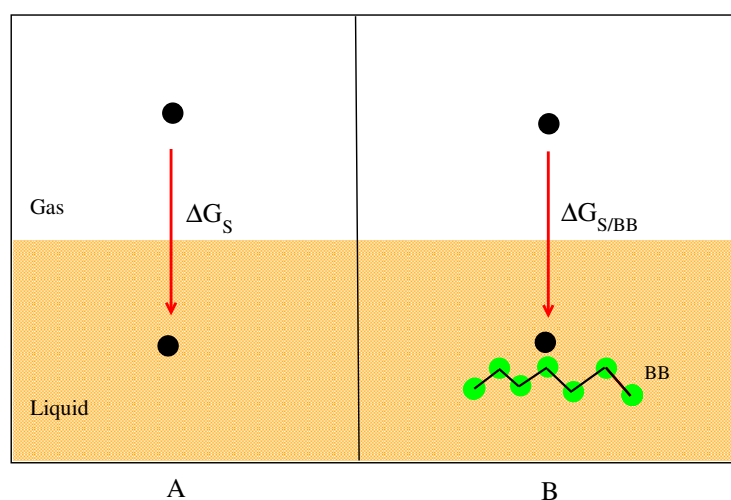


Figure 2.5: A. Normal solvation: A molecule (solid black circle) is transferred from a fixed position in ideal gas phase to a fixed position in liquid phase. B. Conditional solvation: A molecule (solid black circle) is transferred from a fixed position in ideal gas phase to a fixed position in liquid phase next to an already solvated backbone (BB).^[28]

In this thesis, we mainly focus on the *conditional* solvation process in water. The conditional solvation is defined by Ben-Naim^[28] as the free energy change in bringing a molecule (S) from ideal gas phase to a fixed position in liquid phase next to an already solvation backbone (BB) like in the Figure 2.5B. The conditional solvation free energy can be defined like normal solvation free energy using the Eq. 2.30. Here B_S is the bind-

ing energy between the molecule S and the solvent molecules, given the molecule S is fixed next the backbone (BB) like in the Fig. 2.5B.

$$\Delta G_S = -\frac{1}{\beta} \ln \langle e^{-\beta B_S} \rangle_0 \quad (2.28)$$

$$B_S = \sum_{i=1}^{N_v} U(r_{v_i}) \quad (2.29)$$

$$\Delta G_{S/BB} = -\frac{1}{\beta} \ln \langle e^{-\beta B_S} \rangle_{BB} \quad (2.30)$$

The solvation free energy calculation belongs to the category called as alchemical free energy change explained earlier. A thermodynamic cycle is considered to compute the solvation free energy and the detail is available in the chapter 3 and 4. The thermodynamic integration method is used for computing the ΔG_S , $\Delta G_{S/BB}$ of different side-chains in water.

Potential of mean force in terms of solvation free energies

The free energy profile along the reaction coordinate ζ is known as potential of mean force (*PMF*). Estimation of *PMF* using different methods has been discussed already. Here how the *PMF*(r) is correlated with solvation free energies, is the intention to discuss. The Figure 2.6 demonstrates this correlation. Here the free energy change to bring two particles (black and green ellipse from the Fig. 2.6) from distance $r=r_\infty$ to distance $r=r$ in liquid phase is the *PMF*(r).

$$PMF(r) = \Delta G_{12} + U(r) - \Delta G_1 - \Delta G_2 \quad (2.31)$$

Eq. 2.31 is obtained from the thermodynamic cycle in the Figure 2.6 and this Eq. shows the relation between the free energies and the *PMF*(r). Here ΔG_{12} is the total solvation free energy of particle 1 and 2 with a condition that these two particles are at a distance r . ΔG_1 and ΔG_2 are the normal solvation free energy of particle 1 and 2 respectively and $U(r)$ is the interaction potential gaining for bringing two particles from infinity to a distance r in gas phase. The *PMF*(r) has two contributions, direct interaction contribution

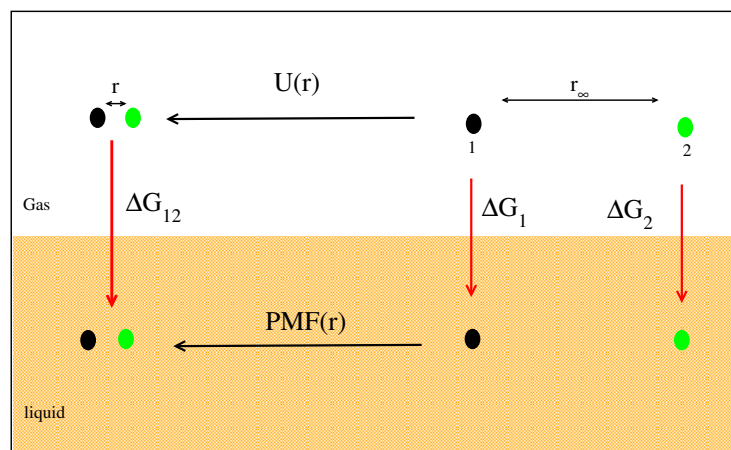


Figure 2.6: Correlation between the $PMF(r)$ and different solvation free energy terms expressed via a thermodynamic cycle. Here the reaction coordinate is the distance (r) between two particles represented by black and green ellipse.

and solvent induced contribution. Here $U(r)$ is the direct interaction contribution in the $PMF(r)$.

$$PMF_{SI}(r) = \Delta G_{12} - \Delta G_1 - \Delta G_2 \quad (2.32)$$

The solvent induced contribution is $PMF_{SI}(r) = PMF(r) - U(r)$, which is related to the solvation free energies of particle 1 and 2 (Eq. 2.32).

Bibliography

- [1] Kollman, P. Free Energy Calculations: Applications to Chemical and Biochemical Phenomena. *Chem. rev.* **1993**, *93*, 2395-2417.
- [2] Christ, C. D.; Mark, A. E.; Van Gunsteren, W. F. Basic Ingredients of Free Energy Calculations: A Review. *J. Comput. Chem.* **2010**, *31*, 1569-1582.
- [3] Chipot, C.; Pohorille, A. *Free Energy Calculations*. Springer-Verlag Berlin Heidelberg, 2007.
- [4] Hansen, N.; van Gunsteren, W. F. Practical aspects of free-energy calculations: A review. *J. Chem. Theory Comput.* **2014**, *10*, 2632-2647.
- [5] Chodera, J. D.; Mobley, D. L.; Shirts, M. R.; Dixon, R. W.; Branson, K.; Pande, V. S. Alchemical Free Energy Methods for Drug Discovery: Progress and Challenges. *Curr. Opin. Struct. Biol.* **2011**, *21*, 150-160.

-
- [6] Zwanzig, R. W. High-Temperature Equation of State by a Perturbation Method. I. Nonpolar Gases. *J. Chem. Phys.* **1954**, *22*, 1420-1426.
- [7] Kirkwood, J. G. Statistical Mechanics of Fluid Mixtures. *J. Chem. Phys.* **1935**, *3*, 300-313.
- [8] Widom, B. Some Topics in the Theory of Fluids. *J. Chem. Phys.* **1963**, *39*, 2808-2812.
- [9] Pohorille, A.; Jarzynski, C.; Chipot, C. Good Practices in Free-Energy Calculations. *J. Phys. Chem. B* **2010**, *114*, 10235-10253.
- [10] Lu, N.; Kofke, D. A. Accuracy of Free-Energy Perturbation Calculations in Molecular Simulation. I. Modeling. *J. Chem. Phys.* **2001**, *114*, 7303-7311.
- [11] Lu, N.; Singh, J. K.; Kofke, D. A. Appropriate Methods to Combine Forward and Reverse Free-Energy Perturbation Averages. *J. Chem. Phys.* **2003**, *118*, 2977-2984.
- [12] Straatsma, T. P.; McCammon, J. A. Multiconfiguration Thermodynamic Integration. *J. Chem. Phys.* **1991**, *95*, 1175-1188.
- [13] Den Otter, W. K.; Briels, W. J. The Calculation of Free-Energy Differences by Constrained Molecular-Dynamics Simulations. *J. Chem. Phys.* **1998**, *109*, 4139-4146.
- [14] Sprik, M.; Ciccotti, G. Free Energy from Constrained Molecular Dynamics. *J. Chem. Phys.* **1998**, *109*, 7737-7744.
- [15] Darve, E.; Pohorille, A. Calculating Free Energies Using Average Force. *J. Chem. Phys.* **2001**, *115*, 9169-9183.
- [16] Hénin J.; Chipot, C. Overcoming Free Energy Barriers Using Unconstrained Molecular Dynamics Simulations. *J. Chem. Phys.* **2004**, *121*, 2904-2914.
- [17] Beutler, T.C.; Mark, A.E.; van Schaik, R.C.; Gerber, P.R.; van Gunsteren, W.F. Avoiding Singularities and Numerical Instabilities in Free Energy Calculations Based on Molecular Simulations. *Chem. Phys. Lett.* **1994**, *222*, 529-539.
- [18] Shirts, M. R.; Pande, V. S. Solvation Free Energies of Amino Acid Side Chain Analogs for Common Molecular Mechanics Water Models. *J. Chem. Phys.* **2005**, *122*, 134508-134520.
- [19] Bennett, C. H. Efficient Estimation of Free Energy Differences from Monte Carlo Data. *J. Comput. Phys.* **1976**, *22*, 245-268.

-
- [20] Torrie, G. M.; Valleau, J. P. *J. Comput. Phys.* **1977**, *23*, 187-199.
- [21] Kumar, S.; Rosenberg, J. M.; Bouzida, D.; Swendsen, R. H.; Kollman, P. A. *J. Comput. Chem.* **1992**, *13*, 1011-1021.
- [22] Kästner, J.; Thiel, W. Bridging the Gap Between Thermodynamic Integration and Umbrella Sampling Provides a Novel Analysis Method:“Umbrella integration”. *J. Chem. Phys.* **2005**, *123*, 144104-144108.
- [23] Kästner, J. Umbrella Sampling. *WIREs Comput. Mol. Sci.* **2011**, *1*, 932-942.
- [24] Trzesniak, D.; Kunz, A. P. E.; van Gunsteren, W. F. A Comparison of Methods to Compute the Potential of Mean Force. *Chem. Phys. Chem.* **2007**, *8*, 162-169.
- [25] Kong, X.; Brooks III, C. L. λ -Dynamics: A New Approach to Free Energy Calculations. *J. Chem. Phys.* **1996**, *105*, 2414-2423.
- [26] Huber, T.; Torda, A. E.; van Gunsteren, W. F. Local Elevation: A Method for Improving the Searching Properties of Molecular Dynamics Simulation. *J. Comput. Aided Mol. Des.* **1994**, *8*, 695-708.
- [27] Laio, A.; Parrinello, M. Escaping Free-Energy Minima. *Proc. Natl. Acad. Sci. USA* **2002**, *99*, 12562-12566.
- [28] Ben-Naim, A. *Molecular Theory of Water and Aqueous Solutions, Part II: The Role of Water in Protein Folding Self Assembly and Molecular Recognition*; World Scientific: Singapore, 2010.



3 Peptide Backbone Effect on Hydration Free energies of Amino Acid Side Chains

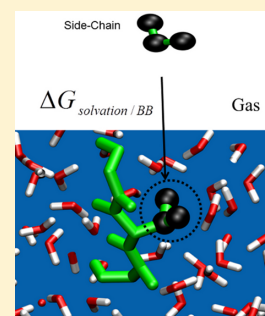
Peptide Backbone Effect on Hydration Free Energies of Amino Acid Side Chains

Timir Hajari and Nico F. A. van der Vegt*

Center of Smart Interfaces, Technische Universität Darmstadt, Alarich-Weiss-Straße 10, 64287, Darmstadt, Germany

Supporting Information

ABSTRACT: We have studied the hydrophobicity of amino acid side chains by computing conditional solvation free energies that account for effects of the peptide backbone on the side chains' solvent environment. The free energies reported herein correspond to a gas–liquid transfer process, which mimics solvation of the side chain under the condition that the backbone has been solvated already, and have been obtained on the basis of free energy calculations with empirical force field models. We find that the peptide backbone strongly impacts the solvation of nonpolar side chains, while its effect on the polar side chains is less pronounced. The results indicate that, in the presence of the short peptide backbone, nonpolar amino acid side chains are less hydrophobic than what is expected based on small molecule (analogue) solvation data.



1. INTRODUCTION

Hydrophilic and hydrophobic interactions play an important role in different biological processes like protein folding and protein–protein association. Because these processes take place in water, a thorough understanding of the aqueous solvation of the amino acid building blocks is prerequisite in identifying the molecular driving forces. In the context of the protein folding, it has been proposed that the hydrophobic effect plays a dominant role.^{1–3} Alternative views in the literature instead emphasize the role of hydrogen bonding of the peptide backbone.⁴ Because solvation free energies provide information on solvent contributions to hydrophobic and hydrophilic interactions between amino acid side groups on the peptide backbone, it is important to quantify them under experimental conditions relevant to folding. On the basis of the simple picture that a hydrophobic side chain, initially exposed to water, moves into a nonpolar protein interior upon folding, Kauzmann¹ proposed that the nature of “hydrophobic bonds” involved in maintaining the native configurations of proteins can be understood by studying solute transfer free energies between water and an organic solvent. Various hydrophobicity scales have been proposed on the basis of this partitioning approach. Solubility data of amino acids in water, ethanol, and dioxane solutions were used by Nozaki and Tanford⁵ to establish a hydrophobicity scale, but also water–octanol transfer free energies⁶ and water–air interface partitioning data⁷ were used. The appropriate choice of an organic solvent in mimicking the protein interior is however not straightforward and carries various discrepancies.⁸ Polar organic solvents like octanol exhibit more hydrogen bonding with amino acids as compared to the realistic scenario inside a protein core, and the organic solvents may partly be soluble in water in the liquid–liquid partitioning approach.⁹ Ben-Naim has moreover

pointed out a fundamental misconception in applying the above liquid–liquid partitioning approaches which originates from incorrectly accounting for the contribution of cavity formation in the organic solvent.¹⁰ Wolfenden et al.¹¹ instead used vapor–liquid free energy data, referred to as the hydration potential, of amino acid analogues and found a correlation between the surface accessible area upon folding (obtained from known protein structures) and the hydration potential. As the interior of a protein is a surrounding providing intramolecular dispersion interactions and hydrogen bonding, a vapor phase is of course incapable of mimicking it. Recently, Baldwin concluded that gas–liquid transfer data of nonpolar and polar groups can be used in determining the thermal stability of protein.¹² Apart from hydrophobicity scales based on phase transfer data, there are the well-known statistical methods^{13–15} where the accessible or buried areas of amino acid residues upon folding from known protein structures are considered to analyze hydrophobicity.

A common but critical assumption in the above approaches is that, in several of these studies based on partitioning data, only side chain analogues (small molecules) are considered which in reality however are attached to the peptide backbone.¹⁶ It is the purpose of this paper to provide data, obtained with molecular simulations, on *conditional* solvation free energies of nonpolar and polar amino acid side chains attached to a short, tripeptide backbone. The conditional solvation free energy corresponds to the process¹⁶ of solvating only the side chain atoms of the peptide, whose backbone remains solvated throughout the process. Hence, it may be interpreted as the side chain

Received: September 17, 2014

Revised: October 17, 2014

Published: October 22, 2014

contribution to the free energy of exposing the peptide to water, or, equivalently, the free energy of a vapor-to-liquid transfer process in which only the side chain is transferred to the liquid next to the already solvated backbone (Figure 1).

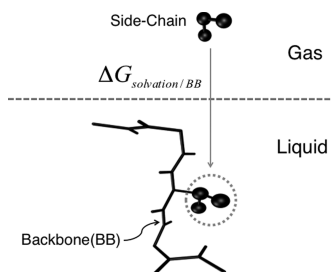


Figure 1. Conditional gas–liquid transfer process. The amino acid side chain is transferred from a fixed position in the gas phase to a fixed position next to the peptide backbone in aqueous solution.¹⁶

This free energy, referred to in this paper as $\Delta G_{\text{solvation/BB}}$, may in first approximation be provided by experimental solvation free energies of side chain analogue molecules, but differences are expected. These differences, which are caused by the effect of the peptide backbone on the local water structure surrounding the side chain, have not been well-characterized to date, yet they are important to better understand hydrophobicity/hydrophilicity variations among the different, polar and nonpolar, side groups. The data reported herein may further prove useful in analysis of folding equilibria based on transfer models^{17–20} and provide a new hydrophobicity scale for amino acid side chains complementing existing ones based on side chain analogue data. There are several computer simulations reported in the literature where conditional solvation effects and nonadditive free energy contributions from side chains have been discussed.^{21–24} Instead of using peptide backbones, these studies have been restricted to (capped) amino acids^{21,22} or nonflexible peptide backbones.²⁴

To mimic the peptide backbone, we consider short tripeptides $\text{CH}_3\text{CO-GLY-X-GLY-NHCH}_3$ with different amino acid residues X. In these short peptides, the side chains are mostly exposed to water. This situation hence mimics the solvent environment of a side chain in the extended backbone conformation. We find that the peptide backbone has a striking effect on the solvation of hydrophobic side chains. It attenuates the hydrophobic effect for the nonpolar side chains considerably, whereas the solvation of polar groups remains mostly unaffected. We also investigate the correlation between $\Delta G_{\text{solvation/BB}}$ and the corresponding amino acid residue's buried area upon folding from known protein structures taken from the work reported by Rose et al.¹⁴

2. COMPUTATIONAL METHODS

We calculated the conditional solvation free energy of each amino acid side chain except for the charged amino acids using a thermodynamic cycle which is presented in Figure 2. The conditional solvation free energy ($\Delta G_{\text{solvation/BB}}$) is determined from two thermodynamic transformations: one is the free energy change (ΔG_{gas}) due to decoupling the nonbonded interactions between the side chain atoms and the rest of the system in a vacuum, and the second one is the free energy change (ΔG_{soln}) due to decoupling the nonbonded interactions

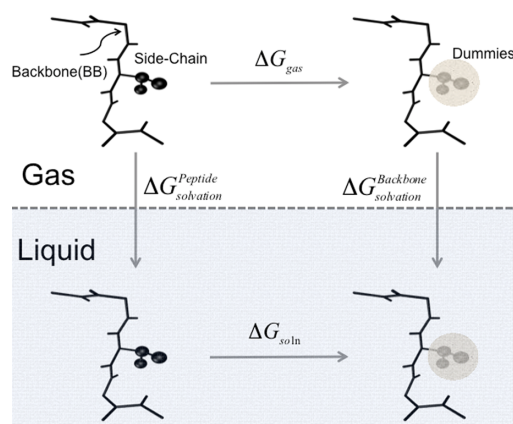


Figure 2. Thermodynamic cycle. The free energy of perturbing the side chain atoms to noninteracting dummies is calculated in the gas phase (ΔG_{gas}) and in water (ΔG_{soln}). The conditional solvation free energy of the side groups is obtained from $\Delta G_{\text{solvation/BB}} = \Delta G_{\text{gas}} - \Delta G_{\text{soln}}$.

between the side chain atoms and the rest of the system in water. The conditional solvation free energy is obtained using

$$\Delta G_{\text{solvation/BB}} = \Delta G_{\text{solvation}}^{\text{Peptide}} - \Delta G_{\text{solvation}}^{\text{Backbone}} = \Delta G_{\text{gas}} - \Delta G_{\text{soln}} \quad (1)$$

The change in free energies of these two transformations (ΔG_{gas} and ΔG_{soln}) was calculated using the thermodynamic integration (TI) method.²⁵ In TI, a coupling parameter (λ) is used to connect two thermodynamic states A and B. λ couples the nonbonded interactions between the side chain and the rest of the system and varies between $\lambda_A = 0$ (full interaction) and $\lambda_B = 1$ (zero interaction). Free energy differences are obtained by integration along λ

$$\Delta G_{AB} = \int_0^1 \left\langle \frac{dU(\lambda)}{d\lambda} \right\rangle_{\lambda} d\lambda \quad (2)$$

We have applied a soft-core potential²⁶ to avoid singularities for $\lambda \rightarrow 1$.

$$U_{\text{sc}}(r, \lambda) = (1 - \lambda)U([\alpha\sigma^6\lambda^p + r^6]^{1/6}) \quad (3)$$

The soft core parameters²⁷ were $\alpha = 0.5$, $p = 1$, and $\sigma = 0.3$ nm.

We further used the Bennett acceptance ratio (BAR) method²⁸ and the Widom test particle insertion method²⁹ for alanine as a consistency check. With all three methods, very similar results were found. The details are provided in the Supporting Information.

Molecular dynamics simulations were performed using the GROMACS software package (versions 4.6.2 and 4.5.1).³⁰ The GROMOS 54a7³¹ force field was used for the amino acids combined with the SPC water model.³² We note that various computer simulations^{27,33–35} have previously been reported to validate solvation free energies of side chain analogues with empirical force field models, which all achieve high accuracy with respect to reproducing experimental data. Hence, we do not expect strong force field effects on the computed data. We considered different peptides $\text{CH}_3\text{CO-GLY-X-GLY-NHCH}_3$ by varying the amino acid residue X. Here the backbone is a triglycine chain with $\text{CH}_3\text{-NH}$ capped C-terminal and COCH_3 capped N-terminal. Although proline does not have any real

side chain, we considered the $-\text{CH}_2-\text{CH}_2-\text{CH}_2-$ unit inside the five membered ring as a side chain. All the peptides are flexible; hence, the solvent exposure of the side chain may be different from rigid extended conformations. The corresponding differences in solvent accessible surface area (SASA)³⁶ are discussed in the Supporting Information where we report the SASA of each side chain in water and compare it with the standard accessible area data³⁷ of the same side chain in the extended state. Note that the difference between conditional solvation free energies of two different side chains corresponds to the difference in solvation free energies ($\Delta\Delta G_{\text{solvation}}^{\text{peptide}}$) of the two corresponding tripeptides $\text{CH}_3\text{CO-GLY-X-GLY-NHCH}_3$. The conditional solvation free energies obtained by the approach in Figure 2 correspond to the process in Figure 1, if we assume that no differences in side group nonbonded interactions with the backbone arise due to differences in conformational sampling in vacuum and in water. This aspect will be examined later on. Alternative to $\Delta G_{\text{solvation/BB}}$, the notation $\Delta\Delta G_{\text{aa}\rightarrow\text{PG}}^{\text{sol}}$ may be used which is the relative solvation free energy of the amino acid (aa) with respect to pseudo-glycine (PG).²² Pseudo-glycine (PG) lacks one hydrogen at α compared to glycine. The unconditional solvation free energies $\Delta G_{\text{solvation}}$ of the free amino acid side chains (without backbone) were calculated as well. Instead of considering the corresponding side chain analogue molecules, we truncated each amino acid topology at the β -carbon to get the corresponding side chain's topology without a backbone. For example, for alanine, CH_4 is generally considered as the side chain analogue molecule, whereas we consider here the chopped side chain CH_3 , which we modeled with the side group's nonbonded interaction parameters. Our considered side chain analogues therefore are not real molecules; nevertheless, it helps to quantify the real influence of the backbone on the side chain solvation. The chopped side chains are all charge neutral.

All covalent bonds of the solutes were constrained using the LINCS algorithm,³⁸ whereas the bonds and angle in water were kept constrained using the SETTLE algorithm.³⁹ The cutoff distance for the LJ nonbonded interactions was 1.4 nm in the gas phase and liquid phase simulations. In both the gas phase and the liquid phase, long-range electrostatic interactions were calculated using the PME method⁴⁰ with a real space cutoff of 1.4 nm and with a grid-spacing of 0.12 nm. The time step was 2 fs.

Liquid Phase. Periodic cubic boxes of ~ 4 nm size were simulated containing ~ 2160 water molecules. In the liquid phase, 26–31 λ points were used to compute ΔG_{soln} using TI for both the side chains on the peptide backbone and the free side chain analogues. For all cases, 26 λ points were used with the basic λ spacing, 0.04 nm. For polar side chains, five additional λ points were used in the interval $0 < \lambda < 0.004$ to capture the curvature of the free energy derivative $\langle dU(\lambda)/d\lambda \rangle$. We further used 4–5 additional λ points in the interval $0.460 < \lambda < 0.760$ for nonpolar groups, as here the softcore overlap occurs.²⁷ NPT simulations were performed at 1 bar pressure and at 298 K temperature using a leapfrog stochastic dynamics integrator⁴¹ with an inverse friction constant of 0.1 ps. The systems were equilibrated at each λ point for 1 ns using the Berendsen barostat⁴² with a coupling time of 0.5 ps. The production runs involved 4 ns data collection at each λ point and were performed using the Parrinello–Rahman barostat⁴³ with a coupling time of 0.5 ps.

Gas Phase. In the gas phase, 51–101 equidistant λ points were used to compute ΔG_{gas} with TI. In applying the BAR method, too small overlap between two successive λ points was achieved with 26–31 λ points. As the peptides have large conformational flexibility in comparison to the liquid phase, we decided to perform long simulations at each λ point. NVT simulations were performed at 298 K temperature using a leapfrog stochastic dynamics integrator with an inverse friction constant of 0.1 ps. Periodic cubic box sizes were used with the same size as in the liquid phase calculations. At each λ point, 40–60 ns production runs were performed to converge the ensemble average $\langle dU(\lambda)/d\lambda \rangle$. To check the effect of using PME in the gas phase calculations, we performed one additional ΔG_{gas} calculation for the Asn polar side chain using a larger cubic box (linear dimension 8 nm) together with a large cutoff of 3 nm for the Lennard-Jones and electrostatic interactions. Within the error bar of the calculation, the result agreed with the PME based calculation.

Errors were estimated using block averaging as

$$\delta\Delta G = \sqrt{\frac{\sum_{i=1}^{\text{Nb}} (\Delta G_i - \Delta\bar{G})^2}{\text{Nb}(\text{Nb} - 1)}} \quad (4)$$

where we have considered number of blocks $\text{Nb} = 5$ and ΔG_i is the value for each individual simulation block. $\Delta\bar{G}$ is the mean value over all blocks. Equation 4 has been used to compute errors in ΔG_{gas} and ΔG_{soln} to obtain the total error in solvation free energy.

3. RESULTS AND DISCUSSION

We have computed $\Delta G_{\text{solvation/BB}}$ for all 14 different, polar and nonpolar, amino acid side chains at amino acid position X in the tripeptide $\text{CH}_3\text{CO-GLY-X-GLY-NHCH}_3$. The unconditional solvation free energy ($\Delta G_{\text{solvation}}$) has also been computed for all 14 amino acid side chains. As our considered analogues are not real molecules (see previous section), small differences are found in comparison with experimentally obtained solvation free energies of the amino acid side chains by Wolfenden et al.¹¹ The conditional solvation free energies ($\Delta G_{\text{solvation/BB}}$) and unconditional solvation free energies ($\Delta G_{\text{solvation}}$) are reported in Table 1. Figure 3 compares these two quantities for each side chain.

Conditional Solvation of Nonpolar Side Chains.

Differences are particularly apparent for the nonpolar side chains, which have remarkably smaller solvation free energies in the presence of the peptidic backbone, i.e., the conditional solvation free energies of Val, Ile, and Leu show a 6-fold up to 20-fold reduction compared to the unconditional solvation free energies, while Ala, Pro, and Phe side chains show negative values and have favorable thermodynamic interaction with water. Thus, nonpolar side chains are significantly less hydrophobic in comparison with the free analogues due to the presence of the peptide backbone. Reduction in hydrophobicity has previously been observed in experiment and in simulations. Ben-Naim analyzed experimental solvation free energy data of different organic compounds to estimate the conditional solvation free energies of different nonpolar and polar groups.¹⁶ To demonstrate Ben-Naim's approach, we here consider two molecules BB-R and BB-H where BB stands for backbone. The difference between the solvation free energies of BB-R and BB-H is defined as the conditional solvation free energy of the R group, in analogy with eq 1. If, for example, we consider the solvation free energy data for propane (8.26 kJ/

Table 1. Conditional Solvation Free Energies ($\Delta G_{\text{solvation/BB}}$) of the Side Chains and the Unconditional Solvation Free Energy ($\Delta G_{\text{solvation}}$) of the Free Amino Acid Side Chains (See the Computational Methods Section)^a

side chain	$\Delta G_{\text{solvation/BB}}$ (kJ/mol)	$\Delta G_{\text{solvation}}$ (kJ/mol)
Val	2.4	13.9
Ile	2.1	14.0
Leu	0.6	12.4
Ala	-3.7	10.0
Pro	-4.0	11.0
Phe	-6.7	1.7
Met	-6.7	-5.9
Cys	-8.2	-8.4
Thr	-13.0	-12.6
Trp	-23.5	-23.3
Ser	-13.0	-18.2
Tyr	-35.1	-24.6
Gln	-36.0	-39.3
Asn	-34.0	-39.5

^aThe error bars, based on block averages of the free energy (five blocks), are in all cases <1 kJ/mol.

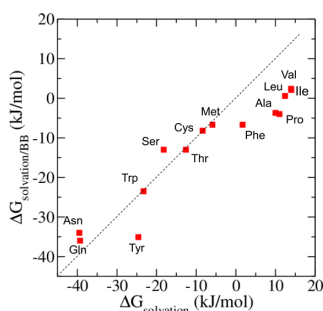


Figure 3. Comparison between the conditional solvation free energy ($\Delta G_{\text{solvation/BB}}$) and the unconditional solvation free energy ($\Delta G_{\text{solvation}}$) of polar and nonpolar amino acid side chains.

mol) and isobutane (9.97 kJ/mol),⁴⁴ then the free energy difference of 1.71 kJ/mol corresponds to the conditional solvation free energy of a methyl (CH_3) group attached to the aliphatic backbone. The experimental solvation free energy of methane (CH_4) is 8 kJ/mol, so the comparison shows that hydrophobicity is remarkably reduced close to the aliphatic backbone. Significant reduction in solvation free energies of several other nonpolar groups has further been found with these groups attached to a hydrocarbon BB chain. Ben-Naim's calculations are however restricted to nonpolar backbones, rather than an actual peptide backbone for which the experimental data are lacking. Using the OPLS-AA force field,⁴⁵ Chang et al.³⁵ computed the side chain's solvation free energies ($\Delta G_{\text{side chain}}$) by subtracting the solvation free energy of glycine (ΔG_{Gly}) from the solvation free energy of an entire amino acid ($\Delta G_{\text{amino acid}}$). They pointed out that, due to the partial burial of the side chain by the backbone, the alkane side chains in amino acids are less hydrophobic. Notably, our calculations show that $\Delta G_{\text{solvation/BB}}$ is negative for the alanine and proline side chains which both are in close proximity to the backbone. In line with the above observations, an enhancement in the probability of cavity formation near unfolded protein surfaces has also been observed,⁴⁶ i.e., nonpolar groups are

more favorably solvated close to extended backbones than in bulk water in agreement with the data presented here and the work of Ben-Naim and Chang et al. Recent studies also found that the change of the van der Waals cavity formation contribution (ΔG_{vdw}) is negative with increasing peptide chain length for alanine peptides in a fixed, extended conformation.⁴⁷

Other simulation studies^{21–24} that used different force fields did not find such significant reductions in the $\Delta G_{\text{solvation/BB}}$ values for Val, Ile, and Leu compared to their analogue molecules data. Even an enhancement in hydrophobicity has been reported²² when a methyl group is conditionally solvated next to a peptide backbone. We therefore decided to perform additional calculations with the CHARMM27 force field⁴⁸ and the TIP3P water model (the model used in refs 21–23). With this model, we calculated $\Delta G_{\text{solvation/BB}}$ for the alanine and valine side chains attached to another "backbone" (the neutral amino acid $\text{H}_2\text{N-X-COOH}$). The results (Ala, -3 kJ/mol; Val, 1.5 kJ/mol) show a similar reduction in hydrophobicity, as was obtained with the GROMOS 54a7 force field applied to the tripeptide.

Conditional Solvation of Polar Side Chains. The data summarized in Table 1 further demonstrate the effect of the backbone on the solvation free energies of the polar side chains. Large negative values of $\Delta G_{\text{solvation/BB}}$ are obtained for the side chains of Thr, Ser, Tyr, Trp, Asn, and Gln owing to hydrogen bonding interactions with water. The side chains like Phe, Met, and Cys are moderately hydrophilic in nature. Tyr and Trp side chains are more hydrophilic than Phe and Met, contrary to other scales.^{5,14} Asn, Gln, and Ser show a positive deviation with respect to the corresponding analogue data, with the biggest deviation observed for Ser. Nonadditivity in the solvation free energies of the polar groups in the presence of a peptide backbone can arise from different sources. Most of the polar side chains are capable of making hydrogen bonds with the peptide backbone either with N—H bonds or C=O bonds. Such polar side chain–backbone intramolecular interactions known as self-solvation (SS) are observed mainly in an apolar phase or in the gas phase. In water, polar side chains are hydrated and intramolecular H-bonds are less pronounced. The interatomic distances between the polar side chains and backbone polar atoms have been computed to investigate whether the side chains participate in making hydrogen bonds with the peptide backbone. Hydrogen bonds between the oxygen atom of the serine side chain and the nearest N—H bonds have been observed in the gas phase, while in the liquid phase they play no role (see the Supporting Information). Thus, in serine, we observed a self-solvation effect arising from its gas phase which is reducing the overall solvation free energy of the side chain in the presence of peptide backbone. Also, for Gln and Asn, self-solvation leads to a slightly increased conditional solvation free energy in comparison with the unconditional free energies. For Thr, on the other hand, we find that the intramolecular hydrogen bonding tendency of the side chain is comparable in the liquid phase and the gas phase (see the Supporting Information). As a consequence of such similar backbone–side chain hydrogen bonding effects for Thr, $\Delta G_{\text{solvation/BB}}$ is unaffected by self-solvation. In recent work by others, a large self-solvation effect for Ser has been found which results in a very small conditional solvation free energy (0.1 kcal/mol) for the serine side chain.²² Effects of self-solvation were seen³⁵ to be more pronounced for the zwitterionic form than for the neutral form of an amino

acid, which indicates that electrostatic interactions are important in determining the strength of these intramolecular hydrogen bonds. The partial charges on polar backbone atoms in the GROMOS54a7 force field are smaller compared to the partial charges in other force fields like OPLS-AA⁴⁵ and CHARMM27; hence, the self-solvation contribution estimated with GROMOS54a7 may be underestimated in comparison with OPLS-AA and CHARMM27.

Interestingly, the conditional solvation free energy of the Tyr side chain is 10.5 kJ/mol more favorable compared with the unconditional solvation free energy. For this system, self-solvation plays no role. Assuming that hydration of the OH group is not affected by the presence of the backbone, one may assign this free energy difference to the effect of the backbone on the aromatic ring. This is supported by comparing the conditional and unconditional solvation free energies of the Phe side chain (Table 1), which shows a difference of 8.4 kJ/mol. The backbone thus seems to increase the hydrophilicity of the Tyr side chain relative to the free side chain, or analogue molecule.

Ben-Naim showed that the conditional solvation free energies of polar groups are unchanged with respect to their analogue data,¹⁶ in agreement with what is found here (except for Tyr). These observations were made by analyzing solvation free energies of model organic compounds, not including backbones that can participate in hydrogen bond formation.

Correlation with Hydrophobicity Scale Based on Residue's Buried Surface Area Information. The hydrophobic behavior of an individual side chain statistically shows a correlation with its occurrence at the interior or at the exterior of a folded protein.^{13–15} We used data on the buried area upon folding from the work by Rose et al.¹⁴ to examine the correlation with our estimated $\Delta G_{\text{solvation/BB}}$ data. Figure 4

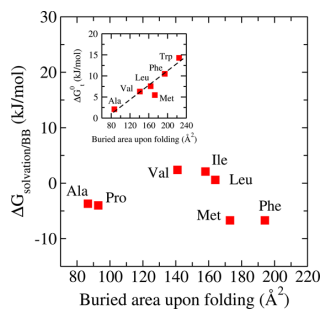


Figure 4. Correlation between the conditional solvation free energy ($\Delta G_{\text{solvation/BB}}$) and the buried area of individual side chains upon folding.¹⁴ The inset shows the correlation between the buried area of individual side chains upon folding and the unconditional liquid–liquid transfer free energies.⁵

shows $\Delta G_{\text{solvation/BB}}$ presented versus the buried area upon folding for different amino acid side chains. Rose et al.¹⁴ observed an almost perfect linear correlation (see inset) between the buried area and the Nozaki–Tanford free energy of transfer from water to organic solvent.⁵ This correlation, however, disappears for the conditional solvation free energies of nonpolar side chains. The data in Figure 4 thus indicate that hydrophobicity cannot be the sole contributor in predicting the location of a side chain in a folded protein. Moelbert et al.⁴⁹ also found various inconsistencies in the correlation between

surface accessibility of each of the amino acids and its hydrophobicity. Cysteine is capable of forming disulfide bonds, and always exists in the interior of a protein irrespective of its hydrophilicity. Small side chains like Ala and Ser can stay in the interior or be exposed to water irrespective of their hydrophobicity.⁵⁰ Even the same amino acid showed different propensities in making two common secondary structures, α -helices and β -strands for folded proteins.^{49,51–53} The probability density functions regarding the tendencies of the 20 amino acid residues to be exposed to water or to be buried inside the protein core have been examined by Nauchitel et al.⁵⁰ These authors observed various mismatches between the hydrophobicity and the surface exposure for the individual amino acids. More recently, the work of Garde and co-workers has shown that hydrophobicity of surface exposed groups is context-dependent.^{46,54}

4. CONCLUSIONS

Molecular simulations have been performed to calculate conditional solvation free energies of the nonpolar and polar amino acid side chains attached to a tripeptide, which serves as a model protein backbone. In this approach, the solvation free energy of the side chain is characterized in a more realistic chemical environment as compared to the free analogue molecule and includes effects of the backbone on the local water structure around the side chain. We find that the polar peptide backbone has a remarkably large effect on the hydrophobicity of nonpolar side chains. The conditional solvation free energies of the nonpolar side chains are strongly reduced relative to the solvation free energies of the corresponding analogue molecules. Interestingly, this effect is significantly larger compared with the prediction made on the basis of the change of the solvent accessible surface areas between free analogues and real side chains. Thus, the existing hydrophobicity scales based on small molecule's free energy data should be improved with including the role of non-additivity in solvation free energies. For the polar side chains except Tyr, we instead find that the conditional solvation free energy does not significantly differ from the unconditional (analogue) solvation free energy. For serine, self-solvation, i.e., the hydrogen bonding between side chain and backbone polar groups in the gas phase, introduces nonadditivity that should be carefully mimicked, as these effects are present in long peptide chains.

The data presented in this work indicates that desolvation of nonpolar side chains provides a driving force for protein folding which is smaller than driving forces estimated from experimental analogue transfer free energies combined with SASA models. Hydrophobic solvation of small molecules is dominated by nonpolar cavity formation in water but, as shown in this work, is strongly attenuated by the presence of a peptide backbone. On the basis of applications of the transfer model, Bolen and co-workers have provided evidence that, instead of nonpolar side chain interactions, peptide hydrogen bonds provide the dominating contribution in controlling folding–unfolding equilibrium.^{4,18,19} The absence of a clear correlation between the conditional solvation free energy and the residue's solvent exposure in known protein structures demonstrated in Figure 4 may support this view. In this context, it is however worth pointing out that, in a very interesting recent study, Moeser and Horinek compared the standard, united residue, transfer model with predictions of a newly proposed, universal backbone, transfer model.²⁰ Their work convincingly demon-

strates that both the side chain and the backbone on average contribute favorably in urea denaturation of proteins. Further work, therefore, is needed to quantify the relative side chain and backbone contributions.

■ ASSOCIATED CONTENT

■ Supporting Information

The comparison between the computed solvent accessible surface area (SASA) of each side chain attached to the peptide and the SASA of the same side chain in the extended conformation from the literature; the relation between the conditional solvation free energies and the side chain SASA; the details of other free energy methods to estimate $\Delta G_{\text{solvation/BB}}$ of the alanine side chain; and the side chain–backbone hydrogen bond analysis in the gas phase and in the liquid phase for Ser and Thr. This material is available free of charge via the Internet at <http://pubs.acs.org>.

■ AUTHOR INFORMATION

Corresponding Author

*E-mail: vandervegt@csi.tu-darmstadt.de. Phone: +49 6151 16-4356.

Notes

The authors declare no competing financial interest.

■ ACKNOWLEDGMENTS

We thank Emiliano Brini for several useful discussions. This research has been carried out as part of the priority program SPP 1569 by the German Science Foundation. We are grateful to the high-performance computing center of the Technische Universität Darmstadt for allocating computer time.

■ REFERENCES

- (1) Kauzmann, W. Some Factors in the Interpretation of Protein Denaturation. *Adv. Protein Chem.* **1959**, *14*, 1–63.
- (2) Tanford, C. The Hydrophobic Effect and the Organization of Living Matter. *Science* **1978**, *200*, 1012–1018.
- (3) Dill, K. A. Dominant Forces in Protein Folding. *Biochemistry* **1990**, *29*, 7133–7155.
- (4) Bolen, D. W.; Rose, G. D. Structure and Energetics of the Hydrogen-Bonded Backbone in Protein Folding. *Annu. Rev. Biochem.* **2008**, *77*, 339–362.
- (5) Nozaki, Y.; Tanford, C. The Solubility of Amino Acids and Two Glycine Peptides in Aqueous Ethanol and Dioxane Solutions. *J. Biol. Chem.* **1971**, *246*, 2211–2217.
- (6) Fauchère, J. L.; Pliska, V. Hydrophobic Parameters of Amino-Acid Side-Chains from the Partitioning of N-Acetyl-Amino-Acid Amide. *J. Med. Chem.* **1983**, *18*, 369–375.
- (7) Bull, H. B.; Breese, K. Surface Tension of Amino Acid Solutions: A Hydrophobicity Scale of the Amino Acid Residues. *Arch. Biochem. Biophys.* **1974**, *161*, 665–670.
- (8) Lee, B. Estimation of the Maximum Change in Stability of Globular Proteins upon Mutation of a Hydrophobic Residue to Another of Smaller Size. *Protein Sci.* **1993**, *2*, 733–738.
- (9) Radzicka, A.; Wolfenden, R. Comparing the Polarities of the Amino Acids: Side-Chain Distribution Coefficients between the Vapor Phase, Cyclohexane, 1-Octanol, and Neutral Aqueous Solution. *Biochemistry* **1988**, *27*, 1664–1670.
- (10) Ben-Naim, A. Solvent Effects on Protein Association and Protein Folding. *Biopolymers* **1990**, *29*, 567–596.
- (11) Wolfenden, R.; Andersson, L.; Cullis, P. M.; Southgate, C. C. Affinities of Amino Acid Side Chains for Solvent Water. *Biochemistry* **1981**, *20*, 849–855.
- (12) Baldwin, R. L. Properties of Hydrophobic Free Energy Found by Gas-Liquid Transfer. *Proc. Natl. Acad. Sci. U.S.A.* **2013**, *110*, 1670–1673.
- (13) Chothia, C. The Nature of the Accessible and Buried Surfaces in Proteins. *J. Mol. Biol.* **1976**, *105*, 1–14.
- (14) Rose, G. D.; Geselowitz, A. R.; Lesser, G. J.; Lee, R. H.; Zehfus, M. H. Hydrophobicity of Amino Acid Residues in Globular Proteins. *Science* **1985**, *229*, 834–838.
- (15) Miller, S.; Janin, J.; Lesk, A. M.; Chothia, C. Interior and Surface of Monomeric Proteins. *J. Mol. Biol.* **1987**, *196*, 641–656.
- (16) Ben-Naim, A. *Molecular Theory of Water and Aqueous Solutions, Part II: The Role of Water in Protein Folding Self Assembly and Molecular Recognition*; World Scientific: Singapore, 2010.
- (17) Tanford, C. Isothermal Unfolding of Globular Proteins in Aqueous Urea Solutions. *J. Am. Chem. Soc.* **1964**, *86*, 2050–2059.
- (18) Auton, M.; Bolen, D. W. Predicting the Energetics of Osmolyte-Induced Protein Folding/Unfolding. *Proc. Natl. Acad. Sci. U.S.A.* **2005**, *102*, 15065–15068.
- (19) Auton, M.; Holthausen, L. M. F.; Bolen, D. W. Anatomy of Energetic Changes Accompanying Urea-Induced Protein Denaturation. *Proc. Natl. Acad. Sci. U.S.A.* **2007**, *104*, 15317–15322.
- (20) Moeser, B.; Horinek, D. Unified Description of Urea Denaturation: Backbone and Side Chains Contribute Equally in the Transfer Model. *J. Phys. Chem. B* **2014**, *118*, 107–114.
- (21) König, G.; Borech, S. Hydration Free Energies of Amino Acids: Why Side Chain Analog Data Are Not Enough. *J. Phys. Chem. B* **2009**, *113*, 8967–8974.
- (22) König, G.; Bruckner, S.; Borech, S. Absolute Hydration Free Energies of Blocked Amino Acids: Implications for Protein Solvation and Stability. *Biophys. J.* **2013**, *104*, 453–462.
- (23) Tomar, D. S.; Weber, V.; Pettitt, B. M.; Asthagiri, D. Conditional Solvation Thermodynamics of Isoleucine in Model Peptides and the Limitations of the Group-Transfer Model. *J. Phys. Chem. B* **2014**, *118*, 4080–4087.
- (24) Staritzbichler, R.; Gu, W.; Helms, V. Are Solvation Free Energies of Homogeneous Helical Peptides Additive? *J. Phys. Chem. B* **2005**, *109*, 19000–19007.
- (25) Kirkwood, J. G. Statistical Mechanics of Fluid Mixtures. *J. Chem. Phys.* **1935**, *3*, 300–313.
- (26) Beutler, T. C.; Mark, A. E.; van Schaik, R. C.; Gerber, P. R.; van Gunsteren, W. F. Avoiding Singularities and Numerical Instabilities in Free Energy Calculations Based on Molecular Simulations. *Chem. Phys. Lett.* **1994**, *222*, 529–539.
- (27) Hess, B.; van der Veegt, N. F. A. Hydration Thermodynamic Properties of Amino Acid Analogs: A Systematic Comparison of Biomolecular Force Fields and Water Models. *J. Phys. Chem. B* **2006**, *110*, 17616–17626.
- (28) Bennett, C. H. Efficient Estimation of Free Energy Differences from Monte Carlo Data. *J. Comput. Phys.* **1976**, *22*, 245–268.
- (29) Widom, B. Some Topics in the Theory of Fluids. *J. Chem. Phys.* **1963**, *39*, 2808–2812.
- (30) Lindahl, E.; Hess, B.; van der Spoel, D. GROMACS 3.0: A Package for Molecular Simulation and Trajectory Analysis. *J. Mol. Model.* **2001**, *7*, 306–317.
- (31) Schmid, N.; Eichenberger, A. P.; Choutko, A.; Riniker, S.; Winger, M.; Mark, A. E.; van Gunsteren, W. F. Definition and Testing of the GROMOS Force-Field Versions 54A7 and 54B7. *Eur. Biophys. J.* **2011**, *40*, 843–856.
- (32) Berendsen, H. J. C.; Postma, J. P. M.; van Gunsteren, W. F.; Hermans, J. *Interaction Models for Water in Relation to Protein Hydration, Intermolecular Forces*; Pullman, B., Ed.; D. Reidel Publishing Company: Dordrecht, The Netherlands, 1981; pp 331–342.
- (33) Villa, A.; Mark, A. E. Calculation of the Free Energy of Solvation for Neutral Analogs of Amino Acid Side Chains. *J. Comput. Chem.* **2002**, *23*, 548–553.
- (34) Shirts, M. R.; Pande, V. S. Solvation Free Energies of Amino Acid Side Chain Analogs for Common Molecular Mechanics Water Models. *J. Chem. Phys.* **2005**, *122*, 134508–134520.

- (35) Chang, J.; Lenhoff, A. M.; Sandler, S. I. Solvation Free Energy of Amino Acids and Side-Chain Analogues. *J. Phys. Chem. B* **2007**, *111*, 2098–2106.
- (36) Lee, B.; Richards, F. M. The Interpretation of Protein Structures: Estimation of Static Accessibility. *J. Mol. Biol.* **1971**, *55*, 379–400.
- (37) Lesser, G. J.; Rose, G. D. Hydrophobicity of Amino Acid Subgroups in Proteins. *Protein* **1990**, *8*, 6–13.
- (38) Hess, B.; Bekker, H.; Berendsen, H. J. C.; Fraaije, J. G. E. M. LINCS: A Linear Constraint Solver For Molecular Simulations. *J. Comput. Chem.* **1997**, *18*, 1463–1472.
- (39) Miyamoto, S.; Kollman, P. A. Settle: An Analytical Version of the SHAKE and RATTLE Algorithm for Rigid Water Models. *J. Comput. Chem.* **1992**, *13*, 952–962.
- (40) Essmann, U.; Perera, L.; Berkowitz, M. L.; Darden, T.; Lee, H.; Pedersen, L. G. A Smooth Particle Mesh Ewald Method. *J. Chem. Phys.* **1995**, *103*, 8577–8593.
- (41) van Gunsteren, W. F.; Berendsen, H. J. C. A Leap-Frog Algorithm for Stochastic Dynamics. *Mol. Simul.* **1988**, *1*, 173–185.
- (42) Berendsen, H. J. C.; Postma, J. P. M.; van Gunsteren, W. F.; DiNola, A.; Haak, J. R. Molecular Dynamics with Coupling to an External Bath. *J. Chem. Phys.* **1984**, *81*, 3684–3690.
- (43) Parrinello, M.; Rahman, A. Polymorphic Transitions in Single Crystals - a New Molecular-Dynamics Method. *J. Appl. Phys.* **1981**, *52*, 7182–7190.
- (44) Ben-Naim, A. *Hydrophobic Interactions*; Plenum Press: New York, 1980; pp 107–108.
- (45) Jorgensen, W. L.; Maxwell, D. S.; Tirado-Rives, J. Development and Testing of the OPLS All-Atom Force Field on Conformational Energetics and Properties of Organic Liquids. *J. Am. Chem. Soc.* **1996**, *118*, 11225–11236.
- (46) Acharya, H.; Vembanur, S.; Jamadagni, S. N.; Garde, S. Mapping Hydrophobicity at the Nanoscale: Applications to Heterogeneous Surfaces and Proteins. *Faraday Discuss.* **2010**, *146*, 353–365.
- (47) Kokubo, H.; Harris, R. C.; Asthagiri, D.; Pettitt, B. M. Solvation Free Energies of Alanine Peptides: The Effect of Flexibility. *J. Phys. Chem. B* **2013**, *117*, 16428–16435.
- (48) MacKerell, A. D., Jr.; Banavali, N.; Foloppe, N. Development and Current Status of the CHARMM Force Field for Nucleic Acids. *Biopolymers* **2001**, *56*, 257–265.
- (49) Moelbert, S.; Emberly, E.; Tang, C. Correlation Between Sequence Hydrophobicity and Surface-Exposure Pattern of Database Proteins. *Protein Sci.* **2004**, *13*, 752–762.
- (50) Nauchitel, V. K.; Somorjai, R. L. Spatial and Free Energy Distribution Patterns of Amino Acid Residues in Water Soluble Proteins. *Biophys. Chem.* **1994**, *51*, 327–336.
- (51) Munoz, V.; Serrano, L. Intrinsic Secondary Structure Propensities of Amino Acids, Using Statistical ϕ - ψ Matrices: Comparison with Experimental Scales. *Proteins* **1994**, *20*, 301–311.
- (52) Minor, D. L., Jr.; Kim, P. S. Context is a Major Determinant of Beta-Sheet Propensity. *Nature* **1994**, *371*, 264–267.
- (53) Minor, D. L., Jr.; Kim, P. S. Context-Dependent Secondary Structure Formation of a Designed Protein Sequence. *Nature* **1996**, *380*, 730–734.
- (54) Patel, A. J.; Garde, S. Efficient Method to Characterize the Context-Dependent Hydrophobicity of Proteins. *J. Phys. Chem. B* **2014**, *118*, 1564–1573.

Supporting Information

Peptide Backbone Effect on Hydration Free Energies of Amino Acid Side Chains

Timir Hajari and Nico F. A. van der Vegt*

*Center of Smart Interfaces, Technische Universität Darmstadt, Alarich-Weiss-Straße 10, 64287,
Darmstadt, Germany*

We present the following information: Section 1 summarizes the comparison between the calculated solvent accessible surface area (SASA) of each side chain attached to the peptide and the SASA of the same side chain in the extended conformation as obtained from literature. In section 2, the relation between the side chain SASA and the conditional solvation free energies is presented. The details of the test particle insertion method and the Bennett Acceptance Ratio (BAR) method to estimate $\Delta G_{solvation/BB}$ of the Alanine side chain are reported in section 3. In section 4, the intramolecular distances between the side chain oxygen atom of Ser or Thr and the hydrogen atoms from H-N units (amide groups) of the peptide are shown to quantify hydrogen bonding tendencies both in the gas phase and in the liquid phase.

1 Computed side chain SASAs

The 2nd column in Table S1 shows the solvent accessible surface areas of side chains X attached to the tripeptide $\text{CH}_3\text{CO-GLY-X-GLY-NHCH}_3$. The SASA values have been computed using the GROMACS code,¹ where the Double Cubic Lattice Model from Eisenhaber *et al.*² has been used, based on 5 ns trajectories in water. The SASA values corresponding to the extended standard states of GLY-X-GLY, taken from the work of Rose and coworkers³ who used the SASA approach of Lee *et al.*,⁴ are presented in the 3rd column for each side chain. The last column contains the SASA values of the isolated side chains calculated with the GROMACS code. The side chain SASA values obtained from the simulations with the GROMOS 54a7 force field⁵ are smaller than the extended standard state values owing to the flexibility of the tripeptide backbone.

Side chain	Side chain SASA (\AA^2)	Extended SASA (\AA^2)	isolated side chains SASA (\AA^2)
Val	106.6	128.4	158.0
Ile	127.5	150.1	183.0
Leu	130.3	157.8	181.0
Ala	54.4	71.9	105.1
Pro	93.0	111.0	158.0
Phe	160.1	184.4	216.0
Met	140.5	164.8	192.6
Cys	90.7	103.5	143.2
Thr	94.8	114.6	145.0
Trp	188.6	228.9	253.0
Ser	68.0	85.8	118.0
Tyr	163.6	198.1	226.1
Gln	127.1	155.4	178.2
Asn	100.5	125.3	154.0

Table S1: Solvent accessible surface areas for each amino acid side chain. The data in the 2nd column correspond to the side chain SASAs of amino acids X in the sequence $\text{CH}_3\text{CO-GLY-X-GLY-NHCH}_3$ simulated in water. The 3rd column contains the extended standard state SASA values from the work of Lesser *et al.*³ The last column contains the SASA values of the isolated side chains.

2 Conditional solvation free energy ($\Delta G_{solvation/BB}$) versus SASA

Figure S1 shows $\Delta G_{solvation/BB}$ of (mainly) nonpolar amino acid side chains X within the tripeptides $\text{CH}_3\text{CO-GLY-X-GLY-NHCH}_3$ versus the side group SASA values. The inset shows the difference between the conditional and unconditional solvation free energies versus the corresponding SASA differences (differences between the data in columns 1 and 3 of Table S1). Solvation free energies of nonpolar groups are often considered to be proportional to their SASA values. It can however be observed that this proportionality does not exist for the data presented in Figure S1.

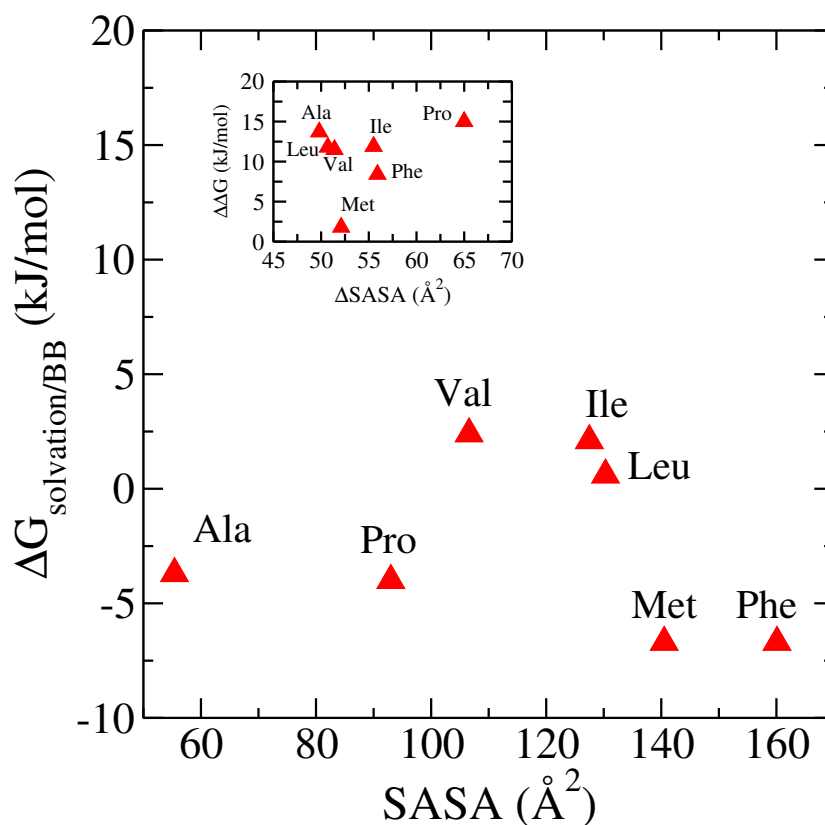


Figure S1: Comparison between the conditional solvation free energies ($\Delta G_{solvation/BB}$) and the corresponding solvent accessible surface areas of nonpolar amino acid (X) side chains in tripeptides $\text{CH}_3\text{CO-GLY-X-GLY-NH-CH}_3$. The inset shows the quantity $\Delta\Delta G$, defined as $\Delta\Delta G \equiv \Delta G_{solvation} - \Delta G_{solvation/BB}$, versus ΔSASA , defined as $\Delta\text{SASA} \equiv \text{SASA}(\text{free side chain analog}) - \text{SASA}(\text{side chain})$.

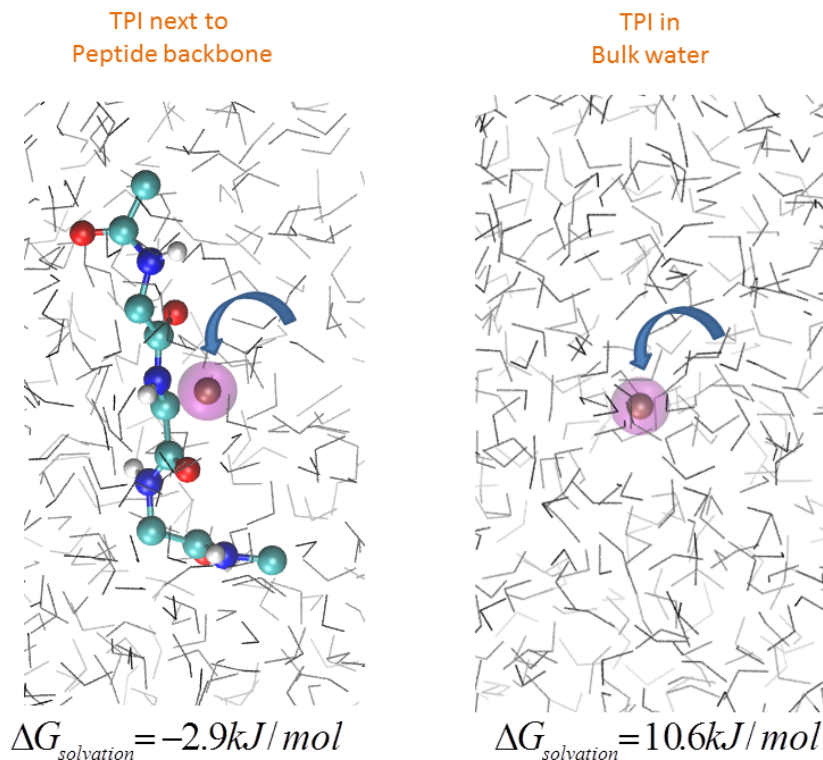


Figure S2: Test-particle insertion of a united atom CH_3 particle next to a tripeptide $\text{CH}_3\text{CO-GLY-PseudoALA-GLY-NH-CH}_3$ (left) and test-particle insertion of the same particle in bulk water (right). The nonbonded interaction parameters of the inserted particle correspond to those of the Ala side chain (CH_3).

3 Alternative free energy calculations for Ala

3.1 Test particle insertion⁶

A simulation system containing a tripeptide $\text{CH}_3\text{CO-GLY-PseudoALA-GLY-NH-CH}_3$ and water in a ~ 4 nm cubic box has been considered. Here, PseudoALA refers to an ALA unit whose side chain is a noninteracting dummy group. In the GROMOS 54a7 force field, the side chain of ALA is an united CH_3 atom. We have performed a 60 ns NPT production run of this system. Every 10 ps an united atom CH_3 test-particle-insertion (TPI) is performed at the position of the dummy side chain of PseudoALA (Figure S2). We used the nonbonded parameters of the alanine side chain for the test particle and computed $\Delta G_{solvation/BB}$ by averaging the Boltzmann factor of the test-particle energy over all configurations. The obtained value of

$\Delta G_{solvation/BB}$ is -2.9 kJ/mol which is in good agreement with the value computed using the TI method (-3.7 kJ/mol). Based on performing TPI in bulk water, a the solvation free energy of 10 kJ/mol is obtained with the same CH₃ test-particle. The results obtained with TI and TPI both indicate that the solvation free energy of the nonpolar CH₃ group is remarkably reduced in the presence of the tripeptide backbone.

3.2 Bennett Acceptance Ratio (BAR) method.⁷

System	No of λ	ns per λ
gas phase	51	50
liquid phase	30	5.0

The leap-frog stochastic dynamics⁸ integrator with an inverse friction constant of 0.1 ps to maintain the system temperature at 298K has been used, both, in the gas phase and in the liquid phase simulations. The production runs at each λ point in the liquid phase have been performed using the Parrinello-Rahman barostat⁹ with a coupling time of 0.5 ps. System sizes and simulation details are identical to those used in the main paper for the TI method. The estimated $\Delta G_{solvation/BB}$ for the Alanine side chain is -4.1 kJ/mol which again is in good agreement with the $\Delta G_{solvation/BB}$ value obtained using the TI method.

4 Intramolecular hydrogen bonding analysis.

The probability distribution of the interatomic distances between the oxygen atom of Ser or Thr side chains and the hydrogen atom of the N-H units (amide groups) are shown in Figure S3 and Figure S4. The interatomic H-O distance in a sidechain-backbone N-H-O hydrogen bond configuration is typically between 0.16 nm and 0.25 nm. In the gas phase, two N-H units participate in hydrogen bonding with the Ser side chain oxygen atom (black and red line in the left panel of Figure S3). In the aqueous phase, intramolecular hydrogen bonding is significantly reduced (black and red line in the right panel of Figure S3). We thus find that in the gas phase, a strong self-solvation (intramolecular hydrogen bonding) of the Ser chain chain occurs while in the aqueous phase self-solvation plays no significant role. For Thr, the side

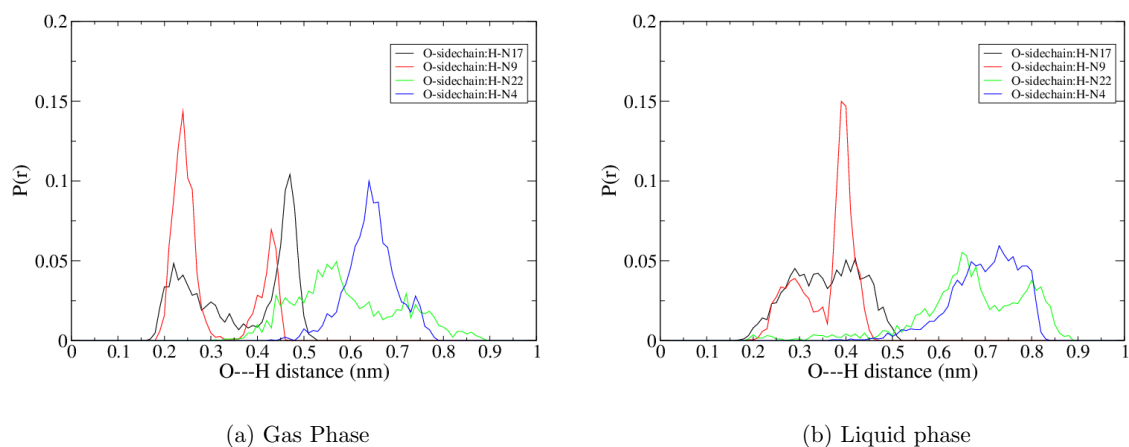


Figure S3: Distance distributions of the oxygen atom in the serine side chain and hydrogen atoms of the H-N units (amide groups) in the tripeptide $\text{CH}_3\text{CO-GLY-SER-GLY-NHCH}_3$. The figure on the left corresponds to the tripeptide in the gas phase; the figure on the right corresponds to the tripeptide in the aqueous phase.

chain oxygen atom has very similar intramolecular hydrogen bonding propensity in, both, the gas phase and the aqueous phase (see Figure S4 black lines). Close inspection shows that self-solvation of the Thr side chain is somewhat weaker in the aqueous phase as compared to the gas phase, but the difference is not as prominent as observed for serine.

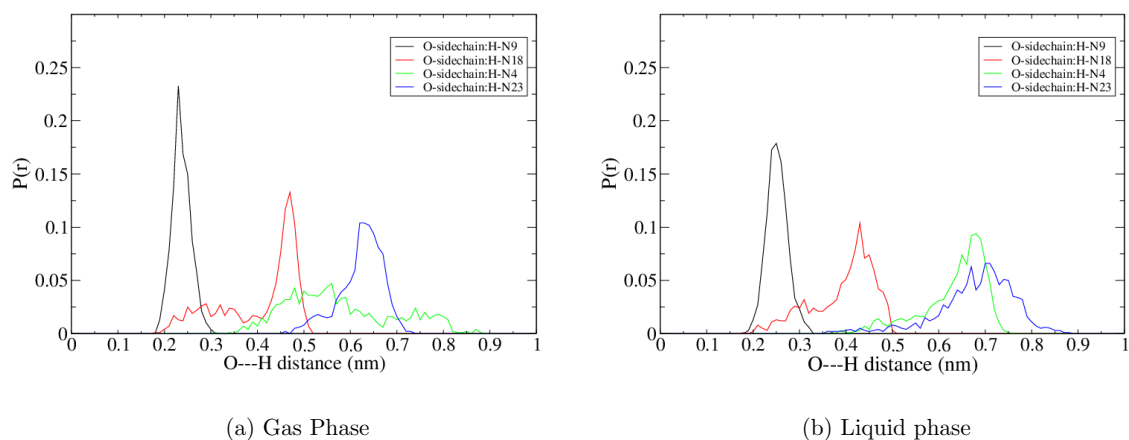


Figure S4: Distances distributions of the oxygen atom in the threonine side chain and hydrogen atoms of the H-N units (amide groups) in the tripeptide $\text{CH}_3\text{CO-GLY-THR-GLY-NHCH}_3$. The figure on the left corresponds to the tripeptide in the gas phase; the figure on the right corresponds to the tripeptide in the aqueous phase.

References

- [1] Lindahl, E.; Hess, B.; van der Spoel, D. GROMACS 3.0: A Package for Molecular Simulation and Trajectory Analysis. *J. Mol. Mod.* **2001**, *7*, 306-317.
- [2] Eisenhaber, F.; Lijnzaad, P.; Argos, P.; Sander, C.; Scharf, M. The Double Cubic Lattice Method: Efficient Approaches to Numerical Integration of Surface Area and Volume and to Dot Surface Contouring of Molecular Assemblies. *J. Comput. Chem.* **1995**, *16*, 273-284.
- [3] Lesser G. J.; Rose, G. D. Hydrophobicity of Amino Acid Subgroups in Proteins. *Protein* **1990**, *8*, 6-13.
- [4] Lee, B.; Richards, F. M. The Interpretation of Protein Structures: Estimation of Static Accessibility. *J. Mol. Biol.* **1971**, *55*, 379-400.
- [5] Schmid, N.; Eichenberger, A. P.; Choutko, A.; Riniker, S.; Winger, M.; Mark, A. E.; van Gunsteren, W. F. Definition and Testing of the GROMOS Force-Field Versions 54A7 and 54B7. *Eur. Biophys. J.* **2011**, *40*, 843-856.

-
- [6] Widom, B. Some Topics in the Theory of Fluids. *J. Chem. Phys.* **1963**, *39*, 2808-2812.
- [7] Bennett, C. H. Efficient Estimation of Free Energy Differences from Monte Carlo Data. *J. Comput. Phys.* **1976**, *22*, 245-268.
- [8] van Gunsteren, W. F.; Berendsen, H. J. C. A Leap-Frog Algorithm for Stochastic Dynamics. *Mol. Sim.* *1988*, *1*, 173-185.
- [9] Parrinello, M.; Rahman, A. Polymorphic Transitions in Single Crystals - a New Molecular-Dynamics Method. *J. Appl. Phys.* **1981**, *52*, 7182-7190.

4 Solvation Thermodynamics of Amino Acid Side Chains on a Short Peptide Backbone

Solvation thermodynamics of amino acid side chains on a short peptide backbone

Timir Hajari and Nico F. A. van der Vegt^{a)}

Eduard-Zintl-Institut für Anorganische und Physikalische Chemie and Center of Smart Interfaces, Technische Universität Darmstadt, Alarich-Weiss-Straße 10, 64287 Darmstadt, Germany

(Received 17 January 2015; accepted 27 March 2015; published online 9 April 2015; publisher error corrected 10 April 2015)

The hydration process of side chain analogue molecules differs from that of the actual amino acid side chains in peptides and proteins owing to the effects of the peptide backbone on the aqueous solvent environment. A recent molecular simulation study has provided evidence that all nonpolar side chains, attached to a short peptide backbone, are considerably less hydrophobic than the free side chain analogue molecules. In contrast to this, the hydrophilicity of the polar side chains is hardly affected by the backbone. To analyze the origin of these observations, we here present a molecular simulation study on temperature dependent solvation free energies of nonpolar and polar side chains attached to a short peptide backbone. The estimated solvation entropies and enthalpies of the various amino acid side chains are compared with existing side chain analogue data. The solvation entropies and enthalpies of the polar side chains are negative, but in absolute magnitude smaller compared with the corresponding analogue data. The observed differences are large; however, owing to a nearly perfect enthalpy-entropy compensation, the solvation free energies of polar side chains remain largely unaffected by the peptide backbone. We find that a similar compensation does not apply to the nonpolar side chains; while the backbone greatly reduces the unfavorable solvation entropies, the solvation enthalpies are either more favorable or only marginally affected. This results in a very small unfavorable free energy cost, or even free energy gain, of solvating the nonpolar side chains in strong contrast to solvation of small hydrophobic or nonpolar molecules in bulk water. The solvation free energies of nonpolar side chains have been furthermore decomposed into a repulsive cavity formation contribution and an attractive dispersion free energy contribution. We find that cavity formation next to the peptide backbone is entropically favored over formation of similar sized nonpolar side chain cavities in bulk water, in agreement with earlier work in the literature on analysis of cavity fluctuations at nonpolar molecular surfaces. The cavity and dispersion interaction contributions correlate quite well with the solvent accessible surface area of the nonpolar side chains attached to the backbone. This correlation however is weak for the overall solvation free energies owing to the fact that the cavity and dispersion free energy contributions are almost exactly cancelling each other. © 2015 AIP Publishing LLC. [<http://dx.doi.org/10.1063/1.4917076>]

I. INTRODUCTION

Hydrophobic effects¹⁻³ play a key role in many biological processes and affect the stability and function of proteins, membranes, and lipid aggregates in aqueous environments. The low solubility of nonpolar solutes in water is commonly known as an important consequence of the hydrophobic effect. The solvation free energy (ΔG_S) of a nonpolar solute in water is large and positive, and weakly temperature dependent. In contrast, the entropy ($T\Delta S_S$) and enthalpy (ΔH_S) changes of solvating nonpolar solutes in water at room temperature are both negative but increase rapidly with increasing temperature.⁴⁻⁸ The stronger temperature dependence of the latter two quantities is owing to a dominant contribution of solvent reorganization, which, despite its significance in understanding heat capacity effects,⁹ does not affect the solvation free energy due to exact enthalpy-entropy compensation.¹⁰⁻¹²

At constant pressure, ΔH_S is local. This means that ΔH_S represents the excess enthalpy of a small subvolume centered on the fixed solute, extending out into the surrounding solvent up to a few solvation shells.^{13,14} This excess can be estimated based on the information about the internal energy of the isolated, non-solvated, solute, the solute-water binding energy, and the solvent-solvent binding energies in the solvation shell of the solute and in the distant bulk. The negative sign of solvation enthalpies ΔH_S of small nonpolar solutes in water results from the remarkable fact that water can host small molecular-sized gaps or cavities without sacrificing its hydrogen bonds. Even though cavity formation contributes a positive solvent reorganization energy,¹⁵⁻¹⁷ this energy cost is overcompensated by weakly attractive solute-solvent dispersion interactions that render the overall enthalpy change negative.

At constant pressure, ΔS_S is also a local property associated with the solvation subvolume mentioned above. The excess is now taken relative to the sum of the internal entropy of the isolated, non-solvated, solute and the entropy per water molecule in the same subvolume after the solute has

^{a)} Author to whom correspondence should be addressed. Electronic mail: vandervegt@csi.tu-darmstadt.de

been removed multiplied with the number of water molecules that were originally there. Given the fact that, in solution, the center of the subvolume is always occupied by the solute, and therefore not available to the solvent, ΔS_S contains an excluded volume, or solute cavity, contribution, which is always negative. This negative contribution to ΔS_S reflects the reduction in accessible solvent configuration space upon creating a molecular-sized cavity that has all solvent molecules in the equilibrium positions and orientations to host the solute.

The solvation enthalpy quantifies the difference between overall system enthalpies before and after solvating the solute and therefore includes the contributions of solute-solvent (SW) interactions (E_{SW}) and changes in solvent-solvent (WW) interactions (ΔH_{WW}), i.e., $\Delta H_S = E_{SW} + \Delta H_{WW}$. As shown by Ben-Naim,¹⁰ Yu and Karplus,¹¹ and others,^{12,18,19} ΔH_{WW} (the solvent reorganization enthalpy) is exactly enthalpy-entropy compensating, i.e., $\Delta S_S = \Delta S_{WW} + S_{SW}$ with $\Delta S_{WW} = \Delta H_{WW}/T$. Based on the use of Gibbs inequalities, Ben-Amotz showed that the “solute-solvent coupling process necessarily produces a decrease in entropy and a release of heat, $TS_{SW} < 0$, out into the solvent degrees of freedom.”²⁰ Part of this heat is absorbed by the solvation shell and contributes to an increase of its entropy $\Delta S_{WW} = \Delta H_{WW}/T$, while the remaining part $T\Delta S_S$ quantifies the net heat exchange with the system surroundings. The solute-solvent entropy $S_{SW} < 0$ quantifies the reduction of configuration space due to repulsive cavity formation. On top of that, introduction of attractive solute-solvent interactions further reduces S_{SW} because attractive interactions bias the solvent configuration space.¹⁸

While the hydration thermodynamics of small nonpolar solutes is dominated by microscopic cavity fluctuations,^{21–25} the hydration of larger nonpolar solutes and extended hydrophobic surfaces is enthalpically dominated above a characteristic length scale (radii $R \geq 1.0$ nm) where the three-dimensional hydrogen bonded network structure of water is perturbed by the introduction of an interface which is incapable of participating in hydrogen bonding.^{25–27} For the nonpolar peptide side chain solvation processes studied in this work, the nonpolar solute radii are all smaller than 1.0 nm.

To characterize hydrophobic effects in processes such as protein folding or protein-protein association, information on the hydrophobicity of small nonpolar molecules (either side chain analogues or amino acids)^{28,29} has frequently been used. The nonpolar and polar amino acid side chains of proteins are however attached to a peptide backbone, which affects the local water structure and, in turn, affects the hydrophobicity/hydrophilicity of the side chains. This effect of the backbone on the solvation free energy of the side chain is accounted for in the conditional solvation process that corresponds to a gas-to-liquid transfer process where an amino acid side chain is solvated next to an already solvated peptide backbone³⁰ and has been discussed in several simulation studies.^{31–35} A recent computer simulation study reported by us³⁵ showed that the conditional solvation of nonpolar amino acid side chains attached to a short peptide backbone is significantly more favorable than unconditional solvation of nonpolar analogue molecules in bulk water. In contrast to this result, it was furthermore found that this backbone has minor effect on the solvation of the polar amino acid side chains.³⁵

To analyze the origin of our previous observations, we here present a molecular simulation study on temperature dependent conditional solvation free energies of nonpolar and polar side chains. We report the conditional solvation enthalpies $\Delta H_{S/BB}$ and entropies $\Delta S_{S/BB}$ (where $/BB$ denotes the condition of the backbone) of the nonpolar and polar side chains together with an analysis in terms of the solute-solvent and solvent-solvent contributions. We further report a cavity ($\Delta G_{C/BB}$) and dispersion attraction ($\Delta G_{D/BB}$) free energy decomposition of the conditional solvation free energies of the nonpolar side chains which provides further insight in the role of cavity fluctuations and dispersion interactions.

The thermodynamically unfavorable process of cavity formation frequently dominates over favorable dispersion interactions in nonpolar solvation in water and water/cosolvent mixtures.^{21,36–38} Garde and coworkers characterized cavity fluctuations close to hydrophobic and hydrophilic surfaces,³⁹ however, it is not well characterized how a short peptide backbone influences the two free energy contributions $\Delta G_{C/BB}$ and $\Delta G_{D/BB}$ in the conditional solvation of nonpolar amino acid side chains. It is moreover frequently assumed that ΔG_C is a linear function of surface area or molecular volume.²⁵ However, a recent study has shown that ΔG_C , ΔG_D , and ΔG_S are complex functions of volume and area and are strongly context dependent.⁴⁰ The dependence of $\Delta G_{C/BB}$ and $\Delta G_{D/BB}$ of different nonpolar side chains on the solvent accessible surface area (SASA)^{41,42} is therefore also studied in this work.

In this work, tripeptides, $\text{CH}_3\text{CO-GLY-X-GLY-NHCH}_3$ are considered to mimic the peptide backbone, where X represents different polar and nonpolar amino acid residues. For each uncharged amino acid, the conditional solvation free energy ($\Delta G_{S/BB}$) is computed at six different temperatures ranging from 278 K to 338 K. $\Delta S_{S/BB}$ and $\Delta H_{S/BB}$ are obtained by fitting the temperature dependence of $\Delta G_{S/BB}$ which further provides information on hydration heat capacity effects. The solvation enthalpies and entropies are further decomposed into their respective solvent-solute and solvent-solvent contributions.

II. COMPUTATIONAL DETAILS

A. Computation of thermodynamic data

Assuming that the heat capacity change in hydrating the amino acid side chains next to a peptide backbone is constant in the temperature range 278 K–338 K,⁴³ we can write the temperature dependency of the condition solvation free energy in the following way:

$$\Delta G_{S/BB} = a + bT + cT \ln(T). \quad (1)$$

The $\Delta G_{S/BB}$ values are estimated for polar and nonpolar side chains at six different temperatures (278 K, 288 K, 308 K, 318 K, 328 K, and 338 K) using the thermodynamic integration (TI) method⁴⁴ discussed in Sec. II B. The conditional hydration free energies—calculated at the above temperatures for each side chain—are fitted to Eq. (1) to obtain the corresponding a , b , and c -values. The solvation entropy ($\Delta S_{S/BB}$) is next computed using Eq. (2). The solvation enthalpy ($\Delta H_{S/BB}$) is

obtained from Eq. (3),

$$\Delta S_{S/BB} = -\left(\frac{\partial \Delta G_{S/BB}}{\partial T}\right)_P = -b - c[1 + \ln(T)], \quad (2)$$

$$\Delta H_{S/BB} = \Delta G_{S/BB} + T\Delta S_{S/BB}. \quad (3)$$

Additional simulation trajectories of 40 to 50 ns have been accumulated at 298 K for all CH₃CO–GLY–X–GLY–NHCH₃ tripeptides in order to compute the side chain-solvent interaction energy $E_{SW/BB}$ of residue X. This quantity includes the short range part of the Coulomb interaction and the van der Waals interaction between water and the side chain. The conditional (solvent-solvent) reorganization enthalpy ($\Delta H_{WW/BB}$) is obtained by applying

$$\Delta H_{S/BB} = E_{SW/BB} + \Delta H_{WW/BB}. \quad (4)$$

B. Simulation details of conditional solvation free energy calculations

The simulation procedure used to compute the conditional solvation free energy of different polar and nonpolar side chains is discussed in detail in our previous work.³⁵ The same procedure is followed in the present work to compute the $\Delta G_{S/BB}$ values at six different temperatures, ranging between 278 K and 338 K.

The conditional solvation free energy ($\Delta G_{S/BB}$) is defined as

$$\Delta G_{S/BB} = \Delta G_S^{Peptide} - \Delta G_S^{Backbone} \quad (5)$$

and is obtained using the thermodynamic cycle shown in Figure 1. Using this cycle, $\Delta G_{S/BB}$ is written in terms of two alchemical transformations (ΔG_{gas} and ΔG_{soln}),

$$\Delta G_{S/BB} = \Delta G_S^{Peptide} - \Delta G_S^{Backbone} = \Delta G_{gas} - \Delta G_{soln}, \quad (6)$$

where ΔG_{gas} corresponds to a free energy change for decoupling the nonbonded interactions between the side chain and rest of the system in vacuum, and similarly, ΔG_{soln} is the free

energy change due to decoupling the nonbonded interactions between side chain and the rest of the system in water. ΔG_{soln} and ΔG_{gas} are computed using the TI method,⁴⁴

$$\Delta G_{soln/gas} = \int_0^1 \left\langle \frac{\partial U_{sc}(\lambda)}{\partial \lambda} \right\rangle_\lambda d\lambda. \quad (7)$$

A soft-core potential⁴⁵ U_{sc} is used for both the van der Waals and electrostatic interactions,

$$U_{sc}(r, \lambda) = (1 - \lambda)U([\alpha\sigma^6\lambda^p + r^6]^{1/6}), \quad (8)$$

with soft-core parameters $\alpha = 0.5$, $p = 1$, and $\sigma = 0.3$ nm to avoid singularities at the end state.

All simulations were performed using the GROMACS software package (versions 4.6.2 and 4.5.1).⁴⁶ The GROMOS 54a7 (Ref. 47) force field for amino acids and the simple point charge (SPC) water model⁴⁸ were chosen for all the simulations. Using the SETTLE algorithm,⁴⁹ the bonds and angle in water were kept rigid. All covalent bonds of the tripeptides were constrained using the LINCS algorithm.⁵⁰ For each tripeptide, the C-terminal was capped with CH₃-NH and the N-terminal was capped with COCH₃. The Lennard-Jones (LJ) nonbonded interactions were evaluated in the gas phase and liquid phase simulations using a cutoff distance of 1.4 nm. The electrostatic interactions were evaluated both in the gas phase and liquid phase using the particle mesh Ewald method⁵¹ with a real space cutoff 1.4 nm and a grid-spacing 0.12 nm. The time step is always 0.002 ps.

1. Simulations in liquid phase

Periodic boxes of size ~4 nm with ~2160 water molecules and one tripeptide were used. In total, 26-31 λ points were chosen to perform the thermodynamic integration. For both the nonpolar and polar side chains, the λ -spacing ($\Delta\lambda$) equals 0.04. Additionally, we considered 5 λ points for polar side chains when λ ranges from 0 to 0.004. A leap-frog stochastic

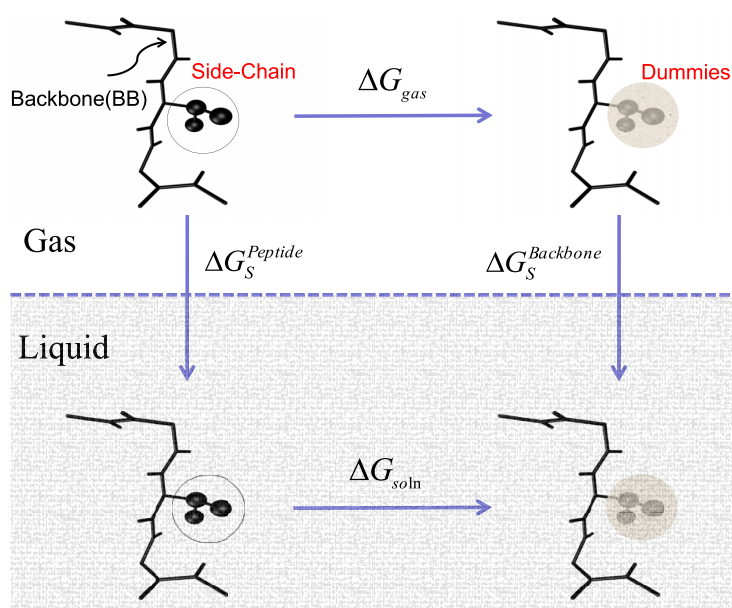


FIG. 1. Thermodynamic cycle to compute the conditional solvation free energies of different side chains. The free energy change due to the transformation of all the side chain atoms into non-interacting dummies in vacuum (upper horizontal arrow) is denoted as ΔG_{gas} ; the same transformation in water (lower horizontal arrow) is denoted as ΔG_{soln} . Using these two free energy changes, the conditional solvation free energy of each side chain is estimated $\Delta G_{S/BB} = \Delta G_{gas} - \Delta G_{soln}$.

dynamics integrator⁵² with an inverse friction constant of 0.1 ps was used to maintain the desired temperature. At each temperature and λ point, the system was equilibrated for 1 ns at 1 bar pressure using the Berendsen barostat⁵³ with a coupling time of 0.5 ps, and afterward, 4.5 ns of production runs were performed using the Parrinello-Rahman barostat⁵⁴ with a coupling time of 0.5 ps to obtain the $\langle \frac{dU(\lambda)}{d\lambda} \rangle_\lambda$.

For the nonpolar side chains, the TI method (Eq. (7)) has further been used to calculate cavity and dispersion free energy contributions to $\Delta G_{S/BB}$. To this end, the attractive r^{-6} and repulsive r^{-12} parts of the side chain-water LJ interactions were removed in two subsequent steps, each using 26 λ points with a λ -spacing of 0.04. The calculations were performed at 298 K using the leap-frog stochastic dynamics integrator with an inverse friction constant of 0.1 ps and 1 ns equilibration runs and 4 ns production runs at each λ point (using the same pressure coupling schemes as above). These calculations provide the free energy cost of creating a soft repulsive van der Waals cavity near the backbone as well as the free energy gain of introducing the attractive side chain-solvent van der Waals interactions for each nonpolar side chain. These calculations were also performed for the free side chains (without backbone) in bulk water.

2. Simulations in gas phase

NVT simulations with 51 equidistant λ points were considered to compute ΔG_{gas} at each temperature. The simulation box size was 4.0 nm. As the peptides are conformationally very flexible in the absence of water, at each λ point, 40 ns–50 ns molecular dynamics simulations were performed for data collection. A leap-frog stochastic dynamics integrator with an inverse friction constant of 0.1 ps was used.

Error bars on ΔG_{gas} and ΔG_{soln} were determined with block averaging. The trajectories at every λ point were split into five individual blocks ($N_b = 5$) and the error, $\delta\Delta G_{soln/gas}$, was estimated using

$$\delta\Delta G_{soln/gas} = \sqrt{\frac{\sum_{i=1}^{N_b} (\Delta G_i - \Delta \bar{G})^2}{N_b(N_b - 1)}}, \quad (9)$$

where ΔG_i is the free energy of the i th block and $\Delta \bar{G}$ is the average over all blocks. The total error in $\Delta G_{S/BB}$ (Eq. (6)) at each temperature was obtained by adding the individual errors in ΔG_{gas} and ΔG_{soln} .

III. RESULTS AND DISCUSSION

A. Solvation entropy and enthalpy

The temperature dependencies of $\Delta G_{S/BB}$ are shown in Figs. 2 and 3, where black circles denote the data obtained with the TI method and the red lines are the fitted lines using the functional form in Eq. (1). Equations (1)–(3) were subsequently used to obtain the conditional solvation free energies ($\Delta G_{S/BB}$), conditional solvation enthalpies ($\Delta H_{S/BB}$), and conditional solvation entropies ($T\Delta S_{S/BB}$) at 298 K. These data, obtained for different polar and nonpolar uncharged amino acid side chains at 298 K, are summarized in Table I and shown in Figure 4. We note that these data do not depend on the chosen functional form (Eq. (1)). By fitting the solvation free energies to a quadratic equation ($\Delta G_{S/BB} = a + bT + cT^2$), the derived entropies, $T\Delta S_{S/BB}$, and enthalpies, $\Delta H_{S/BB}$, were found to differ less than 0.2 kJ/mol from the data obtained using Eq. (1). In order to obtain an independent error estimate, we calculated $\Delta H_{S/BB}$ for two side chains (Ile and Cys) with an alternative method that uses the total potential energies E of the system at the two end states ($\lambda = 0$ and $\lambda = 1$), i.e., $\Delta H_{S/BB} = [\langle E^{gas} \rangle_{\lambda=1} - \langle E^{gas} \rangle_{\lambda=0}] - [\langle E^{soln} \rangle_{\lambda=1} - \langle E^{soln} \rangle_{\lambda=0}]$. To sample the averages $\langle \dots \rangle_\lambda$ at the two end points, 200 ns simulation trajectories of the liquid phase and 400 ns trajectories of the gas phase were used. The estimated solvation enthalpies $\Delta H_{S/BB}$ are -12.7 ± 2.2 kJ/mol and -16.5 ± 1.9 kJ/mol for Ile and Cys, respectively, in good agreement with the data presented in Table I.

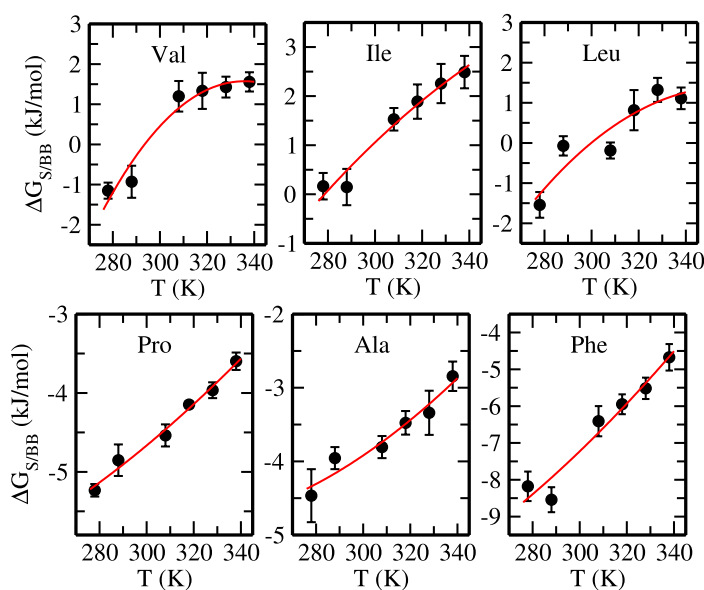


FIG. 2. The temperature dependencies of the conditional solvation free energies ($\Delta G_{S/BB}$) of nonpolar amino acid side chains.

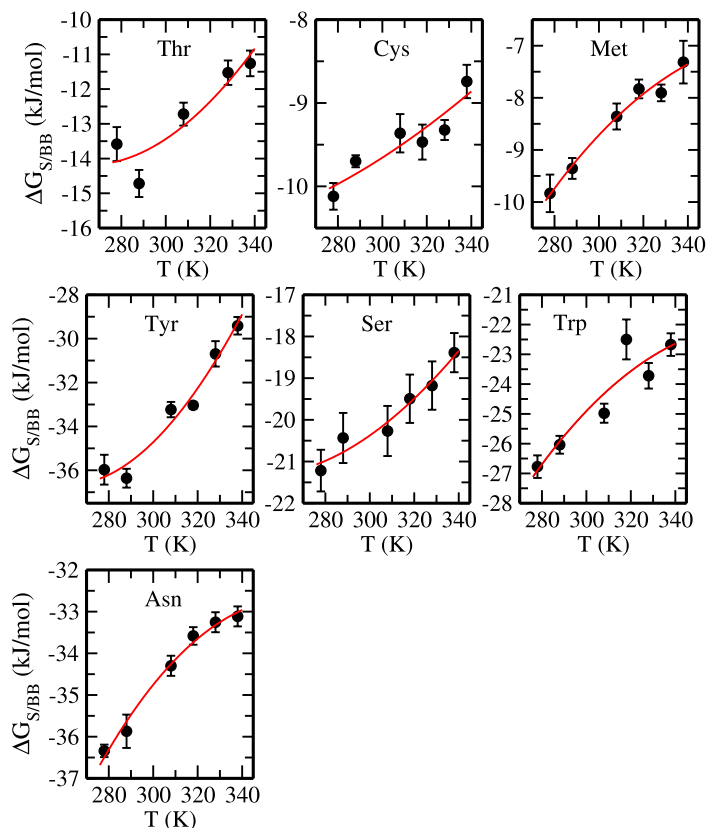


FIG. 3. The temperature dependencies of the conditional solvation free energies ($\Delta G_{S/BB}$) of polar amino acid side chains.

1. Nonpolar side chains

For the nonpolar side chains Val, Ile, and Leu, the favorable, conditional solvation enthalpies are almost exactly compensated by the unfavorable, conditional solvation entropies. As a result, near-zero values for $\Delta G_{S/BB}$ are found for these side chains. For the side chains of Leu, Ala, Pro,

and Phe, $|\Delta H_{S/BB}| > |T\Delta S_{S/BB}|$, i.e., for these side chains the solvation process is enthalpic. As a consequence of that, the conditional solvation free energies for these four side chains are negative, i.e., the hydration process of these nonpolar side chains is favorable. For small nonpolar molecules at room temperature, the solvation entropy generally dominates over solvation enthalpy, i.e., $|T\Delta S_S| > |\Delta H_S|$. The peptide backbone

TABLE I. Conditional solvation free energies ($\Delta G_{S/BB}$) obtained using Eq. (1), conditional solvation enthalpies ($\Delta H_{S/BB}$) obtained using Eq. (3), conditional solvation entropies ($T\Delta S_{S/BB}$) obtained using Eq. (2), side chain-water interaction energies ($E_{SW/BB}$), solvent reorganization enthalpies ($\Delta H_{WW/BB}$), and side chain-water interaction entropies $TS_{SW/BB}$ for the different amino acid side chains. The data are presented in units kJ/mol and the system temperature is 298 K. The enthalpies and entropies are listed with one or two significant figures (see discussion in Sec. III A).

Side chain	$\Delta G_{S/BB}$	$\Delta H_{S/BB}$	$T\Delta S_{S/BB}$	$E_{SW/BB}$	$\Delta H_{WW/BB}$	$TS_{SW/BB}$
Val	0.3	-20	-20	-21.6 ± 0.1	2	-22
Ile	1.0	-13	-14	-28.4 ± 0.1	15	-29
Leu	-0.2	-15	-15	-29.0 ± 0.1	14	-29
Ala	-3.9	-10	-6	-9.1 ± 0.02	-1	-5
Pro	-4.7	-12	-7	-21.0 ± 0.02	9	-16
Phe	-7.3	-25	-18	-54.0 ± 0.7	29	-47
Met	-8.8	-23	-14	-55.7 ± 1.7	33	-47
Cys	-9.7	-15	-5	-36.2 ± 0.2	21	-26
Thr	-13.4	-25	-12	-61.4 ± 0.7	36	-48
Trp	-25.0	-49	-24	-98.1 ± 1.4	49	-73
Ser	-20.4	-31	-11	-67.0 ± 0.7	36	-47
Tyr	-34.9	-63	-28	-110.7 ± 0.4	48	-76
Asn	-34.8	-55	-20	-115.7 ± 0.4	61	-81

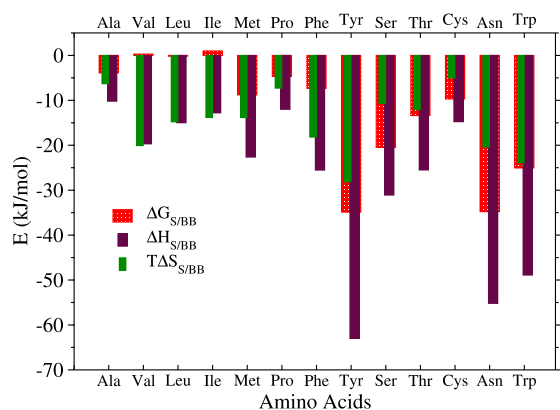


FIG. 4. The conditional solvation free energies ($\Delta G_{S/BB}$), conditional solvation enthalpies ($\Delta H_{S/BB}$), and conditional solvation entropies ($T\Delta S_{S/BB}$) for polar and nonpolar amino acid side chains at 298 K.

therefore alters the entropy-enthalpy balance for the nonpolar side chain hydration process.

It is interesting to compare the conditional solvation entropies $\Delta S_{S/BB}$ of the different side chains with the corresponding analogue solvation entropies ΔS_S taken from experimental and simulation work. The black bars in Figure 5(b) correspond to the solvation entropy data for amino acid side chain analogue molecules taken from experimental work of Makhatadze and Privalov.⁵⁵ Solvation entropy data for side chain analogue molecules obtained from computer simulations reported by Hess and van der Vegt¹⁶ are represented using red bars in Figure 5(b). Hess and van der Vegt calculated the solvation entropies with several different empirical force field models, and for better comparison, we have taken only the data obtained with the GROMOS 53A6 force field for the analogues along with the SPC water model. The conditional solvation entropies are shown with green bars in the same figure. For all nonpolar and polar side chains, the conditional solvation entropies are less negative compared with the respective analogue solvation entropies. Hence, the peptide backbone has a strong impact on the side chain solvation entropies. The conditional solvation enthalpies, presented in Figure 5(a), are instead more negative for the Ala, Val, Leu, and Pro side chains while being (slightly) less negative for the Ile, Met, and Phe side chains. It is clear from Figures 5(a) and 5(b) that the solvation entropies of nonpolar groups are to a greater extent influenced by the backbone than the solvation enthalpies and because of that the overall conditional solvation free energies of the nonpolar side chains become significantly less unfavorable compared with unconditional hydrophobic solvation, attaining near-zero or even negative values.

2. Polar side chains

From the data in Table I and Figure 4, it can be observed that $\Delta H_{S/BB}$ dominates over $T\Delta S_{S/BB}$ for the polar side chains Asn, Tyr, Ser, Trp, and Thr. The most negative value of $\Delta H_{S/BB}$ is obtained for the side chain of Tyr resulting from hydrating the hydroxyl group and the phenyl ring. From Figure 5(b), it is evident that the conditional solvation entropies of polar

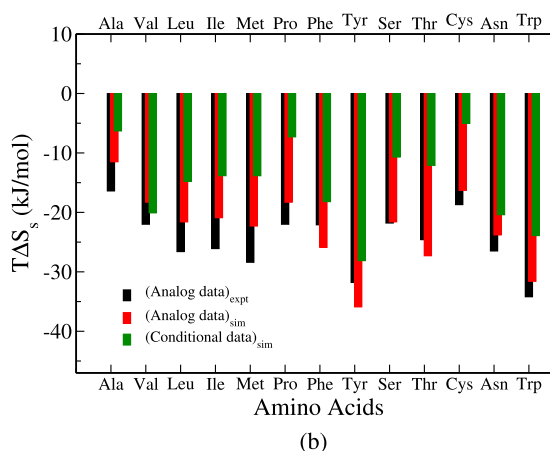
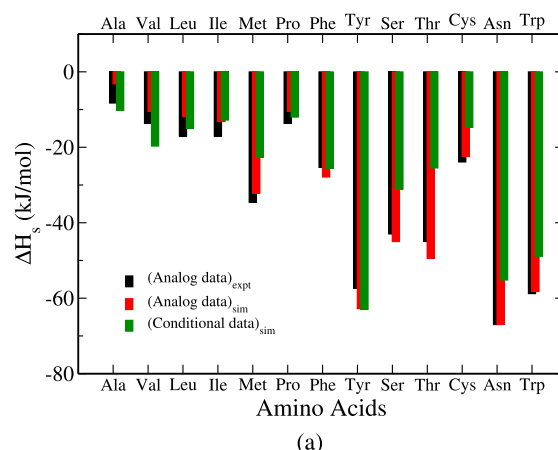


FIG. 5. The solvation enthalpy and entropy data for amino acid analogue molecules (black bars) taken from experimental work of Makhatadze and Privalov;⁵⁵ solvation enthalpy and entropy data for amino acid analogue molecules (red bars) taken from the computer simulation work reported by Hess and van der Vegt¹⁶ using the GROMOS 53A6 force field for amino acid analogues along with the SPC water model; and the conditional solvation enthalpies ($\Delta H_{S/BB}$) and entropies ($T\Delta S_{S/BB}$) for different polar, nonpolar, uncharged amino acid side chains (green bars) estimated in this work. System temperatures are 298 K for all three cases.

side chains are less negative than the analogue solvation entropies. Except for Tyr, the conditional solvation enthalpies for polar side chains are also less negative in comparison with the analogue solvation enthalpies (Figure 5(a)). The enthalpy differences obtained upon subtracting $\Delta H_{S/BB}$ and ΔH_S values for the polar side chains almost perfectly compensate the corresponding entropy differences (except for Tyr). Because of this compensation effect, the conditional solvation free energies of polar side chains do not differ significantly from the corresponding unconditional solvation free energies (ΔG_S), in contrast to the nonpolar side chains whose solvation free energies are strongly affected by the peptide backbone. The detailed comparison between ΔG_S and $\Delta G_{S/BB}$ of the different polar and nonpolar side chains is reported in our previous work.³⁵

$\Delta H_{S/BB}$ of the Tyr side chain is almost unaffected compared with ΔH_S . In contrast to this, a significant difference between $\Delta S_{S/BB}$ and ΔS_S is found. This causes $\Delta G_{S/BB}$ of

the Tyr side group to be more negative than the solvation free energy of its free side chain.³⁵ This observation may be related to the fact that the backbone screens the (mildly) hydrophobic phenyl ring. We note that König *et al.*^{32,33} have reported simulations, which, with a different backbone and a different force field model, show that the backbone has a strong nonadditive effect on the solvation of the polar serine (Ser) side chain due to self-solvation.

B. Hydration heat capacity

The hydration heat capacity is defined as $\Delta c_P = -T(\partial^2 \Delta G_S / \partial T^2)_P$. Makhatadze and Privalov reported positive hydration heat capacities for all (nonpolar, polar, charged) amino acid side chain analogues and also showed that hydration heat capacities of polar and charged groups (e.g., $-\text{OH}$, $-\text{NH}_3^+$) are negative at room temperature while those of nonpolar groups are large and positive.⁵⁶ The curvature in the temperature dependence of $\Delta G_{S/BB}$ in Figs. 2 and 3 determines the conditional heat capacity of hydration $\Delta c_{P/BB}$. Although the data are not sufficiently accurate to provide quantitative information on this quantity, some interesting effects are visible. For example, the data in Fig. 2 indicate that $\Delta c_{P/BB}$ changes sign for the nonpolar side chains Ala, Pro, and Phe, becoming negative in contrast to positive experimental values reported for the corresponding analogue molecules. Tyr and Ser (Fig. 3) also have negative $\Delta c_{P/BB}$, again in contrast with positive values reported for the analogues. Although we have not further studied heat capacity effects here, further work on the nature of the observed effects is warranted.

C. Solute-solvent and solvent-solvent contributions

The solute-solvent and solvent-solvent energy contributions $E_{SW/BB}$ and $\Delta H_{WW/BB}$ to the conditional solvation enthalpies are presented in Table I (columns 5 and 6). For both polar and nonpolar amino acid side chains, solute-solvent interactions provide the dominant contribution to conditional solvation enthalpies. Nevertheless, the solvent-solvent reorganization enthalpy is not negligible, except for Ala and Val whose small side chain sizes may render the reorganization enthalpies negligible. The unfavorable solvation entropy $\Delta S_{S/BB}$ of the nonpolar groups arises from the solute-solvent entropy term (column 7 in Table I), while the solvent reorganization contribution is positive but generally has a smaller magnitude. Similar observations were made by Gallicchio *et al.*¹⁵ Hence, hydrophobic solvation entropies and enthalpies are dominated by the solute-solvent contributions. We compared our data for $E_{SW/BB}$, $TS_{SW/BB}$, and $\Delta H_{WW/BB}$ with those of Gallicchio *et al.* who reported the solvation of alkane molecules in water.¹⁵ The comparison shows that next to the peptide backbone the (negative) solute-solvent and (positive) solvent-solvent energy components are reduced, i.e., $|E_{SW/BB}| < |E_{SW}|$ and $\Delta H_{WW/BB} < \Delta H_{WW}$. The comparison further shows that next to the peptide backbone the solute-solvent entropy component increases, i.e., becomes less negative. This means that the entropic cost of cavity formation close to the backbone is reduced over the entropic cost of cavity formation in bulk.

The hydration process of the polar side chains is enthalpic, i.e., $|\Delta H_{S/BB}| > T|\Delta S_{S/BB}|$. Due to strong electrostatic interactions between polar side chains and water, $E_{SW/BB}$ values are large and negative. The contributions from $\Delta H_{WW/BB}$ are instead positive and also large, nevertheless the overall $\Delta H_{S/BB}$ is highly negative. As mentioned already, the overall $T\Delta S_{S/BB}$ values of polar groups are less negative compared with the analogue data and are in fact comparable with the $T\Delta S_{S/BB}$ values of the nonpolar side chains. The reason is that polar hydration produces two large, partially canceling, entropic contributions: a negative side chain-water entropy $TS_{SW/BB}$ and a positive water reorganization entropy $T\Delta S_{WW/BB}$. Similar cancellation has been reported for ionic and polar hydration where a negative solute-solvent interaction entropy and a positive water reorganization entropy almost perfectly cancel each other.²⁰

D. Cavity and dispersion contributions in hydrophobic solvation

Hydration of nonpolar solutes can be thought of as a two-step process. At first, a repulsive cavity is to form in water. In the second step, the dispersion interactions are introduced in this already existing repulsive cavity. The details of this calculation are described in Sec. II B. In general, the free energy contribution to form a molecular-sized cavity is highly unfavorable in water and dominates over the attractive dispersion contribution. To examine how the peptide backbone influences these two free energy contributions in the solvation of nonpolar solutes, the cavity and dispersion decompositions are performed for alkane side chains in the presence of the tripeptide backbone and also in the absence of the backbone. The resulting cavity and dispersion contributions to the free energy are presented in Table II for the alkane side chains of amino acid residues Ala, Ile, Leu, Pro, and Val. Since the GROMOS 54a7 force field uses a united atom description of the CH_3 , CH_2 , and CH moieties in these side chains, these solvation free energies do not contain contributions from electrostatic interactions with the solvent. Therefore, the total solvation free energy of each of these side chains is the sum of the cavity and the dispersion free energy contributions.

The cavity free energies, ΔG_C , are all positive and overcompensate the favorable (negative) ΔG_D values. The conditional cavity free energies, $\Delta G_{C/BB}$, are also all positive but are overcompensated by stronger negative $\Delta G_{D/BB}$ values. It can further be seen that $\Delta G_{C/BB} < \Delta G_C$. Thus, cavity formation close to the backbone is more favorable than in

TABLE II. Conditional and unconditional van der Waals cavity and dispersion free energies of the nonpolar side chains at 298 K. Units are in kJ/mol. Errors were estimated using Eq. (9).

Side chain	ΔG_C	$\Delta G_{C/BB}$	ΔG_D	$\Delta G_{D/BB}$
Val	59.1 ± 0.1	36.4 ± 0.2	-44.6 ± 0.05	-37.0 ± 0.05
Ile	67.8 ± 0.2	44.1 ± 0.2	-53.9 ± 0.1	-45.3 ± 0.8
Leu	66.8 ± 0.6	43.3 ± 0.3	-54.0 ± 0.1	-44.4 ± 0.1
Ala	34.6 ± 0.05	14.2 ± 0.1	-23.7 ± 0.02	-17.2 ± 0.03
Pro	56.9 ± 0.2	28.5 ± 0.1	-43.5 ± 0.03	-34.1 ± 0.04

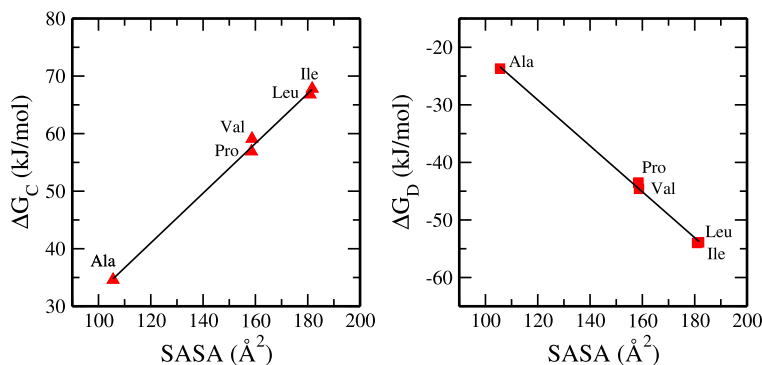


FIG. 6. Correlation between the free energy contribution ΔG_C and the side chain SASA (left) and the correlation between the free energy contribution ΔG_D and the side chain SASA (right). The statistical error bars (see Table II) are smaller than the symbol size.

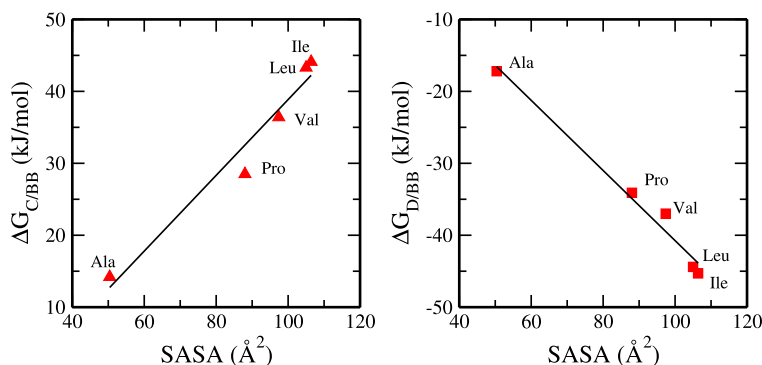


FIG. 7. Correlation between the free energy contribution $\Delta G_{C/BB}$ and the side chain SASA (left) and the correlation between the free energy contribution $\Delta G_{D/BB}$ and the side chain SASA (right). The statistical error bars (see Table II) are smaller than the symbol size.

bulk water. The differences ($\Delta G_C - \Delta G_{C/BB}$) are big and vary between 20 kJ/mol and 28 kJ/mol. The dispersion interaction contributions, $\Delta G_{D/BB}$, are less negative than their unconditional values ΔG_D . Here, the differences ($\Delta G_D - \Delta G_{D/BB}$) vary between 6 kJ/mol and 10 kJ/mol. Thus, the greater ease of nonpolar cavity formation next to the peptide backbone renders nonpolar side chains less hydrophobic than the corresponding free alkane molecules in bulk water. This observation is in agreement with work reported by Garde and co-workers³⁹ who showed that cavity formation is more favorable next to an unfolded protein compared to cavity formation in bulk water.

Figure 6 shows the correlation of ΔG_C and ΔG_D with the SASA of the nonpolar side chain analogues. The SASA values were obtained from 4 ns simulation runs using the Gromacs analysis tool.^{42,46} An almost perfect linear correlation is observed, in agreement with other simulation and experimental studies using alkane molecules.^{15,21} While ΔG_C is positive and increases linearly with SASA, ΔG_D is negative and decreases linearly with SASA. Figure 7 shows the same correlation but now for $\Delta G_{C/BB}$ and $\Delta G_{D/BB}$ presented versus the SASA value of the corresponding side chain obtained from 4 ns simulation runs of the tripeptide. Because the favorable $\Delta G_{D/BB}$ contribution almost perfectly cancels the unfavorable $\Delta G_{C/BB}$ contribution, the overall solvation free energies, $\Delta G_{S/BB}$, are very small (see Table I) irrespective of the side chain SASA values. Resultingly, the $\Delta G_{S/BB}$ values correlate only weakly with SASA. Linear relationships between SASA and hydration free energies of nonpolar groups are frequently assumed to be valid, furthermore assuming a positive slope (positive surface tension γ). For the systems

investigated here, these assumptions are invalid. Related to this observation, recent work by Harris and Pettitt⁴⁰ showed that depending on the geometry and chemistry, the hydrophobic solvation free energy can be negative in agreement with the data presented here. These authors in fact found a negative γ in the correlation between ΔG_S and SASA for extended and denatured configurations of decaalanine. They also concluded that none of the ΔG_C , ΔG_D , and the overall ΔG_S data for nonpolar groups are simple linear function of SASA or molecular volume.

IV. CONCLUSIONS

Thermodynamic solvation properties of small molecules or amino side chain analogues are often used to quantify driving forces in biological processes like protein folding or protein-protein association. This procedure is however approximate and sometimes even qualitatively wrong owing to the nonadditive nature of the solvation free energies and effects of the backbone on the solvation of the side chains.^{31–34} In a recent study, we showed that the presence of a short peptide backbone decreases the hydrophobicity of nonpolar amino acid side chains in comparison with the hydrophobicity of the free side chain analogues.³⁵ It could furthermore be shown that the effect of the backbone on the hydrophilicity of polar amino acid side chains is significantly less pronounced. The present work provides a rationalization of these observations in terms of solvation enthalpies and entropies.

It is found that the hydration process of nonpolar and polar side chains is enthalpic for all side chains except Val and Ile. This result is in strong contrast with the generally accepted

view that hydration of nonpolar side chains is dominated by the entropy. For the nonpolar side chains, an almost perfect enthalpy-entropy compensation is observed which results in near-zero values of the solvation free energy and even small negative values implying favorable side chain solvation. For the polar side chains, solvation free energies depend very little on whether the hydration process of the side chains occurs in the presence or absence of the short peptide backbone. The backbone however strongly affects the solvation enthalpies and entropies of the polar side chains, but these effects almost perfectly cancel out in the solvation free energies. Tyrosine is however an exception; the peptide backbone has no significant effect on the solvation enthalpy, while the unfavorable solvation entropy is reduced. A plausible explanation is that the backbone screens the mildly hydrophobic phenyl ring from unfavorable entropic interactions with water while solvation of the aromatic hydroxyl group remains unaffected due to the relatively large distance that separates it from the backbone. As a result, the backbone acts to significantly increase the hydrophilicity of Tyr relative to the free side chain.

Solvation of all side chains is entropically unfavorable. The backbone however reduces this entropic cost relative to solvation of the free side chain analogues in bulk water. For the nonpolar side chains, this effect results in a remarkable reduction of their hydrophobicity compared to free analogue solvation. By decomposing the nonpolar solvation free energy into repulsive van der Waals cavity and attractive dispersion interaction contributions, it is found that side chain sized cavity formation near the peptide backbone is favored over side chain sized cavity formation in the distant bulk (cavity formation of the free side chain). The reduced hydrophobicity of nonpolar side chains hence results from a smaller cavity formation contribution in the solvation entropies of these side chains. This picture is supported by an analysis of the solvation free energies in terms of the solute-solvent entropy and solute-solvent energy. The solute-solvent entropy characterizes the entropy cost of cavity formation and is found to be much smaller close to the backbone compared with bulk. Hence, cavity fluctuations are enhanced close to the peptide backbone in agreement with work reported by Garde and coworkers who reported enhanced water density fluctuations near hydrophobic surfaces.⁵⁷

The repulsive van der Waals cavity and attractive dispersion interaction contributions to the nonpolar solvation free energies are both found to scale linearly with the SASA. We however also find that the nonpolar side chain solvation free energies do not correlate well with SASA, hence challenging the validity of some simple hydrophobic solvation models. Aspects of these are discussed in more detail in a recent paper by Harris and Pettitt.⁴⁰

Finally, the present work provides some interesting insights in the solvation entropy of nonpolar and polar side chains. For both nonpolar and polar side chains, the entropy has a negative sign. Our analysis in terms of solute-solvent and solvent-solvent contributions shows that the solvation entropy of the nonpolar side chains is dominated by cavity fluctuations described by the solute-solvent contribution. The solvent-solvent entropy contribution in nonpolar solvation is small but of opposite sign and partly cancels the negative solute-

solvent entropy. For the polar side chains, the solute-solvent and solvent-solvent contributions to the entropy are of opposite sign too, but are both bigger. Hence, these contributions also partially cancel and result in net entropies of equal magnitude as the nonpolar solvation entropies.

ACKNOWLEDGMENTS

This research has been carried out as part of the priority program SPP 1569 by the German Science Foundation. We are grateful to the high-performance computing center of the Technische Universität Darmstadt for allocating computer time. We thank Kaustubh Rane for several useful discussions.

¹W. Kauzmann, *Adv. Protein Chem.* **14**, 1 (1959).

²C. Tanford, *Science* **200**, 1012 (1978).

³K. A. Dill, *Biochemistry* **29**, 7133 (1990).

⁴R. L. Baldwin, *Proc. Natl. Acad. Sci. U.S.A.* **83**, 8069 (1986).

⁵D. Paschek, *J. Chem. Phys.* **120**, 6674 (2004).

⁶F. Sedlmeier, D. Horinek, and R. R. Netz, *J. Chem. Phys.* **134**, 055105 (2011).

⁷B. Lee, *Biophys. Chem.* **51**, 271 (1994).

⁸N. T. Southall, K. A. Dill, and A. D. J. Haymet, *J. Phys. Chem. B* **106**, 521 (2002).

⁹B. Madam and K. Sharp, *J. Phys. Chem. B* **101**, 11237 (1997).

¹⁰A. Ben-Naim, *Biopolymers* **14**, 1337 (1975).

¹¹H. A. Yu and M. Karplus, *J. Chem. Phys.* **89**, 2366 (1988).

¹²B. Guillot and Y. Guissani, *J. Chem. Phys.* **99**, 8075 (1993).

¹³N. Matubayasi, E. Gallicchio, and R. M. Levy, *J. Chem. Phys.* **109**, 4864 (1998).

¹⁴R. M. Levy and E. Gallicchio, *Annu. Rev. Phys. Chem.* **49**, 531 (1998).

¹⁵E. Gallicchio, M. M. Kubo, and R. M. Levy, *J. Phys. Chem. B* **104**, 6271 (2000).

¹⁶B. Hess and N. F. A. van der Vegt, *J. Phys. Chem. B* **110**, 17616 (2006).

¹⁷C. Peter and N. F. A. van der Vegt, *J. Phys. Chem. B* **111**, 7836 (2007).

¹⁸I. C. Sanchez, T. M. Truskett, and P. J. in't Veld, *J. Phys. Chem. B* **103**, 5106 (1999).

¹⁹D. Ben-Amotz, F. O. Raineri, and G. Stell, *J. Phys. Chem. B* **109**, 6866 (2005).

²⁰D. Ben-Amotz and R. Underwood, *Acc. Chem. Res.* **41**, 957 (2008).

²¹B. Lee, *Biopolymers* **31**, 993 (1991).

²²B. Lee, *Biopolymers* **24**, 813 (1985).

²³S. Garde, G. Hummer, A. E. García, M. E. Paulaitis, and L. R. Pratt, *Phys. Rev. Lett.* **77**, 4966 (1996).

²⁴G. Hummer, S. Garde, A. E. García, A. Pohorille, and L. R. Pratt, *Proc. Natl. Acad. Sci. U.S.A.* **93**, 8951 (1996).

²⁵D. Chandler, *Nature* **437**, 640 (2005).

²⁶D. M. Huang and D. Chandler, *Proc. Natl. Acad. Sci. U.S.A.* **97**, 8324 (2000).

²⁷R. Zangi and B. J. Berne, *J. Phys. Chem. B* **112**, 8634 (2008).

²⁸Y. Nozaki and C. Tanford, *J. Biol. Chem.* **246**, 2211 (1971), available online at <http://www.jbc.org/content/246/7/2211.full.pdf+html>.

²⁹A. Radzicka and R. Wolfenden, *Biochemistry* **27**, 1664 (1988).

³⁰A. Ben-Naim, *Molecular Theory of Water and Aqueous Solutions. Part II: The Role of Water in Protein Folding, Self-Assembly and Molecular Recognition* (World Scientific, Singapore, 2010).

³¹R. Staritzbichler, W. Gu, and V. Helms, *J. Phys. Chem. B* **109**, 19000 (2005).

³²G. König and S. Boresch, *J. Phys. Chem. B* **113**, 8967 (2009).

³³G. König, S. Bruckner, and S. Boresch, *Biophys. J.* **104**, 453 (2013).

³⁴D. S. Tomar, V. Weber, B. M. Pettitt, and D. Asthagiri, *J. Phys. Chem. B* **118**, 4080 (2014).

³⁵T. Hajari and N. F. A. van der Vegt, *J. Phys. Chem. B* **118**, 13162 (2014).

³⁶N. F. A. van der Vegt and W. F. van Gunsteren, *J. Phys. Chem. B* **108**, 1056 (2004).

³⁷T. A. Özal and N. F. A. van der Vegt, *J. Phys. Chem. B* **110**, 12104 (2006).

³⁸R. L. Baldwin, *FEBS Lett.* **587**, 1062 (2013).

³⁹H. Acharya, S. Vembanur, S. N. Jamadagni, and S. Garde, *Faraday Discuss.* **146**, 353 (2010).

⁴⁰R. C. Harris and B. M. Pettitt, *Proc. Natl. Acad. Sci. U.S.A.* **111**, 14681 (2014).

- ⁴¹B. Lee and F. M. Richards, *J. Mol. Biol.* **55**, 379 (1971).
- ⁴²F. Eisenhaber, P. Lijnzaad, P. Argos, C. Sander, and M. Scharf, *J. Comput. Chem.* **16**, 273 (1995).
- ⁴³W. Becktel and J. A. Schellman, *Biopolymers* **26**, 1859 (1987).
- ⁴⁴J. G. Kirkwood, *J. Chem. Phys.* **3**, 300 (1935).
- ⁴⁵T. C. Beutler, A. E. Mark, R. C. van Schaik, P. R. Gerber, and W. F. van Gunsteren, *Chem. Phys. Lett.* **222**, 529 (1994).
- ⁴⁶E. Lindahl, B. Hess, and D. van der Spoel, *J. Mol. Model.* **7**, 306 (2001).
- ⁴⁷N. Schmid, A. P. Eichenberger, A. Choutko, S. Riniker, M. Winger, A. E. Mark, and W. F. van Gunsteren, *Eur. Biophys. J.* **40**, 843 (2011).
- ⁴⁸H. J. C. Berendsen, J. P. M. Postma, W. F. van Gunsteren, and J. Hermans, in *Intermolecular Forces*, edited by B. Pullman (Reidel, Dordrecht, 1981), pp. 331–342.
- ⁴⁹S. Miyamoto and P. A. Kollman, *J. Comput. Chem.* **13**, 952 (1992).
- ⁵⁰B. Hess, H. Bekker, H. J. C. Berendsen, and J. G. E. M. Fraaije, *J. Comput. Chem.* **18**, 1463 (1997).
- ⁵¹U. Essmann, L. Perera, M. L. Berkowitz, T. Darden, H. Lee, and L. G. Pedersen, *J. Chem. Phys.* **103**, 8577 (1995).
- ⁵²W. F. van Gunsteren and H. J. C. Berendsen, *Mol. Simul.* **1**, 173 (1988).
- ⁵³H. J. C. Berendsen, J. P. M. Postma, W. F. van Gunsteren, A. DiNola, and J. R. Haak, *J. Chem. Phys.* **81**, 3684 (1984).
- ⁵⁴M. Parrinello and A. Rahman, *J. Appl. Phys.* **52**, 7182 (1981).
- ⁵⁵G. I. Makhatadze and P. L. Privalov, *J. Mol. Biol.* **232**, 639 (1993).
- ⁵⁶G. I. Makhatadze and P. L. Privalov, *J. Mol. Biol.* **213**, 375 (1990).
- ⁵⁷R. Godawat, S. N. Jamadagni, and S. Garde, *Proc. Natl. Acad. Sci. U.S.A.* **106**, 15119 (2009).

5 The Influence of Graphite Surface on Ion-Pairing of Hofmeister Ions and Hydrophobic Association

The Influence of Graphite Surface on Ion Pairing of Hofmeister Ions and Hydrophobic Association

Timir Hajari, Fereshte Teherian and Nico F. A. van der Vegt*

Eduard-Zintl-Institut für Anorganische und Physikalische Chemie and Center of Smart Interfaces, Technische Universität Darmstadt, Alarich-Weiss-Straße 10, 64287, Darmstadt, Germany

Abstract

Ion pairing near water interfaces has important implications in many chemical and biological processes. In this work, ion pairing of sodium-halides, potassium-halides and CsI are quantified near a model hydrophobic surface (graphite) using molecular dynamics simulations. The potentials of mean force between the cations and the anions are estimated in bulk water solution and near graphite interface. For salts with strongly solvated small cations and strongly solvated small anions, two oppositely charged ions tend to pair in greater extent near graphite surface than what is observed in bulk solution. Ion pairing tendencies for the salts composed of small cations and weakly solvated, large anions are also amplified near graphite surface, however the effect is smaller in comparison with small-small ion combinations. Pairing between large cation and large anion near the surface is even weakly unfavorable compared with that in bulk. Interestingly, ion pairing (different cations, anions combinations) is even more favorable when the graphite-water interaction strength is artificially reduced. From these findings a simple explanation of how hydrophobic surfaces influence ion pairing propensity of salt solutions is established using Collins's law of matching water affinities. The enhancement of ion-ion association near hydrophobic surface is further found due to the stabilization of solvent shared ion-pair (SIP) state near graphite surface and near more hydrophobic surface. The free energies of the contact ion-pair (CIP) and SIP states at the surface have a larger entropic component in comparison to bulk. Here the larger entropic component at the SIP states near the surface is because of the lower water density around the ions. Hydrophobic association study shows that the stability of contact pair state in the potential of mean force between two methane particles near graphite surface is enhanced than that in bulk water. However the desolvation barrier at the interface is quite similar to bulk, that is in contrast with other hydrophobic surfaces. The hydrophobic solvation process near graphite surface which is also quite different compared with that near other hydrophobic surfaces. It all indicates that the nature of graphite surface is weakly hydrophobic or even slightly hydrophilic because of the high water density near the surface.

Introduction

Ion solution and ion interactions at (macro)molecular surfaces are important in many biological processes. Hofmeister ordered different ions based on their ability to precipitate proteins and hence the ranking of ions depending on their efficiency in precipitating proteins is known as *Hofmeister series*.¹ The Hofmeister effect is not only limited there, the ion specific effect on water surface tension or ion's propensity toward air-water interface, the stability of colloids, the viscosity B coefficient of salt solutions, salting out of nonpolar molecules or macromolecules by Hofmeister ions; all follow similar trends like Hofmeister ion series.²⁻¹¹ Both the anionic and the cationic Hofmeister series are explored for past decades and it is observed that the differences in the strength among different Hofmeister anions to precipitate or stabilize proteins are more prominent. Here our discussion will mostly focus on the Hofmeister anionic rankings. Ions with high charge density (*e.g.* F^-) are strongly solvated in water, are capable of stealing water from proteins occurring precipitation, whereas this ability is absent for weakly hydrated and low charge density containing ions. However from experimental and computer simulation studies, it is apparent that the size of ions either large or small is not enough to explain such specificity specially in protein precipitation.¹¹⁻¹⁶ On the same line, the ions with low charge density show propensity to be absorbed at air-water, solid (hydrophobic)-water interfaces and the ion with high charge density does not show such propensity. For ion specific interaction with protein, ion absorption at air-water interface or solid-water interface, an important aspect that helps to govern such ion specific effect is the balance of ion-ion, ion-water, water-water interaction near such water interfaces and in bulk water solution. Instead of rationalizing only the role of cationic or anionic series separately,

Jungwirth and Cremer emphasis on non-additive effects in understanding such specific ion effects.¹⁵ A recent work from Xie et al.¹⁷ discussed in detail how ion cooperativity or ion pairing governs properties like water activity coefficient, air-water surface tension, solubility of model protein. Despite having the importance of ion-pairing, many works had explored only the individual ion's propensity to exist preferentially at water interfaces like protein-water interface, air-water interface, solid-water interface. To explain the role of ion cooperativity/pairing in governing Hofmeister series, the ion-ion interaction in bulk water is generally used¹⁷⁻²⁰ and the nature of ion-ion interaction for different Hofmeister ions at such interfaces are not well investigated. The interfacial water molecules behave differently than bulk water and ion pair are surrounded by water asymmetrically because of the dehydration around ions in presence of the surface. Hence it is not straightforward how ion-ion interaction is influenced there. It is therefore important to study systematically how ion-pairing propensities for Hofmeister series change from bulk solution to interfacial environments. In our current work, we analyze ion-pairing propensities of Hofmeister anions with Na^+ , K^+ , Cs^+ ions in bulk solution and at a contact distance with an extended hydrophobic graphite surface as a model water interface. The experiment and simulations predicted the contact angle of water on graphene in the range of values from 75° to 95° .²¹⁻²⁴ Thus, from the contact angle values graphite is weakly hydrophobic material. We also study ion pairing between different cations and anions near a more hydrophobic surface than graphite surface by weakening artificially the graphite carbon-water interaction. We have to be aware of the fact that protein surfaces contain peptide backbone and different type of side-chains, thus a Hofmeister ion series for graphite surface can potentially differ than the ion series for protein surfaces. On a positive note, our work helps to gain an insight

of ion-pairing at hydrophobic interfaces which could facilitate an better understanding of Hofmeister effect.

To rationalize ion-ion association or ion-pairing at water interfaces, at first what causes ion association in bulk salt solution is necessary to understand. Collins’s view, “the law of matching water affinities” is useful in this regard.^{18–20} He categorised ions based on their surface charge density. The ions having high charge density are strongly hydrated and have stronger ion-water interaction than water-water interaction. The ions with low charge density have opposite behaviours compared to small ions. According to Collins’s view, the dissolved salts of small-small ion combinations and large-large ion combinations stay together (contact ion-pair state) whereas the salts of large-small ion combinations stay apart (fully dissociated ion-pair state). Many useful properties of salt solutions like solubilities of salts in water, heat of solutions of alkali halides, viscosity B coefficient of salt solutions, effect of ions on water surface tension, osmotic coefficient of electrolyte solutions can easily be explained using Collins’s law.¹⁸ Simulation work from Dill and his coworkers proved the validity of this physical law.²⁵ Their work provided also the molecular level explanation why bulk ionic solution follows Collins’s law. The simulation works from van der Vegt and coworkers^{26,27} further have validated Collins’s physical law for salts having biologically relevant anions (phosphate and acetate ions) and alkali cations. They showed that the thermodynamic property for example the osmotic coefficients of salts with constituent ions like alkali ions and phosphate, acetate anions are determined by the population of solvent shared ion-pair state. Our current work also provides information on different ion-pair state’s populations at graphite-water interface which is an important component in controlling thermodynamic properties of salt solution. Even it could be further useful in studying ion pair dissociation dynamics at interfaces²⁸ from the information about the stability of solvent shared ionpair (SIP), contact ion pair (CIP) states and the barrier height between CIP and SIP states.

Hydrophobic association has wide applications from protein folding, association to micelle formation.^{29–31} Small scale and large scale hydrophobic association in bulk water solution were investigated in past.^{32–35} Various biological systems like proteins, membranes have hydrophobic, hydrophilic interfaces partially or fully exposed to water. Few studies focused on hydrophobic association³⁶ or hydrophobic solvation³⁷ near hydrophobic interface which has potential application in determining the hydrophobicity effect near such interfaces. It is found that the low water density (vapor like behaviors) near hydrophobic surfaces favors the hydrophobic association or solvation in comparison to that in bulk water.^{36,37} Whereas near hydrophilic surfaces, the hydrophobic association or solvation is similar to that in bulk water solution. However, the impact on hydrophobic association or hydrophobic solvation near relatively higher water density containing weakly hydrophobic graphite surface is not known and worthwhile to investigate.

We attempt to understand how a hydrophobic surface influences ion pairing of Hofmeister ions and also hydrophobic association of two methane. Using molecular dynamic simulation, the potentials of mean force (PMF) between cations (Na^+ , K^+ , Cs^+) and anions (Cl^- , Br^- , I^-) near graphite interface are computed and compared with the respective cation-anion PMFs in bulk water. The same PMF calculations are

performed near a relative stronger hydrophobic surface (compared to graphite) for quantifying the role of water density and the surface-water interaction strength in ion-pairing phenomena. Similarly the PMF between two methane particles are computed near two aforementioned surfaces and in bulk water solution to rationalize about the hydrophobic association process at such interfaces. The PMFs are further decomposed to get the entropic and enthalpic components in ion association/pairing and methane-methane association.

Computational Methods

Molecular Dynamics (MD) simulations are performed using GROMACS³⁸ software package (4.6.2) with a time step of 2 fs. All simulations are done in NVT ensemble with the box dimensions (4.18nm×4.26nm×7nm). Fyta and Netz parameters³⁹ for the following ion pairs NaCl, NaBr, NaI and I-I, are used in our calculations and these parameters are actually derived from Dang parameters. The Dang parameters^{40,41} are considered for KCl, KBr, KI and CsI. The SPC/E water model⁴² are used in combination with Fyta and Netz and Dang parameters for ions. The bonds and angle from water molecules are constrained using SETTLE algorithm.⁴³ The parameters σ_{cc} and ϵ_{cc} for graphite carbon atoms are from the work of Walther et. al.⁴⁴ and the interaction parameters between graphite and oxygen atom of water (σ_{cow} , ϵ_{cow}) are same as Werder’s work.⁴⁵ All the parameters are represented in the Table 1. Lorentz-Berthelot mixing rules ($\sigma_{ab}=(\sigma_{aa}+\sigma_{bb})/2$, $\epsilon_{ab}=\sqrt{\epsilon_{aa}\epsilon_{bb}}$) are utilized for the rest of the interaction parameters (ion-ion, ion-water, ion-graphite, graphite-water) except for NaI where $\epsilon_{NaI}=0.9\sqrt{\epsilon_{NaNa}\epsilon_{II}}$.

Table 1: Ions and Graphite parameters

Ion ^a	σ_{ii}	ϵ_{ii}	σ_{iow}	ϵ_{iow}
Na^+	0.2583	0.4186	0.2876	0.5216
Cl^-	0.440	0.4186	0.3785	0.5216
Br^-	0.4631	0.412	0.39	0.52
I^-	0.5831	0.015	0.45	0.1
Ion ^b	σ_{ii}	ϵ_{ii}	σ_{iow}	ϵ_{iow}
K^+	0.315	0.42	0.316	0.52
Cs^+	0.372	0.42	0.344	0.52
Cl^-	0.44	0.42	0.378	0.52
Br^-	0.463	0.42	0.390	0.52
I^-	0.517	0.42	0.417	0.52
Graphite	σ_{cc}	ϵ_{cc}	σ_{cow}	ϵ_{cow}
C	0.3851	0.4396	0.319	0.392
Graphite*	σ_{cc}	ϵ_{cc}	σ_{cow}	ϵ_{cow}
C*	0.3851	0.4396	0.319	0.20

^a represents the parameters from Fyta and Netz and ^b corresponds to the Dang parameters. The units for σ and ϵ are nm and kJ/mol respectively.

Four planar layers of graphene are considered to represent the graphite surface. A distance of 0.34 nm between two adjacent layers and at each layer the C-C distance of 0.142 nm, are chosen based on crystallographic positions. All the carbon atoms are fixed during the simulation.

Potentials of mean force (PMFs) are estimated using constraint force calculations.⁴⁶ The interionic distance (r) is taken as the reaction coordinate. During PMF calculation, ion pairs are only allowed to move along XY directions(parallel

to graphite layers) with a fixed z distance.^{36,47} To compute PMF at bulk water, ion pairs are placed at $z=4.0$ nm away from the closest graphene layer. Similarly for computing PMF at graphite-water interface, the ion pair are kept at a z plane which is far from the closest graphite layer with a z -distance equal to the anion-graphite carbon contact distance ($2^{1/6} \sigma_{\text{anion-carbon}}$). The final PMF ($\text{PMF}(r) = \int_{\infty}^r \langle F_c(r) \rangle dr + RT \ln(r)$) at a particular r , is obtained after correcting the additional free energy contribution, $-RT \ln(r)$ arising for a motion in a 2D plane.⁴⁶ The constraint forces are estimated at 30-32 different distances (r), ranging from 0.25 nm to 1.2 nm. At every cation-anion separation(r), 2 ns of equilibration run and an additional 10 ns of simulation for data collection are performed. The system temperature is maintained at 298K using velocity rescaling⁴⁸ thermostat with a stochastic term and a relaxation time of 0.2 ps is considered. The cut off distance for all nonbonded interactions is 1.0 nm. Particle mesh Ewald (PME)⁴⁹ method with a real space cut off of 1.0 nm and a grid space of 0.12 nm, is utilized to treat the long range electrostatic interaction.

The free energy change along the reaction coordinate r , has entropic and enthalpic contributions at each ion-ion separation. The entropy contribution ($\Delta S(r)$) in $\text{PMF}(r)$ or $\Delta G(r)$ are obtained from the Eq. 1 using finite difference method. Here the values of T and ΔT are 298K and 20K respectively. The enthalpy contribution($\Delta H(r)$) is then obtained from $\text{PMF}(r)$ at 298K and $\Delta S(r)$ using Eq. 2.

$$-\Delta S(r) = \frac{\Delta G(r, T + \Delta T) - \Delta G(r, T - \Delta T)}{2\Delta T} \quad (1)$$

$$\Delta H(r) = \Delta G(r) + T\Delta S(r) \quad (2)$$

Entropy and enthalpy contributions from $\text{PMF}(r)$ s are estimated in bulk water and interface for two ion pairs (NaBr, KBr) and methane-methane association.

Errors in the CIP and SIP states from each $\text{PMF}(r)$ are estimated using block averaging technique. For that purpose, the entire 10 ns trajectory is splitted into five individual blocks. The errors in CIP and SIP states are < 0.25 kJ/mol.

Results and Discussion

Ion-Ion Association

The changes in potentials of mean force ($\text{PMF}(r)$) with ion-ion distance for sodium-halides, iodide-iodide, potassium-halides and CsI are shown in Figure 1 and 2. Here ion-ion association at bulk water is represented by each black line and the red lines correspond to ion-ion association at graphene-water interface. The locations of ion pairs in the simulation box for these two cases are explained in the previous section. In the $\text{PMF}(r)$ s from bulk water, the first minimum, contact ion pair (CIP) is equally deep as the second minimum, solvent shared ion pair (SIP) for salts like NaCl, NaBr, NaI, so both states are equally stable. Similar behaviours are found in graphite-water interfacial region (see Fig. 1). The thermodynamic stability of CIP state in bulk is similar to the CIP state near graphite interface for following ion pairs, NaCl, NaBr, NaI. However, going from bulk water to interfacial case, both the SIP and the third minimum, solvent separated ionpair state (SSIP) for each ion pair are becoming more favorable.

For potassium-halides and CsI, their CIP states are found to

be more stable than their SIP states in bulk water (black lines from the Fig. 2). Figure 2 shows that the deepest minima in the PMFs (red lines) are at CIP distance for potassium-halides and CsI near the interface. According to Collins's convention,^{18,19} the large cation (K^+ , Cs^+) tends to pair off with large anion which favors the CIP state. Hence the CIP state is more favorable for potassium-halides and CsI. Again for K-halides, the SIP state of each ion pair is more stable near graphite-water interface than the SIP state of the same ion pair in bulk water. The CIP state of KCl, KBr ion pairs are unaffected at interface. Interestingly, the CIP state becomes less stable near graphite-water interface in comparison to that at bulk water for large(cation)-large(anion) combination (CsI, KI).

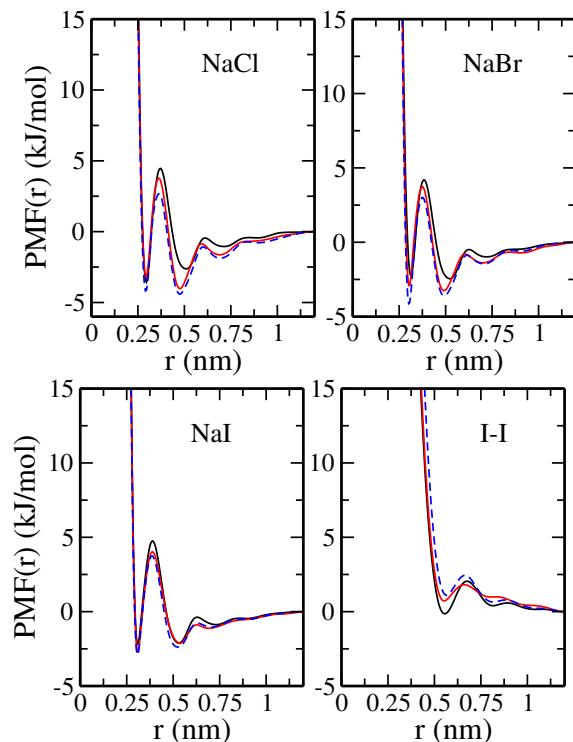


Figure 1: The plots of $\text{PMF}(r)$ s with ion-ion separation (r) for NaCl, NaBr, NaI and I-I. The black lines are the $\text{PMF}(r)$ s when ion pair are at bulk water and the red and blue (dotted) lines are the $\text{PMF}(r)$ s when ion pair are in contact with graphite surface and in contact with modified graphite surface respectively.

So from these all $\text{PMF}(r)$ studies of Hofmeister ions (Fig. 1 and 2), we find that the SIP state of an ion pair becomes thermodynamically more favorable for switching the location of ion pairs from bulk water to graphite-water interface region. We also varied the z -positions of ion-pairs (z -distance from graphite surface) at graphite interface, even-though our main finding (stabilization of SIP) remains same (not shown). The stabilization of SIP state in ion pairing near planar surface

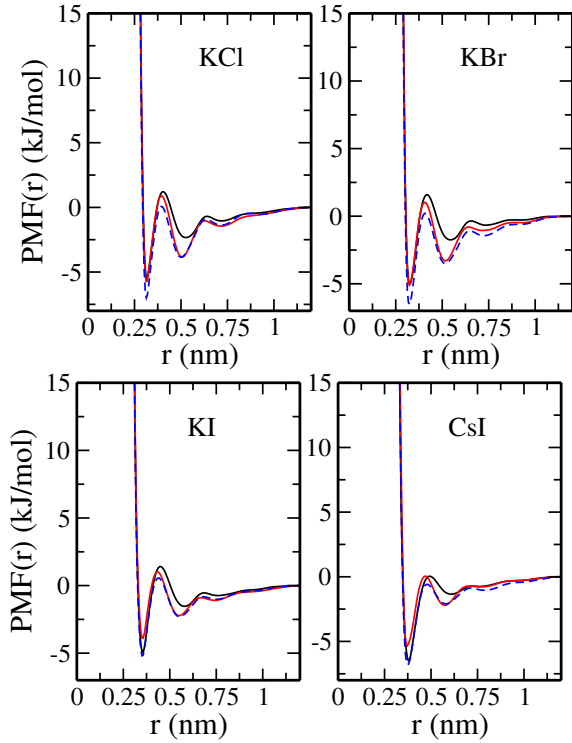


Figure 2: The plots of $PMF(r)$ s with ion-ion separation(r) for KCl, KBr, KI and CsI. The black lines are the PMF s when ion pair are at bulk water and the red and blue (dotted) lines are the PMF s when ion pair are in contact with graphite surface and in contact with modified graphite surface respectively.

or surface with curvature also found by Chorny et al.⁵⁰ So a similar finding from our current work as well as work from Chorny et al. may support the observation that protein crystal structures contain salt bridges via solvent shared state.^{26,51} Work of Garde⁴⁷ also found a stronger water mediated cation-anion interaction (both CIP and SIP states) at water-vapor interfacial region compare to bulk. The process that brings Na^+ and Cl^- from far distance to CIP state, is also found to be more favorable at liquid-liquid interface in comparison with bulk water.⁵⁴ On the contrary, our result shows that CIP states are mostly unaffected or even become less favorable at graphite-water interface. Our current work shows that ion-ion association enhances as the SIP state are more stabilized near graphite interface.

As the graphite surface contains high density of carbon atoms eventually owing strong carbon-water van der Waals interactions which makes the surface weakly hydrophobic. We artificially reduced the carbon-water interaction (ϵ_{cow}) to make the graphite surface more hydrophobic. The detail is in the last row from the table 1. With the chosen value of ϵ_{cow} (0.2 kJ/mol), the water contact angle is around 120° .^{55,56} This surface is called as modified graphite surface throughout the article. The blue lines from the Figures 1 and 2, represent

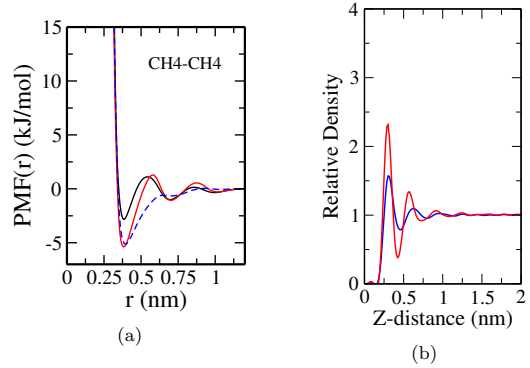


Figure 3: (a) PMF s between two methane particles with methane-methane distance (r) as reaction coordinate in bulk water (black line) and near graphite interface (red line) and near modified graphite surface (blue dotted line) and (b) water density relative to bulk is plotted against the z -distance from graphite surface (red line) and modified graphite surface (blue line). A bin size of 0.0875 nm is used in estimating water density.

the $PMF(r)$ s with ion-ion distance for sodium halides, iodide-iodide, potassium-halides and CsI near such modified graphite surface or strongly hydrophobic surface. Whereas the black lines from the Figures 1 and 2 are for the bulk water solution. Moving from bulk water to such interfacial case, the features in the PMF s are quite similar like near normal graphite surface (red lines). Ion-ion association is enhanced in greater extent near this modified graphite surface compared with that near normal graphite surface. For all ion pairs, the SIP state of an ion pair becomes systematically more stable than its SIP state at pure water. Whereas the CIP state stabilizations are there, but not that prominent. Figure 1 and 2 shows that the impact of surface on the PMF s is more prominent for the following ion pairs, NaCl, NaBr, KCl, KBr. Compare to other salts, their CIP, SIP and SSIP states are stabilized in greater extent than their respective CIP, SIP and SSIP states in pure water. The CIP states of ion pairs, KI and CsI, turn out to be equally stable like in bulk water solution in contrast to normal graphite surface. So this modified graphite surface or more hydrophobic surface induces more ion pairing compared to bulk and even compared to normal graphite surface.

Ion-Ion Association Constant

The water density near normal graphite (red line) and modified graphite surface (blue line) are shown in the Figure 3b. As observed from Figure 3b, the water density is relatively lower at modified graphite surface. Such reduced water density enhances ion pairing which is clear from the comparison among the PMF s from the Figures 1 and 2. The ion-ion association is further quantified following $A_{bulk/sur} = \int_0^{r_{cut}} \exp(-PMF(r)/k_bT) 2\pi r dr$, where “A” is termed as the ion-ion association constant and r_{cut} is considered just beyond the SSIP distances (0.80 nm). Here “A” is a measure of ion-ion association. A larger positive value of “A” corresponds to a greater ion pairing between cation and anion. Figure 4 represents the enhancement in ion-ion association near the surfaces compared to bulk water solution ($[A_{sur} - A_{bulk}]/A_{bulk}$).

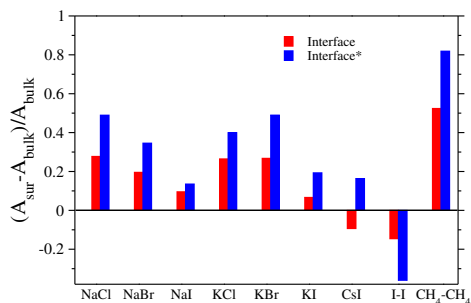


Figure 4: The enhancement in the ion-ion, CH₄-CH₄ association constants near graphite (red bars) and modified graphite (blue bars) surfaces. Here A_{sur} and A_{bulk} are the association constants at surface and at bulk respectively.

The red and blue bars are for graphite surface and modified graphite surface respectively. More hydrophobic surface induces more ion pairing (blue bars) for all different cation-anion combinations. The water density around ion pair near hydrophobic surfaces is less than that in bulk that enhances ion pairing. The normalized water density around ion pair are discussed in the section–Entropy-Enthalpy Decomposition. The relative increase in interfacial pairing propensity follows a Hofmeister series: NaCl>NaBr>NaI. Moving from Cl⁻ to I⁻ anion for Na⁺ cation, the highest and lowest ion-ion association relative to bulk solution are found for NaCl and NaI ion pairs respectively near graphite surface (red bars). Both Na⁺ and Cl⁻ have strong interaction with water in bulk solution. For ion pairing of NaCl, the ion-water interactions have to be overcompensated by the cation-anion interaction. Now near graphite surface, the number of water molecules around these strongly solvated ions are reduced. Hence the cation feels strong attractive force from the anion in absence of water which causes a stronger association. Interfacial ion pairing of NaCl is further amplified near modified graphite surface. Here the interfacial water density is even much smaller (the high contact angle surface) and, consequently, the ion-ion electrostatic attraction is effectively stronger. For weakly solvated, large anion, I⁻, the I⁻-water interaction is not such strong like Cl⁻, hence the influences of hydrophobic surfaces on Na-I ion pairing is less pronounced. So ion pairing with small-large ion combinations weakly favored over ion pairing in bulk.

The increments in ion pairing propensities near graphite interface follows the following order: KCl≈KBr>KI. Ion pairing between K⁺ and Cl⁻ is more amplified than pairing between K⁺ and I⁻ near graphite surface (red bars). Again near stronger hydrophobic surface, the ion-ion association for KCl, KBr, KI are even more pronounced (blue bars). The enhancement in ion-ion association near modified graphite surface with respect to bulk follows KCl<KBr>KI. The combination between small cation, K⁺ and large anion, I⁻ for KI, pairing is affected a little near hydrophobic interfaces. The Cl⁻ interacts strongly with water compare with I⁻. So a less water density near hydrophobic interface reduces the cost of Cl⁻-water interaction lose due to K-Cl pairing owing to strong ion pairing. As the I⁻-water interaction is weaker than Cl⁻-water interaction, the surface does not influence pairing between K⁺

and I⁻.

Ion pairing tendency between a large cation, Cs⁺ and a large anion, I⁻ is even reduced near graphite interface (red bar). The large-large combination always pair off in bulk as ion pairing brings the gain of water-water interaction. Additionally the water-ion interaction is weaker which costs less free energy penalty in ion pairing. Now near the graphite surface, the reduced water density does not help to gain much water-water interaction. It may cause such slightly reduced ion pairing between Cs⁺ and I⁻ slightly reduced near graphite surface. But, ion pairing near modified graphite surface where the water density is even reduced, then the ion-ion interaction dominates owing to a relative higher ion-ion association than in bulk (blue bar).

According to Collins’s view, the aqueous salts solution with strongly solvation small sized cation (Na⁺, K⁺) and small sized anion (Cl⁻, Br⁻) tend to pair off in water. Near hydrophobic surface, these strongly solvation ions tend to pair off even strongly because of the water density which is relatively less around the ions near hydrophobic surface. The salts with large anion (I⁻) and relatively small sized cations (Na⁺, K⁺) tend to stay apart in water and similarly near hydrophobic surface ion pairing tendencies for such ion pairs remain almost unaffected. Ion pairing tendency in bulk for salt with large(cation)-large(anion) combination is even more favorable than near graphite surface and is less favorable than near more hydrophobic surface.

Anion(I⁻)-Anion(I⁻) PMF(r) shows two shallow minima at about 0.55 nm and 0.8 nm in bulk water (black line from Fig. 1). Like charge pairing becomes less favorable at graphite interface, albeit two shallow minima are present but they are less pronounced (red line) than in bulk case. This effect is even enhanced near modified graphite surface (blue line). The Anion-anion PMF(r) values at different r near interface are more positive (repulsive) compare with the PMF(r) values in bulk water. The possible explanation for our current finding could be the presence low dielectric medium (hydrophobic surface) near to two anions that enhance the same charge repulsion. That is why the red line and blue line are always more positive than the black line in the Fig. 1. For the similar reason, the values of PMF(r) at r ≥ 0.75 nm at interface region are always less than the corresponding values of PMF(r) at bulk water in opposite charge ion pairing from figure 1 and 2. Nevertheless, the nature of PMF(r) at shorter distances is governed by the effects of explicit water, ion-ion interaction, ion-water interaction. So our current results are not just simply because of the influence from the low dielectric medium, but rather due to presence of complicated molecular level effects.

Simulation work from Cummings et al.⁵² found that an ion pair (NaCl at CIP or SIP state) has more negative interfacial free energy than single ion (Cl⁻) along at air-water interface. Even Experimentally, it was found that anion and cation, both strongly absorb to the interface as a contact ion pair.⁵⁷ We computed the free energy change to bring a contact ion pair of NaBr or a solvent shared ion pair of NaBr and a single Br⁻ ion from bulk water to graphite-water interfacial region. These calculations are performed using PLUMED⁵³ package in combination with GROMACS software. Both processes with SIP and CIP states of NaBr ion pair, are seen to be favorable (red and black lines from figure 5). Bringing a single Br⁻ anion from bulk to contact distance with graphite surface (green

line from figure 5) is free energetically most favorable. Na^+ is strongly solvated in water and it has less propensity to lose water around it's solvation shell and to be absorbed in graphite surface as well. Hence the SIP and CIP ion pair states from NaBr have less propensity compare with single anion (Br^-) to go in contact with graphite surface. These findings emphasis on the importance to account the role of counterion or ion pairing in determining Hofmeister effect.

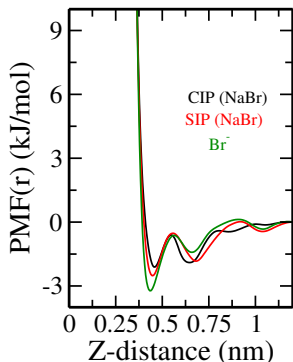


Figure 5: The change in free energy as a function of z-distance from graphite surface. The black line refers to the free energy change to bring a CIP state of NaBr along z-axis (normal to the graphite surface) from bulk water to interface. The red line is for the same process but with a SIP state of NaBr. The inter-ionic axis is always perpendicular to z-axis during PMF calculations. The green line represents the PMF of a single Br^- ion along z-axis.

Hydrophobic Association

Two united methane molecules (OPLS⁵⁸ force field) are considered to compute PMF in bulk water and at graphite interface. Figure 3a shows that a deep minimum at contact distance around 0.375 nm, called as contact minimum (CM) and another relatively less deeper minimum at solvent shared distance around 0.675 nm, called as solvent separated minimum (SSM) are present both in bulk and at interface. The hydrophobic interaction between two methane molecules is affected by graphite surface. The value of PMF(r) at contact distance becomes more negative as one approaches near interface from bulk. The solvent shared and solvent separated states remain unaffected. Figure 3a also indicates that the desolvation barrier in going from solvent shared distance to contact distance near the surface is quite similar compared with the same barrier at bulk water. Work of Vembanur et al.³⁶ found that the contact formation between two or more nonpolar solutes becomes more feasible and the desolvation barrier also disappears at extended hydrophobic surface ($\text{CH}_3\text{-SAM}$). The decrease in the desolvation barrier is explained there based on the fact that water near such hydrophobic surface is like at vapor-water interface. We keep two methane particles in between first and second water layers from rigid graphite surface. Relative water density (ρ_z/ρ_{bulk}) on top graphite surface is shown in Figure 3b. The water density is significantly higher than the water density at a vapor-water in-

terface. Hence the desolvation barrier exists there in contrast to what Vembanur et al. reported. Now the same PMF calculations are done with the more hydrophobic surface which has relatively less water density next to the surface (blue line from Fig 3b). The blue dotted line from figure 3a shows the PMF(r)s between two methane particles near this surface. The desolvation barrier between CM and SSM disappears in the methane-methane PMF(r). Here our result supports the work of Vembanur et al. The PMF studies indicate that the relative higher water density makes graphite surface less hydrophobic and quite different from other hydrophobic surface like $\text{CH}_3\text{-SAM}$ surface.

Entropy-Enthalpy Decomposition

Ion-Ion Association

Figure 6 and 7 show the entropy ($-\text{T}\Delta\text{S}(r)$) and enthalpy ($\Delta\text{H}(r)$) parts from the PMFs at bulk and at graphite interface. We consider only two ion pairs (KBr, NaBr) in our current work. The $\Delta\text{H}(r)$ and $-\text{T}\Delta\text{S}(r)$ shown in Figure 6 and 7, are at temperature 298 K.

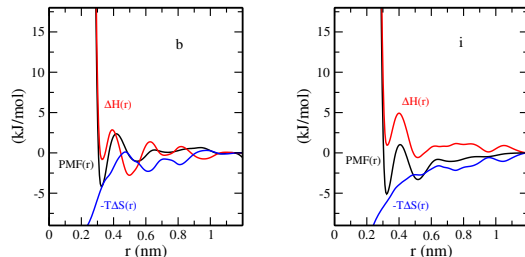


Figure 6: Enthalpy contribution, $\Delta\text{H}(r)$ (red lines) and entropy contribution, $-\text{T}\Delta\text{S}(r)$ (blue lines) in the PMFs of KBr ion pair. Left panel is in bulk solution and right panel is at interface.

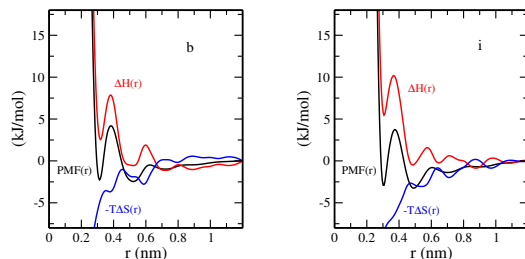


Figure 7: Enthalpy contribution, $\Delta\text{H}(r)$ (red lines) and entropy contribution, $-\text{T}\Delta\text{S}(r)$ (blue lines) in the PMFs of NaBr ion pair. Left panel is in bulk solution and right panel is at interface.

If we see the Figure 6, the $-\text{T}\Delta\text{S}(r)$ values at CIP state of KBr in bulk (left panel) and at interface (right panel), both are negative and the entropic contribution is larger at graphite interface. However the enthalpy part is more negative in bulk water. Here Due to the entropy-enthalpy cancellation, the

overall thermodynamic stabilities in the PMFs at CIP distances in figure 2 are similar in bulk and at interface. Positive entropy contribution ($T\Delta S_{SIP}$) in cation-anion association or hydrophobic association were found already in bulk water previously in simulations.^{59–61} Moving from SIP to CIP causes the release of restricted water molecules from the common hydration shell of two ions that brings such entropy gain. On the other hand, the KBr ion pair at SIP state near interface is enthalpically less favorable and entropically more favorable than in bulk (Figure 6). Nevertheless the more stable KBr SIP configuration or more negative PMF value at interface in figure 2 are arising because of the ΔS_{SIP} values which is more positive for KBr SIP state at interface. For bulk SIP configuration of KBr, the ΔS_{SIP} is around zero, whereas it is positive ($T\Delta S_{SIP} = 2.6$ kJ/mol) at interface.

Similarly, the entropy-enthalpy decomposition in the PMFs of NaBr are shown in the figure 7. The ΔS_{CIP} and ΔS_{SIP} values near interface are more positive than their respective values at bulk. The ΔH_{CIP} in bulk water is more favorable. Entropy-enthalpy cancellation at CIP states makes the overall PMF or ΔG_{CIP} values at bulk and at interface are almost same. Although, the ΔH_{SIP} values are similar in both cases, a more positive ΔS_{SIP} is found at interface. So a more positive ΔS_{SIP} makes the PMF or ΔG_{SIP} value more negative at interface in the figure 1 for NaBr and KBr.

We compute the water density around the SIP state of ion pairs (NaBr, KBr) at bulk water and near graphite interface. The water densities around Na^+ , Br^- ions and K^+ , Br^- ions at their respective SIP distances are shown in the Figure 8. we compute the normalized (with respect to bulk) water density around ion pair by considering a slab of thickness 1 nm. Near the interface, the slab is parallel to the graphite surface. Similarly, the normalized water density around ion pair at bulk water are estimated using a slab of thickness 1 nm. On average the water density is relative higher when the SIP state of ion pairs (NaBr, KBr) is in bulk water. Specially in bulk water, the normalized water density is relative higher around the shared region between the cation and the anion for both NaBr and KBr SIP states. The water molecules around the ions feel strong electrostatic interaction that makes those water molecules orientationally constrained. In bulk water, the SIP state has higher water density around the ions which means a more number of orientationally constrained water molecules are present around NaBr and KBr ion pairs. The significance of such orientationally constrained water molecules around different ion-pair states are nicely explained in the work of Fennell et al.²⁵ Their work showed that a higher orientationally ordered water molecules in the solvation shell of a certain ion pair state, brings more entropic penalty. Here, the SIP states of NaBr or KBr in bulk water contains more number of orientationally ordered water molecules around ion's solvation shell than near interface. So the SIP states of NaBr and KBr near interface has larger entropic contribution in comparison with the corresponding SIP states at bulk water. This observation supports our finding obtained from entropy-enthalpy decomposition in the Figures 6 and 7. We already saw there that a more positive entropic contribution at SIP distance for NaBr and KBr ion pairs is present when these ionpairs' SIP states are at graphite interface.

Hydrophobic Association

Figure 9 represents the entropic and enthalpic components in bulk and interface PMFs along methane-methane separa-

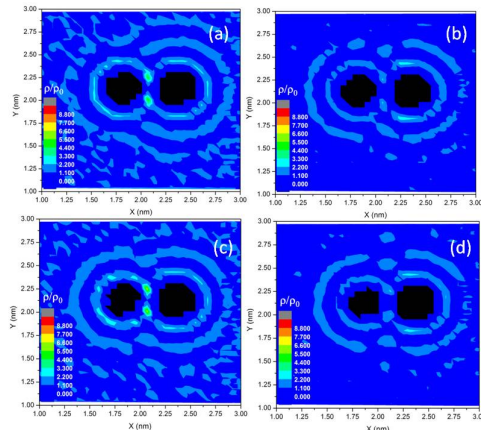


Figure 8: Normalized water density (relative to bulk density) around the SIP states of NaBr and KBr ion pairs. (a) K^+ and Br^- at bulk water solution (b) K^+ and Br^- near graphite interface (c) Na^+ and Br^- at bulk water solution (d) Na^+ and Br^- near graphite interface. The normalized water density is computed using a slab of thickness 1 nm. Here the XY planes are parallel to the graphite layers.

tion distance.

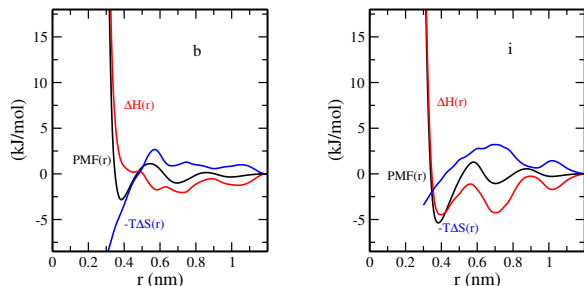


Figure 9: Enthalpy contribution, $\Delta H(r)$ (red lines) and entropy contribution, $-T \Delta S(r)$ (blue lines) in the PMFs of two methane particles. Left panel is in bulk solution and right panel is at interface.

At contact minimum (CM), ΔH_{CM} (red lines) are slightly negative or little positive and $-T\Delta S_{CM}$ (blue lines) are negative at bulk (left panel). Whereas the ΔH_{CM} , red line from the right panel, is more negative and the $-T\Delta S_{CM}$ is around zero near interface. So a favorable hydrophobic association or a negative value of PMF at CM, is caused by mainly entropic term in bulk solution. On the contrary, a negative ΔH_{CM} near graphite interface causes a more favorable hydrophobic association. There have been many works done in past on temperature dependent hydrophobic interactions using nonpolar solutes. Entropy driven hydrophobic association is commonly found there in bulk water.⁶¹ Here we find a large negative enthalpic contribution in hydrophobic association next to rigid hydrophobic graphite surface in agreement with the finding

from Vembanur et al.³⁶. They showed that the hydrophobic association free energy near hydrophobic $-\text{CH}_3$ SAM surface is very weakly dependent on temperature which means that this association process does not contain a large positive entropic contribution, rather a large negative enthalpic part is present. Similar observation is also found when we use the modified graphite surface (not shown). So, a higher methane-methane association at graphite interface relative to bulk is arising from the large enthalpic contribution at interface.

The $\Delta H(r)$ values at solvent shared minimum (SSM) and solvent separated minimum (2SSM) are negative in bulk water (left panel). Near graphite surface, the ΔH_{SSM} and ΔH_{2SSM} are even more negative than in bulk solution (right panel). So, the ΔS_{SSM} and ΔS_{2SSM} are negative both in bulk and interface region. These two quantities are more negative at interface.

Hydrophobic Solvation

The solvation free energies of methane next to graphite surface and at bulk are estimated at different temperatures. The increase in solvation free energy of methane with temperature is shown with temperature in bulk water and near graphite surface in Figure 10. The temperature dependence of solvation free energy changes ($\Delta G_s - \Delta G_s(298\text{K})$) of methane at three different temperatures (278K, 298K, 318K) are presented in bulk water solution using black circles and near interface using red squares. The solvation entropies, obtained from the slopes of two curves, are negative that indicates the solvation of methane next to graphite surface has negative solvation entropy like in bulk. The negative solvation entropy contribution is obtained for the cavity formation in bulk and near hydrophilic surfaces from the simulation work of Patel et al.³⁷ However they found that the solvation entropy is almost zero at hydrophobic surface. So from the hydrophobic solvation study near graphite surface reveals that the surface is not sufficiently hydrophobic and even little hydrophilic in nature.

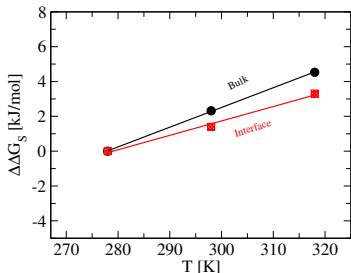


Figure 10: The relative solvation free energies ($\Delta\Delta G_s = \Delta G_s - \Delta G_s(298\text{K})$) of methane molecule at 278K, 298K and 318K at bulk water (black circles) and at graphite interface (red squares). Here methane molecule is allowed to move in a z-plane in solvation free energy calculations in bulk or at interface and the corresponding z positions are like methane-methane PMF calculations.

Conclusions

The ion-ion and ion-water interaction is crucial in understanding many chemical and biological processes occurring in ionic

solution. Despite of the importance of ions in solution, the origin of various ion specific effects are not completely understood. On this context, the ion specific behaviors near water interfaces such as protein-water, air-water and solid-water interfaces are still not fully resolved. Various studies focused on the single ion behaviors near such interfaces, whereas the ion-ion interactions in such contexts are not known. A complete balance of ion-ion, ion-water, water-water interactions in bulk as well as near such water interface, is crucial to determine such specificity. In our current work, we systematically study the ion-ion interactions using different small, large cations and anions near a model hydrophobic surface (graphite) to shed some light on ion specific effects. Ion pairing propensities of cations, Na^+ , K^+ , Cs^+ with anions such as Cl^- , Br^- , I^- near graphite surface and near a modified graphite surface (more hydrophobic) are characterized by PMF calculations and the PMFs are compared with that in bulk.

In bulk water, small ions of higher charge density tends to pair together because the cation-anion interaction overcompensates the strong ion-water interaction.^{18,19} On the other hand, a small ion tends to stay apart from a large ion as the small ion-water interaction dominates over ion-ion interaction.^{18,19} A large-large combination always stays in contact to each other as the ion-water interaction is not stronger than the ion-ion interaction and more importantly, the water-water interaction is gained.^{18,19} Now near hydrophobic surface, ion-pairing propensities are changed because of the water density and water structure which are different relative to that in bulk water. Ion pairing at graphite interface shows some interesting features. Ion pairing propensities between cations and anions are enhanced with some distinct characteristics. Ion pairing between small cation such as Na^+ , K^+ and relative small anions Cl^- , Br^- is amplified in greater extent compare with that in bulk. Ion pairing between small cations Na^+ , K^+ and relatively large anion like I^- is also increased relative to that in bulk, nevertheless the effect is not that strong like for the case of small-small combination. Near graphite surface, the water density around ion pair is found to be less than the water density around ion pair at bulk water. A relatively less number of water molecules around small ion reduces the ion-water interaction penalty arising due to ion pairing. Hence the highest enhancement in ion pairing compared with bulk is seen for small cation and small anion. If the anion is relatively large then the ion-water interaction strength is not so strong in bulk. Although the cost (ion-water interaction) is reduced near interface that helps to enhance pairing but not that extent like the case of small-small combinations. The ion pairing for the combination of large cation, Cs^+ and large anion I^- seems to even become slightly less favorable. The water-water interaction gained at interface due to pairing is also less. Here the ion(large)-water interaction is also weak and does not play important role. Once the surface hydrophobicity is increased then ion pairing between Cs^+ and I^- becomes more favorable than that in bulk water. Similarly, ion pairing between small cations (Na^+ , K^+) and small anions (Cl^- , Br^-) or large anion (I^-) are also amplified than that either in bulk or near graphite surface. For all ion pairs, ion pairing enhances as the solvent shared ion pair state becomes more favorable near graphite surface or modified graphite surface. At least for NaBr and KBr, the entropy and enthalpy components indicate that the more stabilization of SIP states near interface is for entropic reason which is related to the water

density around ion pair at SIP state.

Hydrophobic associations take place in protein folding, protein-protein association and self-assembly of micelles. Water drives such associations. The environment where such association occurs, has potential to alter hydrophobic association. We compute the potential of mean force between two methane particles near a model water interface, graphite interface to analyse the hydrophobic association process. The contact pair state near interface is favoured over the same contact pair state at bulk water. Hence the graphite surface enhances hydrophobic association. A desolvation barrier between the contact minimum and the solvent-separated minimum in the potential of mean force exists in bulk water. This free energy barrier governs the kinetics of hydrophobic association. Like in pure water, the same barrier height in the PMF is also present near graphite interface. This result is in contrast to other hydrophobic surface such as CH₃-SAM surface where this barrier is reduced significantly.³⁶ Once the graphite surface-water interaction is artificially reduced, the desolvation barrier in the PMF disappears like CH₃-SAM surface. This result and also hydrophobic solvation study near graphite surface together indicate the graphite surface is weakly hydrophobic or even slightly hydrophilic in nature in agreement with other experimental²² data. Further studies are required to quantify the nature of graphite surface.

References

- [1] Hofmeister, F. Zur Lehre von der Wirkung der Salze. Zweite Mittheilung. *Arch. Exp. Pathol. Pharmacol.* **1888**, *24*, 247-260.
- [2] Lo Nostro, P.; Ninham, B. W. Hofmeister Phenomena: An Update on Ion Specificity in Biology. *Chem. Rev.* **2012**, *112*, 2286-2322.
- [3] Zhang, Y.; Cremer, P. S. Chemistry of Hofmeister Anions and Osmolytes. *Annu. Rev. Phys. Chem.* **2010**, *61*, 63-83.
- [4] Marcus, Y. Effect of Ions on the Structure of Water: Structure Making and Breaking. *Chem. Rev.* **2009**, *109*, 1346-1370.
- [5] Baldwin, R. L. How Hofmeister Ion Interactions Affect Protein Stability. *Biophys. J.* **1996**, *71*, 2056-2063.
- [6] Collins, K. D.; Washabaugh, M. W. The Hofmeister Effect and the Behaviour of Water at Interfaces. *Q. Rev. Biophys.* **1985**, *18*, 323-422.
- [7] Cacace, M. G.; Landau, E. M.; Ramsden, J. J. The Hofmeister Series: Salt and Solvent Effects on Interfacial Phenomena. *Q. Rev. Biophys.* **1997**, *30*, 241-277.
- [8] Ganguly, P.; Hajari, T.; van der Vegt, N. F. A. Molecular Simulation Study on Hofmeister Cations and the Aqueous Solubility of Benzene. *J. Phys. Chem. B* **2014**, *118*, 5331-5339.
- [9] Jungwirth, P.; Winter, B. Ions at aqueous interfaces: From water surface to hydrated proteins. *Annu. Rev. Phys. Chem.* **2008**, *59*, 343-366.
- [10] Jungwirth, P.; Tobias, D. J. Specific ion effects at the air/water interface. *Chem. Rev.* **2006**, *106*, 1259-1281.
- [11] Zhang, Y.; Cremer, P. S. Interactions between Macromolecules and Ions: The Hofmeister Series. *Curr. Opin. Chem. Biol.* **2006**, *10*, 658-663.
- [12] Rembert, K. B.; Paterová, J.; Heyda, J.; Hilty, C.; Jungwirth, P.; Cremer, P. S. Molecular Mechanisms of Ion-Specific Effects on Proteins. *J. Am. Chem. Soc.* **2012**, *134*, 10039-10046.
- [13] Boström, M.; Tavares, F. W.; Finet, S.; Skouri-Panet, F.; Tardieu, A.; Ninham, B. W. Why Forces between Proteins Follow Different Hofmeister Series for pH above and below pI. *Biophys. Chem.* **2005**, *117*, 217-224.
- [14] Zhang, Y.; Cremer, P. S. The Inverse and Direct Hofmeister Series for Lysozyme. *Proc. Natl. Acad. Sci. USA* **2009**, *106*, 15249-15253.
- [15] Jungwirth, P.; Cremer, P. S. Beyond Hofmeister. *Nature Chemistry* **2014**, *6*, 261-263.
- [16] Schwierz, N.; Horinek, D.; Netz, R. R. Reversed Anionic Hofmeister Series: The Interplay of Surface Charge and Surface Polarity. *Langmuir* **2010**, *26*, 7370-7379.
- [17] Xie, W. J.; Gao, Y. Q. A Simple Theory for the Hofmeister Series. *J. Phys. Chem. Lett.* **2013**, *4*, 4247-4252.
- [18] Collins, K. D. Charge Density-Dependent Strength of Hydration and Biological Structure. *Biophys. J.* **1997**, *72*, 65-76.
- [19] Collins, K. D. Ions from the Hofmeister Series and Osmolytes: Effects on Proteins in Solution and in the Crystallization Process. *Methods* **2004**, *34*, 300-311.
- [20] Collins, K. D.; Neilson, G. W.; Enderby, J. E. Ions in Water: Characterizing the Forces that Control Chemical Processes and Biological Structure. *Biophys. Chem.* **2007**, *128*, 95-104.
- [21] Wang, S.; Zhang, Y.; Abidi, N.; Cabrales, L. Wettability and Surface Free Energy of Graphene Films. *Langmuir* **2009**, *25*, 11078-11081.
- [22] Li et al. Effect of Airborne Contaminants on the Wettability of Supported Graphene and Graphite. *Nat. Mater.* **2013**, *12*, 925-931.
- [23] Raj, R.; Maroo, S. C.; Wang, E. N. Wettability of Graphene. *Nano lett.* **2013**, *13*, 1509-1515.
- [24] Taherian, F.; Marcon, V.; van der Vegt, N. F. A.; Leroy, F. What is the Contact Angle of Water on Graphene?. *Langmuir* **2013**, *29*, 1457-1465.
- [25] Fennell, C. J.; Bizjak, A.; Vlachy, V.; Dill, K. A. Ion Pairing in Molecular Simulations of Aqueous Alkali Halide Solutions. *J. Phys. Chem. B* **2009**, *113*, 6782-6791.
- [26] Hess, B.; van der Vegt, N. F. A. Cation Specific Binding with Protein Surface Charges. *Proc. Natl. Acad. Sci. USA* **2009**, *106*, 13296-13300.
- [27] Ganguly, P.; Schravendijk, P.; Hess, B.; van der Vegt, N. F. A. Ion Pairing in Aqueous Electrolyte Solutions with Biologically Relevant Anions. *J. Phys. Chem. B* **2011**, *115*, 3734-3739.

- [28] Wick, C. D. NaCl Dissociation Dynamics at the Air Water Interface. *J. Phys. Chem. C* **2009**, *113*, 2497-2502.
- [29] Kauzmann, W. Some Factors in the Interpretation of Protein Denaturation. *Adv. Protein Chem.* **1959**, *14*, 1-63.
- [30] Tanford, C. The Hydrophobic Effect and the Organization of Living Matter. *Science* **1978**, *200*, 1012-1018.
- [31] Dill, K. A. Dominant Forces in Protein Folding. *Biochemistry* **1990**, *29*, 7133-7155.
- [32] Hummer, G.; Garde, S.; Garcia, A. E.; Pohorille, A.; Pratt, L. R. An Information Theory Model of Hydrophobic Interactions. *Proc. Natl. Acad. Sci. USA* **1996**, *93*, 8951-8955.
- [33] Setny, P.; Baron, R.; McCammon, J. A. How Can Hydrophobic Association be Enthalpy Driven?. *J. Chem. Theory Comput.* **2010**, *6*, 2866-2871.
- [34] Zangi, R.; Berne, B. J. Temperature Dependence of Dimerization and Dewetting of Large-Scale Hydrophobes: A Molecular Dynamics Study. *J. Phys. Chem. B* **2008**, *112*, 8634-8644.
- [35] Choudhury, N.; Pettitt, B. M. On the Mechanism of Hydrophobic Association of Nanoscopic Solutes. *J. Am. Chem. Soc.* **2005**, *127*, 3556-3567.
- [36] Vembanur, S.; Patel, A. J.; Sarupria, S.; Garde, S. On the Thermodynamics and Kinetics of Hydrophobic Interactions at Interfaces. *J. Phys. Chem. B* **2013**, *117*, 10261-10270.
- [37] Patel, A. J.; Varilly, P.; Jamadagni, S. N.; Acharya, H.; Garde, S.; Chandler, D. Extended Surfaces Modulate Hydrophobic Interactions of Neighboring Solutes. *Proc. Natl. Acad. Sci. USA* **2011**, *108*, 17678-17683.
- [38] Hess, B.; Kutzner, C.; Spoel, D. V. D.; Lindahl, E. GROMACS 4: Algorithms for Highly Efficient, Load-Balanced, and Scalable Molecular Simulation. *J. Chem. Theory Comput.* **2008**, *4*, 435-447.
- [39] Fyta, M.; Netz, R. R. Ionic Force Field Optimization Based on Single-Ion and Ion-Pair Solvation Properties: Going Beyond Standard Mixing Rules. *J. Chem. Phys.* **2012**, *136*, 124103-124108.
- [40] Chang, T. M.; Dang, L. X. Detailed Study of Potassium Solvation Using Molecular Dynamics Techniques. *J. Phys. Chem. B* **1999**, *103*, 4714-4720.
- [41] Dang, L. X. The Nonadditive Intermolecular Potential for Water Revised. *J. Chem. Phys.* **1992**, *97*, 2659-2660.
- [42] Berendsen, H. J. C.; Grigera, J. R.; Straatsma, T. P. The Missing Term in Effective Pair Potentials. *J. Phys. Chem.* **1987**, *91*, 6269-6271.
- [43] Miyamoto, S.; Kollman, P. A. Settle: An Analytical Version of the SHAKE and RATTLE Algorithm for Rigid Water Models. *J. Comput. Chem.* **1992**, *13*, 952-962.
- [44] Walther, J. H.; Jaffe, R.; Halicioglu, T.; Koumoutsakos, P. Carbon Nanotubes in Water: Structural Characteristics and Energetics. *J. Phys. Chem. B* **2001**, *105*, 9980-9987.
- [45] Werder, T.; Walther, J. H.; Jaffe, R. L.; Halicioglu, T.; Koumoutsakos, P. On the Water-Carbon Interaction for Use in Molecular Dynamics Simulations of Graphite and Carbon Nanotubes. *J. Phys. Chem. B* **2003**, *107*, 1345-1352.
- [46] Hess, B.; Holm, C.; van der Vegt, N. F. A. Osmotic Coefficients of Atomistic NaCl (aq) Force Fields. *J. Chem. Phys.* **2006**, *124*, 164509-164518.
- [47] Venkateshwaran, V.; Vembanur, S.; Garde, S. Water-Mediated Ion-Ion Interactions are Enhanced at the Water Vapor-Liquid Interface. *Proc. Natl. Acad. Sci. USA* **2014**, *111*, 8729-8734.
- [48] Bussi, G.; Donadio, D.; Parrinello, M. Canonical Sampling Through Velocity Rescaling. *J. Chem. Phys.* **2007**, *126*, 014101-014107.
- [49] Essmann U.; Perera L.; Berkowitz M. L.; Darden T.; Lee H.; Pedersen L. G. A Smooth Particle Mesh Ewald Method. *J. Chem. Phys.* **1995**, *103*, 8577-8593.
- [50] Chorny, I.; Dill, K. A.; Jacobson, M. P. Surfaces Affect Ion Pairing. *J. Phys. Chem. B* **2005**, *109*, 24056-24060.
- [51] Yu, Z.; Jacobson, M. P.; Josovitz, J.; Rapp, C. S.; Friesner, R. A. First-Shell Solvation of Ion Pairs: Correction of Systematic Errors in Implicit Solvent Models. *J. Phys. Chem. B* **2004**, *108*, 6643-6654.
- [52] Cummings, O. T.; Wick, C. D. Computational Study of Cation Influence on Anion Propensity for the Air-Water Interface. *Chem. Phys. Lett.* **2010**, *500*, 41-45.
- [53] Bonomi, M.; Branduardi, D.; Bussi, G.; Camilloni, C.; Provasi, D.; Raiker, P.; Donadio, D.; Marinelli, F.; Pietrucci, F.; R.A. Broglia, R. A.; Parrinello, M. PLUMED: A Portable Plugin for Free-Energy Calculations with Molecular Dynamics. *Comp. Phys. Comm.* **2009**, *180*, 1961-1972.
- [54] Schweighofer, K.; Benjamin, I. Ion Pairing and Dissociation at Liquid/Liquid Interfaces: Molecular Dynamics and Continuum Models. *J. Chem. Phys.* **2000**, *112*, 1474-1482.
- [55] Taherian, F.; Leroy, F.; van der Vegt, N. F. A. Interfacial Entropy of Water on Rigid Hydrophobic Surfaces. *Langmuir* **2013**, *29*, 9807-9813.
- [56] Driskill, J.; Vanzo, D.; Bratko, D.; Luzar, A. Wetting Transparency of Graphene in Water. *J. Chem. Phys.* **2014**, *141*, 18C517-18C524.
- [57] Otten, D. E.; Onorato, R.; Michaels, R.; Goodknight, J.; Saykally, R. J. Strong Surface Adsorption of Aqueous Sodium Nitrite as an Ion Pair. *Chem. Phys. Lett.* **2012**, *519*, 45-48.

-
- [58] Jorgensen, W. L.; Maxwell, D. S.; Tirado-Rives, J. Development and Testing of the OPLS All-Atom Force Field on Conformational Energetics and Properties of Organic Liquids. *J. Am. Chem. Soc.* **1996**, *118*, 11225-11236.
- [59] Hajari, T.; Ganguly, P.; van der Vegt, N. F. A. Enthalpy-Entropy of Cation Association with the Acetate Anion in Water. *J. Chem. Theory Comput.* **2012**, *8*, 3804-3809.
- [60] Dang, L. X. Temperature Dependence of Interactions of an Ion Pair in Water: A Molecular Dynamics Study. *J. Chem. Phys.* **1992**, *97*, 1919-1921.
- [61] Smith, D. E.; Zhang, L.; Haymet, A. D. J. Entropy of Association of Methane in Water: A New Molecular Dynamics Computer Simulation. *J. Am. Chem. Soc.* **1992**, *114*, 5875-5876.

6 Enthalpy-Entropy of Cation Association with the Acetate Anion in Water

Enthalpy–Entropy of Cation Association with the Acetate Anion in Water

Timir Hajari, Pritam Ganguly, and Nico F. A. van der Vegt*

Center of Smart Interfaces, Technische Universität Darmstadt, 64287 Darmstadt, Germany

S Supporting Information

ABSTRACT: Negatively charged carboxylate and phosphate groups on biomolecules have different affinity for Na^+ and K^+ ions. We performed molecular simulations and studied the pair potential of mean force between monovalent cations and the carboxylate group of the acetate anion in aqueous solution at 298 K. The simulations indicate that a larger affinity of Na^+ over K^+ in the contact ion pair (CIP) state is of entropic origin with the CIP state becoming increasingly populated at higher temperature. Differences between the osmotic activities of these two ions are however governed by interactions with acetate in the solvent-shared ion pair (SIP) state as was previously shown (Hess, B.; van der Vegt, N. F. A. *Proc. Natl. Acad. Sci. U.S.A.* **2009**, *106*, 13296). SIP states with Na^+ are slightly more stable than SIP states with K^+ , resulting in a smaller osmotic activity of sodium. We discuss the different affinities of Na^+ and K^+ in the SIP state in terms of an enthalpy–entropy reinforcement mechanism which involves a water-mediated hydrogen-bonding interaction between the oppositely charged ions. SIP states are enthalpically favorable and become decreasingly populated at higher temperature.

1. INTRODUCTION

Oppositely charged ions attract. In a dielectric medium, such as liquid water, this attraction is attenuated with a factor of approximately 78 (the dielectric constant, 298 K) and is independent of the specific ions involved, provided that the distance between them is large. However at small distances, where the attraction becomes appreciable in comparison to the thermal energy $k_B T$, the effective ion–ion interaction depends on the ion types and on the balance of ion–ion, ion–water, and water–water interactions.^{1,2} The potential corresponding to the mean force between two ions separated by a distance r exhibits multiple minima.^{3–14} At small distances, the first minimum corresponds to the contact ion pair (CIP). The second minimum corresponds to the solvent-shared ion pair (SIP) and is located at a slightly larger distance where the hydration sheaths of the two ions share a common water molecule. A third minimum, the solvent-separated ion pair (2SIP), can further be identified at a distance where the ions are separated by two water molecules. The stabilities (energy minima) of the CIP, SIP, and 2SIP states depend on the ion type.

Ion pairing in water affects dynamic and thermodynamic properties of the electrolyte solution. It has been long known that activity and osmotic coefficients of aqueous electrolyte solutions follow ion-specific series upon varying the cations or anions in solution.¹⁵ The salt activity coefficient of an aqueous alkali chloride solution decreases with increasing crystallographic radius of the cation ($\text{Li}^+ > \text{Na}^+ > \text{K}^+ > \text{Rb}^+ > \text{Cs}^+$). Contrarily, an exactly reversed series applies to aqueous alkali acetate solutions, with activity coefficients that increase as the crystallographic radius of the cation increases ($\text{Li}^+ < \text{Na}^+ < \text{K}^+ < \text{Rb}^+ < \text{Cs}^+$). A recent explanation provided for this reversal of the ion series has been based on molecular simulations where it was analyzed how the excess occupation of CIP and SIP states varies among the ion types.¹⁶ Ion specific variations in the activity coefficient of alkali chloride solutions could be

correlated with the excess occupation of CIP states, while the corresponding variations for alkali acetates could instead be correlated with the excess occupation of SIP states. In SIP configurations, the cation–anion interaction is solvent-mediated and becomes stronger with decreasing cation radius. This picture (see Figure 1), in which the anion accepts a hydrogen

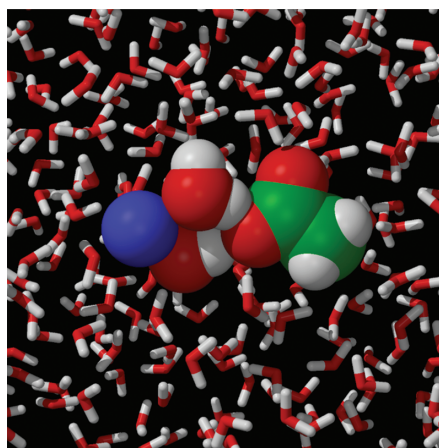


Figure 1. Solvent-shared ion pair between sodium (blue) and acetate in aqueous solution. The ions and the ion bridging water molecules are shown in van der Waals representation.

Special Issue: Wilfred F. van Gunsteren Festschrift

Received: January 31, 2012

Published: April 23, 2012

bond from water in the cation's first hydration shell, not only applies to carboxylate-based anions but also to dimethylphosphates, as was shown in subsequent work by Ganguly et al.¹⁷

Negatively charged carboxylate and phosphate groups on biomolecules interact differently with Na⁺ and K⁺ ions.^{18–23} The water-mediated interaction of sodium and potassium with these biological anions plays a key role in determining differences in their osmotic activities. Owing to its hydrogen-bonding nature, the expected, subtle differences between the interaction of sodium and potassium are sensitive to the thermodynamic conditions of temperature and pressure. In this paper, we study the effective interactions of three cations (Li⁺, Na⁺, K⁺) with the carboxylate group of the acetate ion. To this end, we consider the cation–anion pair potential of mean force (PMF) in a temperature range between 278 and 328 K. We discuss some thermodynamic aspects of ion pairing based on analyses of the enthalpy and entropy contributions to the PMFs.

2. SIMULATION DETAILS

Molecular dynamics (MD) simulations have been performed using the GROMACS package (version 4.0 and 4.5).²⁴ The nonbonded force field parameters for acetate and the cations are reported in References 16 and 17, the OPLS UA force-field²⁵ was used for the bonded parameters of acetate. The SPC/E model²⁶ was taken for water. Particle Mesh Ewald electrostatics²⁷ was used with a direct space cutoff of 1.0 nm and a grid spacing of 0.12 nm. For nonbonded van der Waals interactions, a 1.0 nm cutoff was used. All bond lengths for acetate molecules were kept constant using shake algorithm.²⁸ The temperature was kept constant using velocity rescale thermostat²⁹ with a relaxation time of 0.1 ps. The pressure was kept constant at 1 bar using the Berendsen barostat³⁰ with a relaxation time of 1 ps. All systems were equilibrated in a 10 ns NpT simulation. NpT trajectories of 90 ns were accumulated. The integration time step was 2 fs. All systems contained 5556 water molecules and 50 ion pairs, corresponding to a salt concentration of 0.5 m.

3. RESULTS

Figures 2–4 show cation–acetate radial distribution functions $g(r)$ (RDFs) in the upper panels and the corresponding PMFs, $\Delta G(r) = -RT \ln g(r)$, in the lower panels at three different temperatures. The cation–acetate distances were computed with respect to the closest carboxylate oxygen, and the nonspherical volume for the normalization was taken into

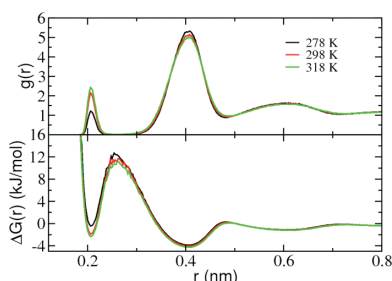


Figure 2. Radial distribution function between Li⁺ and carboxyl oxygen in 0.5 m solution (upper panel). PMF between Li⁺ and carboxyl oxygen in 0.5 m salt solution (lower panel).

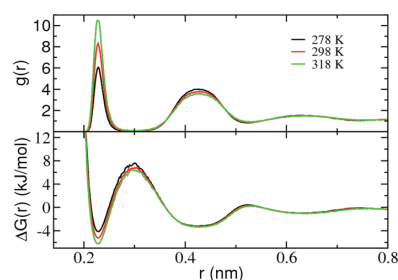


Figure 3. Radial distribution function between Na⁺ and carboxyl oxygen in 0.5 m solution (upper panel). PMF between Na⁺ and carboxyl oxygen in 0.5 m salt solution (lower panel).

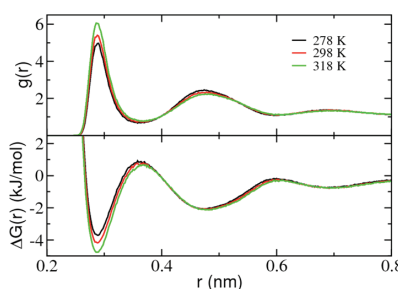


Figure 4. Radial distribution function between K⁺ and carboxyl oxygen in 0.5 m solution (upper panel). PMF between K⁺ and carboxyl oxygen in 0.5 m salt solution (lower panel).

account (for details we refer to the Supporting Information). The first peak in the RDF corresponds to the CIP, the second peak corresponds to the SIP. The stability (ΔG) of the CIP follows the order Na⁺ > K⁺ > Li⁺, while the stability of the SIP follows the order Li⁺ > Na⁺ > K⁺. Ion-specific thermodynamic properties are determined by the stability of SIPs.¹⁶ With increasing temperature, we observe a larger CIP peak but a smaller SIP peak for all three cations. Hence, at higher temperature, the CIP population increases at the expense of the SIP population. Since the temperature derivative of $g(r)$ is given by $[\partial g(r)/\partial T]_p = g(r)\Delta H(r)/RT^2$, we see that the enthalpy, ΔH , in the CIP state is positive, while the enthalpy in the SIP state is negative (relative to large distances $r \rightarrow \infty$). The lower panels in Figures 2–4 show the temperature dependence of the PMFs. Since the temperature derivative of the PMF, $[\partial \Delta G(r)/\partial T]_p = -\Delta S(r)$, provides the entropy,³¹ it becomes clear that in the CIP state the entropy is positive for all cations. The same holds for the SIP states, but the temperature dependence, and therefore the entropy, is considerably smaller. We point out that in the simulations the entropies are calculated by taking finite temperature differences. The entropy calculated therefore assumes a constant heat capacity in the temperature range used for its calculation.

Before we analyze the free energies, enthalpies, and entropies in more detail, it is interesting to consider the predictions obtained with the primitive model, which views ions as point charges in a dielectric medium with dielectric permittivity ϵ . The PMF of the primitive model is given by

$$\Delta G(r) = \frac{-1}{\epsilon r} \quad (1)$$

where we have ignored the constant factor $e^2/4\pi\epsilon_0$. Note that the primitive model in eq 1 is a free energy: the electrostatic screening results from averaging over solvent degrees of freedom at fixed ion distance r and is assumed to attenuate the Coulomb interaction between the two ions with a factor $1/\epsilon$. The dielectric permittivity of the solvent contains the information on the entropic changes of the solvent molecules involved in the charge–charge interaction. Taking the appropriate temperature derivatives provides the enthalpy and entropy:

$$\Delta H(r) = \Delta G(r) \left[1 + \frac{T}{\epsilon} \left(\frac{\partial \epsilon}{\partial T} \right) \right]$$

$$T\Delta S(r) = \Delta G(r) \left[\frac{T}{\epsilon} \left(\frac{\partial \epsilon}{\partial T} \right) \right] \quad (2)$$

For liquid water at 298 K,³²

$$\frac{T}{\epsilon} \left(\frac{\partial \epsilon}{\partial T} \right) = -1.36 \quad (3)$$

which shows that the primitive model predicts a positive change enthalpy change as well as a positive entropy change upon the approach of two oppositely charged ions in water, i.e., the polarization of the dielectric medium by the two ions contributes to a negative enthalpy and entropy but is reduced when the two ions are brought together.

Figure 5 shows the temperature dependence of the CIP free energies ΔG_{CIP} of the systems containing Li^+ , Na^+ , and K^+ . The

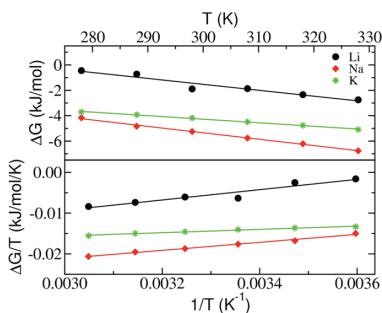


Figure 5. Temperature dependence of the CIP free energy minimum ΔG_{CIP} . The slopes in the upper panel provide the CIP entropy $-\Delta S_{\text{CIP}}$, and the slopes in the lower panel provide the CIP enthalpy ΔH_{CIP} .

free energies, ΔG_{CIP} , enthalpies, ΔH_{CIP} , and entropies, $T\Delta S_{\text{CIP}}$, obtained from the simulations are listed in Table 1 for $T = 298$ K together with the predictions of the primitive model (values in parentheses). The CIP enthalpies and entropies are both positive, in agreement with the expectation based on the primitive model. Entropies $T\Delta S_{\text{CIP}}$, computed using the primitive model (eqs 1–3, using CIP and SIP distances r from the peak positions in Figures 2–4), are remarkably close to the values obtained from the simulations. The enthalpies ΔH_{CIP} obtained from the simulations are however significantly larger (a factor of 2–4) than the values obtained with the primitive model, in particular for the strongly hydrated (kosmotropic)^{1,2,33} Li^+ and Na^+ ions. Upon CIP formation, these ions release part of their hydration water, which contributes to a positive change in enthalpy and entropy.

Table 1. Thermodynamic Properties (units kJ/mol) of the CIP and SIP with Acetate (298 K, 1 bar)^a

CIP state	ΔG_{CIP}	ΔH_{CIP}	$T\Delta S_{\text{CIP}}$
Li^+	-1.4 ± 0.2 (−8.6)	12.6 ± 1.9 (3.1)	14.0 ± 1.7 (11.7)
Na^+	-5.3 ± 0.1 (−7.8)	9.8 ± 0.9 (2.8)	15.1 ± 0.8 (10.6)
K^+	-4.4 ± 0.0 (−6.2)	4.0 ± 0.2 (2.2)	8.4 ± 0.2 (8.4)
SIP state	ΔG_{SIP}	ΔH_{SIP}	$T\Delta S_{\text{SIP}}$
Li^+	-4.0 ± 0.01 (−4.4)	-1.1 ± 0.1 (1.6)	2.9 ± 0.1 (6.0)
Na^+	-3.3 ± 0.03 (−4.2)	-1.8 ± 0.2 (1.5)	1.5 ± 0.2 (5.7)
K^+	-2.1 ± 0.02 (−3.7)	-1.4 ± 0.1 (1.3)	0.7 ± 0.1 (5.0)

^aStatistical errors have been obtained by block averaging. The numbers in parentheses are the predictions of the primitive model (eqs 1–3).

Interestingly, the enthalpy and entropy changes in the CIP state are significantly smaller for the (chaotropic) K^+ ion (Table 1), which is a weaker water binder.

Figure 6 shows the temperature dependence of the SIP free energies, ΔG_{SIP} , of the systems containing Li^+ , Na^+ , and K^+ .

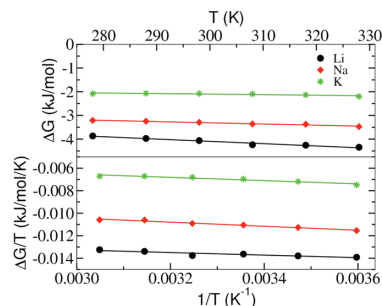


Figure 6. Temperature dependence of the SIP free energy minimum ΔG_{SIP} . The slopes in the upper panel provide the SIP entropy $-\Delta S_{\text{SIP}}$, and the slopes in the lower panel provide the SIP enthalpy ΔH_{SIP} .

The free energies, ΔG_{SIP} , enthalpies, ΔH_{SIP} , and entropies, $T\Delta S_{\text{SIP}}$, are listed in Table 1 for $T = 298$ K. The temperature dependence of ΔG_{SIP} is significantly weaker than the temperature dependence of ΔG_{CIP} . While the entropies $T\Delta S_{\text{SIP}}$ are all small and positive, the enthalpies ΔH_{SIP} are all small and negative. This type of enthalpy–entropy reinforcement is not predicted by the primitive model and warrants further comment, in particular because the salt activities of this system owe their cation specificity from differences in SIP stability.^{16,17} Interestingly, the entropies $T\Delta S_{\text{SIP}}$ obtained from the simulations are significantly smaller than the corresponding entropies predicted by the primitive model (see Table 1). A possible explanation for this may be sought in a water-mediated interaction that stabilizes the SIP state. The water molecule shared between the cation and the carboxylate group of the anion coordinates the cation with its oxygen atom while donating a hydrogen bond to one of the carboxyl oxygen atoms (see Figure 1). This cation–anion bridging interaction via hydrogen-bonding decreases the enthalpy; the entropy tends to decrease too due to the ordering of the bridging water molecules. Fennell et al. observed orientationally constrained water molecules in SIP states of alkali halides.¹⁴ Although these authors did not calculate the entropies of the different ion pair states, their results indicate that SIP states of alkali halides also have a low entropy. Interestingly, Baron et al.³⁴ reported two

examples of enthalpy dominated ion pairing for a model cavity–ligand system. In both cases described, enthalpy dominated ion pairing is solvent separated.³⁴

Enthalpy–entropy compensation is a general property of weak intermolecular interactions,^{35–37} which in SIP formation between monovalent cations and a carboxylate-based anion in water as studied here leads to lower enthalpies and entropies than expected based on simple electrostatic considerations. To investigate if the bridging water molecule is indeed configurationally confined compared to similar water molecules not hydrogen bonded to carboxylate, we considered the angle defined by the positions of the cation and the water oxygen and hydrogen atoms. Only those water molecules in the first hydration shell of the cation that donate a hydrogen bond to a carboxyl oxygen atom were considered in the analysis. The angle distribution functions are shown as solid lines in Figure 7.

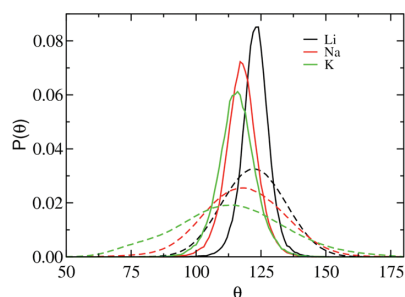


Figure 7. Distribution functions of the cation–oxygen(water)–hydrogen(water) angle for water molecules in the first hydration shell of the cation (298 K). $\int_0^\pi P(\theta)d\theta = 1$. The solid lines show the distribution functions for water molecules that are furthermore hydrogen bonded to the carboxyl oxygen in SIP configurations. The dashed lines show the distribution functions for water molecules in the cation first hydration shell but in the absence of the carboxylate group.

An angle of 125° corresponds to a water molecule that orients its dipole vector along the cation–oxygen(water) connecting vector. Similar angle distribution functions were calculated for cations in bulk water (in absence of an acetate ion), where, instead of hydrogen bonding with acetate, the cation's first shell hydration water molecule donates hydrogen bonds to the bulk. The corresponding distribution functions are shown as dashed lines in Figure 7. The comparison between the dashed and solid lines clearly indicates that bridging water molecules in SIP configurations sample a significantly narrower range of angles, therefore providing support for the idea that the water-mediated hydrogen-bonding interaction between the two ions lowers the water entropy. We further note that the widths of the distribution functions in Figure 7 decrease in the order $K^+ > Na^+ > Li^+$, which is also the order in which the cation–water interaction becomes stronger.

We finally examined the hydrogen-bond angle between the bridging water molecule and the acetate anion. The data are shown in Figure 8 (solid lines) and are compared with the acetate–water hydrogen bond angle distribution of 'free' acetate (dashed lines) far away from any cation. The comparison again shows that a smaller range of angles is sampled in the SIP state. Hydrogen bonds are slightly more bendable in the SIP state, as indicated by a small shift of the peaks to smaller angles in comparison to the free acetate case.

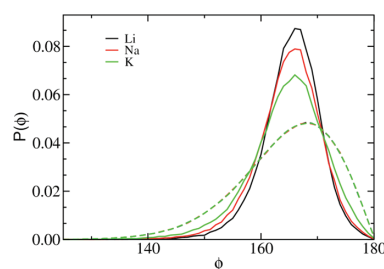


Figure 8. Distribution functions of the oxygen(carboxyl)–hydrogen(water)–oxygen(water) hydrogen-bond angle (298 K). $\int_0^\pi P(\phi)d\phi = 1$. The solid lines show the distribution functions for water molecules that furthermore belong to the first hydration shell of the cation in SIP configurations. The dashed lines show the distribution functions in absence of the cation.

4. DISCUSSION AND CONCLUSIONS

Solvated ions are a common component of nearly all biological systems. In this work we have been interested in the interaction of monovalent cations with the negatively charged carboxylate group of the acetate anion. This anion serves as a model of negatively charged groups on biomolecules. There have been many studies that illustrate pronounced effects of dissolved, specific salts on properties, such as enzymatic activity, protein stability, and protein–protein interaction. Water plays an important, but ill-understood, role in these hydrophilic interactions, and the link to solution thermodynamic properties remains largely unexplored. Studies on the structure and thermodynamics of aqueous electrolyte solutions may potentially provide useful insights that advance our understanding of electrostatic interactions in biomolecular systems.

Salt activities and osmotic pressures of aqueous electrolyte solutions are ion specific. At high enough electrolyte concentrations, the osmotic pressures of NaCl and KCl solutions are different owing to different affinities of cation–anion pairing in these systems. The osmotic pressures of alkali chloride solutions thus depend on the choice of the cation. This dependence is uniquely determined by differences in the contact ion pairing propensities as was shown by Hess and van der Vegt,¹⁶ who applied the thermodynamic solution theory of Kirkwood and Buff³⁸ to molecular dynamics simulation trajectories. Because Kirkwood–Buff theory provides an exact link between the solution thermodynamics and the solution structure (with the structure being expressed in terms of RDFs), our discussion of the solution thermodynamics can be limited to analyzing pair correlations only. Fennell et al.¹⁴ computed various alkali–halide pair PMFs in aqueous solutions based on molecular dynamics simulations. These simulation studies^{14,16} confirm Collins' law of matching water affinities,^{1,2} which states that the relative affinities of ions in solution depend on the matching of cation and anion sizes: small pairs with small and large pairs with large, while small–large ion combinations should remain dissociated. Collins' law is based on enthalpic considerations, and entropy effects are assumed unimportant.

The appellations "chaotrope" and "kosmotrope" are sometimes used as synonyms of "large" and "small", respectively. Chaotropes are "structure breaking" ions, kosmotropes are "structure making" ions.³³ Among a plethora of quantities that can be used to characterize "structure", the ion–water and water–water RDFs provide one possible choice, which is

probably the most meaningful one because Kirkwood–Buff solution theory relates the RDFs to the solution thermodynamics. While certain aspects of the ion–water radial distribution function of chaotropic and kosmotropic ions can be correlated with single ion hydration entropies,³⁹ it was shown previously that differences in ion–water and water–water pair correlations in solutions with different cations do not explain the differences in the solution osmotic pressures.^{16,17} Hence, ion-specific trends in the solution osmotic pressures of these systems can be explained by studying the ion–ion correlations only. These ion–ion correlations contain information on CIPs, SIPs, and 2SIPs, which can in principle be probed with dielectric relaxation spectroscopy. This promising experimental technique has had considerable success in measuring ion pairing.^{40–42}

In this paper, we have reported molecular simulations and calculated ion pair PMFs to study the interaction of monovalent cations (Li^+ , Na^+ , K^+) with the carboxylate group of the acetate anion in water. Previous simulations of this system¹⁶ showed that cation–carboxylate CIPs and SIPs are stronger for Na^+ than for K^+ . It was furthermore shown that the resulting salt activity/osmotic coefficients are cation specific and follow the order $\text{Li}^+ < \text{Na}^+ < \text{K}^+$, exclusively owing to a decreasing stability of water-mediated SIPs in passing from Li^+ to K^+ within this series. The purpose of the present paper has been to characterize the thermodynamic properties of CIPs and SIPs in terms of their enthalpic and entropic stabilization. Because, also in this system, the ion–water and water–water correlations do not explain the ion specificity of the osmotic coefficients,¹⁶ we have exclusively studied the cation–anion pair PMFs together with the contributions of the enthalpy and entropy. We find that for all three cations, the CIP and SIP states have positive entropy relative to the solvent-separated state at large ion separations. The magnitude of the entropy change follows the order $\text{Na}^+ > \text{Li}^+ > \text{K}^+$ (CIP) and $\text{Li}^+ > \text{Na}^+ > \text{K}^+$ (SIP). Ion pairing causes a significantly larger entropy gain for the strong water-binding (kosmotropic) cations Li^+ and Na^+ than for the weak water-binding (chaotropic) K^+ ion. In the CIP state, positive entropies are compensated by a positive enthalpy. This enthalpy–entropy compensation phenomenon results in increased stability (ΔG) and population of CIP configurations with increasing temperature above 298 K. In the SIP state, enthalpy–entropy reinforcement stabilizes the SIP configuration, but its population decreases with increasing temperature above 298 K. The favorable enthalpy of SIP configurations results from a hydrogen-bonding interaction mechanism in which water molecules in the first shell of a cation donate hydrogen bonds to one of the carboxylate oxygens.

It is interesting to point out that surface salt bridges on hyperthermophilic proteins are believed to contribute to protein stability at elevated temperatures by a mechanism which is similar to the one described here.^{43,44} At room temperature, desolvation of the charged side chains penalizes salt bridge formation and leads to little contribution of salt bridges to protein stability. At elevated temperatures, reduced solvation removes this penalty causing a favorable change in the intraprotein Coulomb energy due to the tightening of salt bridges.⁴⁴ The results presented in this work pertain to simple, spherical alkali cations. It would be interesting to further study ammonium or guanidinium-based cations in order to shed further light on the role of hydration and solvent entropy in salt bridge formation at different temperatures.

■ ASSOCIATED CONTENT

📄 Supporting Information

The normalization of the cation–oxygen(carboxylate) radial distribution functions with a nonspherical volume is described. This information is available free of charge via the Internet at <http://pubs.acs.org>.

■ AUTHOR INFORMATION

Corresponding Author

*E-mail: vandervegt@csi.tu-darmstadt.de

Notes

The authors declare no competing financial interest.

■ ACKNOWLEDGMENTS

N.F.A.v.d.V. is indebted to Wilfred van Gunsteren for encouragement and support at a decisive stage of his career and for introducing him to the field of entropy calculations.

■ DEDICATION

This work is dedicated to Wilfred van Gunsteren on the occasion of his 65th birthday.

■ REFERENCES

- (1) Collins, K. D. *Biophys. J.* **1997**, *72*, 65.
- (2) Collins, K. D. *Methods* **2004**, *34*, 300.
- (3) Neilson, G. W.; Enderby, J. E. *Proc. R. Soc. London, Ser. A* **1983**, *390*, 353.
- (4) Patey, G. N.; Valleau, J. P. *J. Chem. Phys.* **1975**, *63*, 2334.
- (5) Mezei, M.; Beveridge, D. L. *J. Chem. Phys.* **1981**, *74*, 6902.
- (6) Pettitt, B. M.; Rossky, P. J. *J. Chem. Phys.* **1986**, *84*, 5836.
- (7) Dang, L. X. *J. Chem. Phys.* **1992**, *97*, 1919.
- (8) Chen, S. W.; Rossky, P. J. *J. Phys. Chem.* **1993**, *97*, 6078.
- (9) Pratt, L. R.; Hummer, G.; Garcia, A. E. *Biophys. Chem.* **1994**, *51*, 147.
- (10) Koneshan, S.; Rasaiah, J. C. *J. Chem. Phys.* **2000**, *113*, 8125.
- (11) Bergdorf, M.; Peter, C.; Hünenberger, P. H. *J. Chem. Phys.* **2003**, *119*, 9129.
- (12) Hess, B.; Holm, C.; van der Vegt, N. F. A. *Phys. Rev. Lett.* **2006**, *96*, 147801.
- (13) Hess, B.; Holm, C.; van der Vegt, N. F. A. *J. Chem. Phys.* **2006**, *124*, 164509.
- (14) Fennell, C. J.; Bizjak, A.; Vlachy, V.; Dill, K. A. *J. Phys. Chem. B* **2009**, *113*, 6782.
- (15) Robinson, R. A.; Stokes, R. H. *Electrolyte Solutions*, 2nd ed.; Dover Publications: Mineola, NY, 2002.
- (16) Hess, B.; van der Vegt, N. F. A. *Proc. Natl. Acad. Sci. U.S.A.* **2009**, *106*, 13296.
- (17) Ganguly, P.; Schravendijk, P.; Hess, B.; van der Vegt, N. F. A. *J. Phys. Chem. B* **2011**, *115*, 3734.
- (18) Vrbka, L.; Vondrasek, J.; Jagoda-Cwiklik, B.; Vacha, R.; Jungwirth, P. *Proc. Natl. Acad. Sci. U.S.A.* **2006**, *103*, 15440.
- (19) Savelyev, A.; Papoian, G. A. *J. Am. Chem. Soc.* **2006**, *128*, 14506.
- (20) Jagoda-Cwiklik, B.; Vacha, R.; Lund, M.; Srebro, M.; Jungwirth, P. *J. Phys. Chem. B* **2007**, *111*, 14077.
- (21) Aziz, E. F.; et al. *J. Phys. Chem. B* **2008**, *112*, 12567.
- (22) Uejio, J. S.; Schwartz, C. P.; Duffin, A. M.; Drisdell, W. S.; Cohen, R. C.; Saykally, R. J. *Proc. Natl. Acad. Sci. U.S.A.* **2008**, *105*, 6809.
- (23) Savelyev, A.; Papoian, G. A. *J. Phys. Chem. B* **2008**, *112*, 9135.
- (24) Hess, B.; Kutzner, C.; van der Spoel, D.; Lindahl, E. *J. Chem. Theory Comput.* **2008**, *4*, 435.
- (25) Jorgensen, W. L.; Maxwell, D. S.; Tirado-Rives, J. *J. Am. Chem. Soc.* **1996**, *118*, 11236.
- (26) Berendsen, H. J. C.; Grigera, J. R.; Straatsma, T. P. *J. Phys. Chem.* **1987**, *91*, 6269.

- (27) Essmann, U.; Perera, L.; Berkowitz, M. L.; Darden, T.; Lee, H.; Pedersen, L. G. *J. Chem. Phys.* **1995**, *103*, 8577.
- (28) Ryckaert, J. P.; Ciccotti, G.; Berendsen, H. J. C. *J. Comput. Phys.* **1977**, *23*, 327.
- (29) Bussi, G.; Donadio, D.; Parrinello, M. *J. Chem. Phys.* **2007**, *126*, 014101.
- (30) Berendsen, H. J. C.; Postma, J. P. M.; van Gunsteren, W. F.; DiNola, A.; Haak, J. R. *J. Chem. Phys.* **1984**, *81*, 3684.
- (31) Smith, D. E.; Zhang, L.; Haymet, A. D. J. *J. Am. Chem. Soc.* **1992**, *114*, 5875.
- (32) Israelachvili, J. N. *Intermolecular and Surface Forces*, 3rd ed., Academic Press: Burlington, MA, 2011.
- (33) Marcus, Y. *Chem. Rev.* **2009**, *109*, 1346.
- (34) Baron, R.; Setny, P.; McCammon, J. A. *J. Am. Chem. Soc.* **2010**, *132*, 12091.
- (35) Dunitz, J. *Chem. Biol.* **1995**, *2*, 709.
- (36) van der Vegt, N. F. A.; van Gunsteren, W. F. *J. Phys. Chem. B* **2004**, *108*, 1056.
- (37) van Gunsteren, W. F.; Bakowies, D.; Baron, R.; Chandrasekhar, I.; Christen, M.; Daura, X.; Gee, P.; Geerke, D. P.; Glättli, A.; Hünenberger, P. H.; Kastenholz, M. A.; Oostenbrink, C.; Schenk, M.; Trzesniak, D.; van der Vegt, N. F. A.; Yu, H. B. *Angew. Chem., Int. Ed.* **2006**, *45*, 4064.
- (38) Kirkwood, J. G.; Buff, F. P. *J. Chem. Phys.* **1951**, *19*, 774.
- (39) Lynden-Bell, R. M.; Rasaiah, J. C. *J. Chem. Phys.* **1997**, *107*, 1981.
- (40) Buchner, R.; Chen, T.; Hefter, G. *J. Phys. Chem. B* **2004**, *108*, 2365.
- (41) Wachter, W.; Kunz, W.; Buchner, R.; Hefter, G. *J. Phys. Chem. A* **2005**, *109*, 8675.
- (42) Marcus, Y.; Hefter, G. *Chem. Rev.* **2006**, *106*, 4585.
- (43) Elcock, A. H. *J. Mol. Biol.* **1998**, *284*, 489.
- (44) de Bakker, P. L.; Hünenberger, P. H.; McCammon, J. A. *J. Mol. Biol.* **1999**, *285*, 1811.

Supporting Information

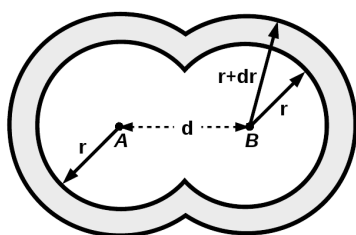
Enthalpy-Entropy of Cation Association with the Acetate Anion in Water

Timir Hajari ¹, Pritam Ganguly ¹ and Nico F.A. van der Vegt ¹

¹ Center of Smart Interfaces, Technische Universität Darmstadt, Petersenstrasse 32, 64287 Darmstadt, Germany

Radial distribution functions with a non-spherical volume normalization.

The radial distribution function (RDF) between the cations and the carboxyl oxygens of acetate (shown in the upper panels of Figs. 1-3) were calculated by considering the nearest oxygen (among the two oxygen atoms of the acetate anion) to the cation. This requires a non-spherical volume for the normalization of the RDF as shown in the picture below.



The two oxygen atoms of the acetate anion are denoted *A* and *B*. The atoms are separated by distance *d*. The grey shaded area is used for normalizing the RDF and is obtained from the volume $V(r,d)$ of two overlapping spheres, *i.e.* the volume of two spheres of radius *r* minus the common volume of the two spheres:

$$V(r,d) = \frac{8}{3}\pi r^3 - \frac{1}{12}\pi(4r+d)(2r-d)^2 \quad (\text{S.1}).$$

The RDF, denoted $g(r)$ in Eq. (S.2), is calculated by counting the number of cations $N(r)$ found at a distance between r and $r+dr$ from the closest acetate oxygen atom:

$$g(r) = \frac{N(r)}{\rho dV(r)} \quad (\text{S.2}),$$

where ρ is the molar cation concentration. The volume element $dV(r)$ in Eq. (S.2) is defined as:

$$dV(r) = V(r+dr, d) - V(r, d) \quad (\text{S.3}).$$

7 Conclusions and Outlook

We have focused on two types of thermodynamic processes, solvation of different polar, nonpolar side-chains present in peptide backbone and ion-pairing in bulk water solution and at hydrophobic interfaces.

The solvation free energy of nonpolar side-chain attached to peptide backbone is significantly reduced compared with the side-chain analogs data. The polar side-chains are barely affected in presence of backbone. Many hydrophobicity scales for studying protein stability utilize the side-chain analog solvation data. Our data could be useful on these regards with the advantage of having the effect of peptide backbone which is not considered in many hydrophobicity scales. The hydrophobicity of nonpolar side-chains is considered to play an important role in protein folding in aqueous solution. Our finding indicates that the nonpolar side-chains are less hydrophobic than what was believed on the basis of free nonpolar side-chain solvation data. In this thesis, capped tripeptides are considered to compute the solvation free energy of side-chains and no adjacent side-chains have been considered in our model peptide backbone. To make a general comment on hydrophobicity reduction, it would be useful to estimate the conditional solvation free energy of nonpolar side-chains in longer peptide backbone or in protein and also to include the effect of adjacent side-chains present in the real scenario. The entropy of solvation for different nonpolar side-chains in presence of backbone is reduced that causes such hydrophobicity reductions. More specifically, the entropy of cavity formation next to backbone is relative more favourable than a same sized cavity formation in bulk water. The highly unfavourable solvation entropy of nonpolar solutes is one of the important characteristics of hydrophobicity effect. Both solvation entropy and enthalpy of polar side-chains are affected. However the entropy-enthalpy cancellation takes place and because of that the overall solvation free energy of polar side-chains is the same as the solvation free energy of corresponding free side-chains. Hence the nonadditive entropy, enthalpy contribution in the solvation of nonpolar and polar groups in presence of context should be analyzed thoroughly in macromolecules such as protein and lipid. The study of protein folding/unfolding equilibrium in different water-cosolvent mixtures utilizes liquid(water)-liquid(water-cosolvent) transfer free energies of different polar and nonpolar side-chains and peptide backbone. The free energy contribution from

side-chains and peptide backbone in controlling folding/unfolding equilibrium is still under debate. In future work, it would be useful to estimate the solvation free energies of side-chains including the effect of backbone in water-cosolvent mixtures to get those transfer free energies.

From our study in this thesis on ion-pairing shows that ion-pairing for small(cation)-small(anion) combination is greatly amplified near hydrophobic surfaces. However pairing between small-large and large-large ion combinations are weakly affected near hydrophobic interface. The water density around ions is smaller near interfaces than that in bulk water. Water density near hydrophobic surface plays important role to bring such specific enhancement in ion-pairing. Same work can be extended near other aqueous interfaces such as protein, air-water and pattern surfaces. The thermodynamic properties of CIPs and SIPs are characterized in terms of their enthalpic and entropic stabilization for acetate ion with different alkali cations. The enthalpy-entropy compensation phenomenon at CIP states and enthalpy-entropy reinforcement stabilization at SIP configurations of different ion pairs are found. Water-mediated hydrogen-bonding interaction between the oppositely charged ions decreases the entropy at SIP state. While at CIP states due to a release part of hydration water around ions, a positive change in enthalpy and entropy is observed for all pairs. It would be interesting to study using positively charged side-chains like Arginine or Lysine and different Hofmeister anions in order to shed further light on the role of ion-pairing in ion specific protein stability.

Curriculum Vitae

Name: Timir Hajari
Place of Birth: Rasulpur, Hooghly, India
Date of Birth: 19.03.1989
Nationality: Indian

Education:

1998 – 2006: High School: Jangalpara B. C. K. M. High School , India.

2006 – 2009: Bachelor of Science (Honours in Chemistry), University of Calcutta, India.

2009 – 2011: Master of Science (Chemistry), Indian Institute of Technology- Bombay, India.

2011 – 2015: Center of Smart Interfaces, Technische Universität Darmstadt, Germany.

(Timir Hajari)

Timir Hajari
Center of Smart Interfaces
Alarich-Weiss-Straße 10
64287 Darmstadt

Tel.: 06151 16 4478
E-mail: hajari@csi.tu-darmstadt.de

Darmstadt, den 1. Juni 2015

Erklärung

Ich erkläre hiermit, noch keinen Promotionsversuch unternommen zu haben.

(Timir Hajari)

Timir Hajari
Center of Smart Interfaces
Alarich-Weiss-Straße 10
64287 Darmstadt

Tel.: 06151 16 4478
E-mail: hajari@csi.tu-darmstadt.de

Darmstadt, den 1. Juni 2015

Eidesstattliche Erklärung

Ich erkläre mich hiermit an Eides Statt, dass ich meine Dissertation selbständig und nur mit den angegebenen Hilfen angefertigt habe.

(Timir Hajari)

